

1 Introduction

1.1 Motivation

During a heterogeneous photochemical reaction, photogenerated electrons and holes migrate to the solid surface where they can participate in reactions with adsorbed species. One goal of photochemistry research during the past three decades has been to promote the efficient photolysis of water using solid oxide catalysts. The efficient photoassisted decomposition of water into hydrogen and oxygen gas is a promising means of converting solar energy into storable fuel (H_2 gas). In contrast to petroleum or nuclear energy sources, hydrogen gas produced through this route is a clean energy source. Also, energy sources based on H_2 fuel from sunlight will provide remote parts of world, which are not connected to power grids for electricity, an alternative to the traditional diesel generator [1].

The bulk of photolysis research has focused on two routes for splitting water. The first is the use of a photoelectrochemical cell in which the photoanode is typically the photoactive material. To avoid limitations associated with the high costs of these systems, a second route using high surface area colloidal suspensions of oxide photocatalysts has been explored. The recombination of photogenerated carriers and the back reaction of reduced and oxidized products (atomic H and hydroxyl radicals, respectively) to reform water are frequently cited as factors limiting the efficiency of photolysis using particulate materials. For this reason, more recent work has been directed toward the development of catalyst structures that separate the charge

carriers and the reduction and oxidation production sites where the precursors to H_2 and O_2 are formed [2].

1.2 Objective

The research described in this thesis is aimed at understanding how the efficiencies of photochemical reactions are influenced by electric fields within the catalyst and by the catalyst's surface orientation. Static dipolar fields can occur in some insulating ceramics because of either a spontaneous internal polarization or the presence of a charged surface. The experiments described here are motivated by the idea that these fields have the potential to separate photogenerated carriers and increase photolysis efficiency by reducing losses associated with carrier recombination and the reverse reaction of products. Studies of the orientation dependence of photochemical reactions on known oxide photolysis catalysts were motivated by prior experiments on TiO_2 , the most studied photolysis catalyst, which has orientation dependent reactivity. These present experiments are guided by the hypothesis that special structural features on different surfaces will promote either reduction or oxidation processes and that this will lead to a geometric separation of O_2 and H_2 generation sites. To test the feasibility of these ideas, experiments were performed to answer the following questions:

1. Do permanent dipoles separate photogenerated charge carriers and the locations of photochemical oxidation/reduction half reactions on the surfaces of polar oxides?
2. Do other materials besides TiO_2 have orientation dependent photochemical reactivities?
3. Is the internal dipolar field or the crystal structure of the catalyst an important materials property for compounds with high photochemical activity such as $Sr_2Nb_2O_7$, $Sr_2Ta_2O_7$, and $BaTi_4O_9$?

1.3 Approach

The approach taken in this research relies on the use of photochemical reactions that leave insoluble products on the catalyst surface at the reaction site. The reaction products, and therefore the reaction sites, can be located on the surface following the reaction using atomic force microscopy. The crystallography of the reaction sites and their relative reactivities are then used to form a structure-property relation for these catalyst/reaction systems. For all materials used in this study, randomly oriented polycrystalline ceramics were used to observe the reactivity over the range of all possible orientations. When available, single crystals were used to study the reactivity of specific orientations. Finally, particulate materials were used to examine the reactivity on the micron scale to see if conclusions derived from experiments on bulk materials can be transferred to the much smaller crystals used for photolysis reactions.

To answer the first two questions posed above, the reactivity of ferroelectric BaTiO_3 and non-ferroelectric SrTiO_3 were studied. These materials were chosen because of the similarity of their perovskite structures and their differing ferroelectric behavior. BaTiO_3 was used to determine the effect of permanent dipoles caused by ferroelectric domains on photochemical reactivity while SrTiO_3 was used to determine the effect of charged surface terminations on photochemical reactivity. SrTiO_3 was also chosen to study the structure sensitivity of another Ti-based catalyst as a comparison to the orientation dependent reactivity of TiO_2 . To answer the third question, the reactivities of BaTi_4O_9 , $\text{Sr}_2\text{Nb}_2\text{O}_7$, and $\text{Sr}_2\text{Ta}_2\text{O}_7$, materials with highly anisotropic crystal structures, were studied.

1.4 Organization

This document is organized in the following way. Chapter 2 presents the relevant background material on polar oxides, heterogeneous photochemical reactions, water photolysis, and the orientation dependence of TiO_2 . Chapter 3 is devoted to describing the crystallography of

the materials studied in this work. The experimental approach taken in this research is described in Chapter 4. Chapters 5 and 6 present the results of experiments aimed at determining if permanent dipoles separate photogenerated charge carriers and the locations of photochemical half reactions on the surface of polar oxides. The reactivity of ferroelectric BaTiO₃ is presented in Chapter 5 and the reactivity of SrTiO₃ is described in Chapter 6. Chapter 6 also discusses the orientation dependence of the photochemical reactivity of SrTiO₃. The experiments in Chapter 7 were designed to determine if either the presence of internal dipolar fields or specific surface structures are important materials properties for compounds with high photolysis efficiencies. The reactivities of BaTi₄O₉ (tunnel structure), Sr₂Nb₂O₇ (layered structure, ferroelectric), and Sr₂Ta₂O₇ (layered structure) are presented in this chapter. Finally, Chapter 8 is devoted to summarizing the observations made in this thesis and present the conclusions formed from this work. Questions to be answered by further experiments are also presented in this final chapter.

1.5 References

- (1) T.H. Maugh III, *Science*, **221** (1983) 1358.
- (2) K. Doman, *Surface Photochemistry*; M. Anpo, Ed.; J. Wiley and Sons: Chichester, England, 1996; p. 1.

2 Background

2.1 Introduction

The purpose of this chapter is to present the relevant background material for the research presented in this document. There are sections devoted to polar oxides, heterogeneous photocatalysis, water photolysis, and the orientation dependence of titania's reactivity. Embedded in these sections is information on why the materials used in this study were selected.

2.2 Polar Oxides

2.2.1 *Ferroelectrics*

Almost all noncentrosymmetric crystals are piezoelectric [1], meaning that a polarization is induced by an applied stress and, conversely, that a mechanical strain is induced by an applied electric field. Pyroelectrics are a special class of piezoelectrics that include all noncentrosymmetric, polar crystals. Pyroelectrics are spontaneously and permanently polarized only in a certain temperature range. As the temperature of the pyroelectric is increased the amount of polarization decreases and then disappears at its Curie temperature, T_c .

If the pyroelectric crystal has more than one polar axis and the direction of the polarization can be switched upon the application of an electric field, it is called a ferroelectric. Below T_c , the crystal takes on a spontaneous polarization and, therefore, has charged surfaces which is an unfavorable energy situation. This depolarization field can be compensated (the energy, $W_E = \int \mathbf{D} \cdot \mathbf{E} dV$, goes to zero), and the electric field both inside and outside the crystal vanishes, by either conduction in the crystal with the establishment of a space charge region, the adsorption of

charged species on the surface, or the formation of a domain structure [2]. Domains are volumes of crystal with a uniform polarization. Because ferroelectrics have more than one polarization direction, the combination of domains with different polarization directions results in the crystal having no net polarization. The pattern of naturally occurring domains depends on the crystal symmetry, defect structure, conductivity, and preparation. Also, the magnitude of the spontaneous polarization, the dielectric and elastic compliances, and the sample geometry can affect the domain pattern. The crystal can, however, be forced to have a single domain by poling – under the influence a strong enough electric field, the polarization in individual domains is switched to align with the direction of the field.

In this study, barium titanate, BaTiO_3 , is used to examine the effects of spontaneous polarization on photochemical activity. BaTiO_3 undergoes a paraelectric-to-ferroelectric phase transition when cooled through $T_c = 120\text{ }^\circ\text{C}$ ($P_s = 0.26\text{ C/m}$ at $23\text{ }^\circ\text{C}$ [3]). The crystal structure at room temperature is a tetragonal distortion of the higher temperature cubic perovskite phase. The crystallography of BaTiO_3 will be described in greater detail in the next chapter, and its reactivity is described in Chapter 5.

2.2.2 Polar Surface Terminations

Polar surface terminations result when an ionic crystal is cleaved and the two new surfaces are oppositely charged with an induced dipole perpendicular to the surface. These charged surfaces produce polarizing electric fields in the bulk that make them unstable and, therefore, they have been assigned infinite surface energies [4]. Of course, this is not an accurate description of a real surface where the charge is usually compensated by surface reconstruction, adsorption of additional charge, or the formation of a space charge region adjacent to the surface.

Zinc oxide (ZnO) is a classic example of a material with two polar terminations. ZnO has the hexagonal wurzite structure and is polar along the c-axis; the $\{0001\}$ surface is a positively charged Zn layer and the $\{000\bar{1}\}$ surface is a negatively charged O layer. It has been suggested that the bulk-terminated surfaces can be stabilized by a charge transfer step that reduces the ionicity of both surfaces [5]. These different surfaces exhibit different properties. For example, the $\{000\bar{1}\}$ -O surface is preferentially etched with acid; the entire surface appears rough after etching. On the other hand, the $\{0001\}$ -Zn surface etches evenly except for the appearance of dislocation etch pits [6]. Acid etched prism $\{10\bar{1}0\}$ faces reveal etch pits with a pointed top and a flat base (a pointed needle shape). The apex is pointed in the $\langle 0001 \rangle$ direction, toward the Zn surface. This differential etching behavior is attributed to dangling electrons at the oxygen terminated surface (electronegativity of O > Zn). This surface ionicity difference also leads to differences in surface conductivity and molecular adsorption [7].

Strontium titanate (SrTiO_3) was chosen to study the effect of polar terminations on photochemical activity. SrTiO_3 has a cubic perovskite structure ($a = 3.905 \text{ \AA}$, $E_g = 3.2 \text{ eV}$). This material was chosen because of its similarity of its structure to BaTiO_3 and the similarity of the Ti-coordination to TiO_2 (rutile). The $\{100\}$ surface of SrTiO_3 is nonpolar while both the $\{110\}$ and $\{111\}$ SrTiO_3 terminations are polar. The influence of Ti coordination can be examined since each of the three low index surfaces of SrTiO_3 has a different number of broken Ti-O bonds ($\{100\} = 1$, $\{110\} = 2$, $\{111\} = 3$). The crystallography of SrTiO_3 and its surfaces are discussed in more detail in Chapter 3, with its reactivity discussed in Chapter 6.

2.3 Heterogeneous Photochemistry

Heterogeneous photochemical reactions take place on semiconductor surfaces when the solid adsorbs photons with an energy greater than its bandgap. This energy excites electrons into

the conduction band and creates holes in the valance band. These photogenerated charge carriers can either recombine, giving off heat or, if there are energy states available at the surface to trap the carriers, they can react with adsorbed species at the semiconductor surface.

For a redox reaction to take place at the semiconductor surface, the electrochemical potentials of the half reactions must lie within the band gap of the semiconductor. Figure 2.1 shows the relationship of the energy bands or TiO_2 , ATiO_3 ($A = \text{Ba}, \text{Sr}$), and the highly active $\text{Sr}_2\text{M}_2\text{O}_7$ ($M = \text{Nb}, \text{Ta}$) materials to the electrochemical potentials of the photochemical reactions discussed in this document: water photolysis, silver reduction, and lead oxidation from aqueous solution. The Fermi level (E_f) for TiO_2 was chosen to reflect that these oxides are most likely to be n-type. This drawing shows that all of the reactions should be possible for the materials used.

Band bending at the surface of the semiconductor is also important because it determines which charge carrier is most likely to react at the surface. Figure 2.2 is a schematic drawing of shows the relationship of the energy bands for both an n-type (a) and p-type (b) semiconductor (band gap = 3 eV). Both of the schematic drawings in Figure 2.2 show the relationship of these

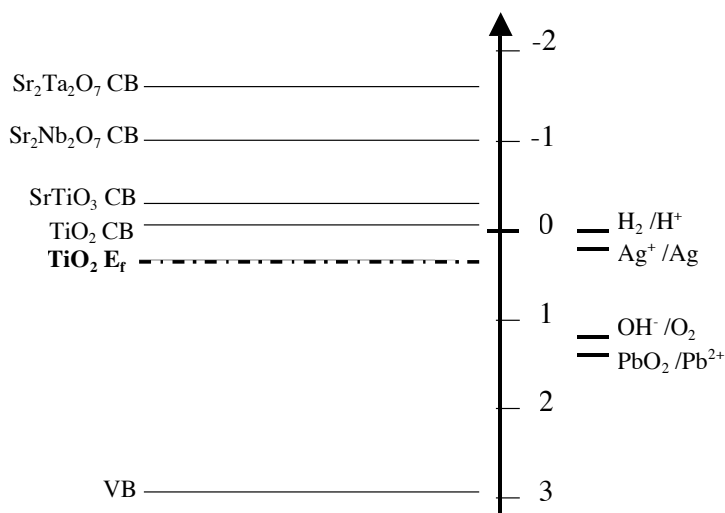


Figure 2.1: Schematic drawing of the flat band potentials of TiO_2 , SrTiO_3 (BaTiO_3), $\text{Sr}_2\text{Nb}_2\text{O}_7$, and $\text{Sr}_2\text{Ta}_2\text{O}_7$ in relation to the electrochemical potentials of the reactions presented in this document. The NHE scale is used (H_2/H^+ vs. NHE = 0 V).

bent bands with the H_2O redox couple. Electrons are the dominant charge carrier in an n-type semiconductor. In typical ambient conditions, the adsorption of electrophilic species on the surface traps excess electrons and creates a negative surface that causes the bands to bend upwards as shown in Figure 2.2a. This upward bending of the bands serves as a barrier for the removal of electrons to adsorbed species at the surface. Therefore, it is easier for new adsorbed species to remove a hole and be oxidized. In a p-type semiconductor (Figure 2.2b), the bands are bent downward because the adsorption of nucleophilic species traps excess holes creating a positive surface charge. Therefore, it is easy for a new adsorbed species at the surface to remove an electron and be reduced. Hence, reduction is more difficult on an n-type semiconductor while, oxidation is difficult on a p-type semiconductor and these are the rate-limiting photochemical reactions.

Figure 2.3 shows the energy bands for the special case of a polarized crystal [2]. The internal polarization (P_s) causes one end of the crystal to be positively charged and the opposite end to be negatively charged. The energy bands on the positively charged surface bend

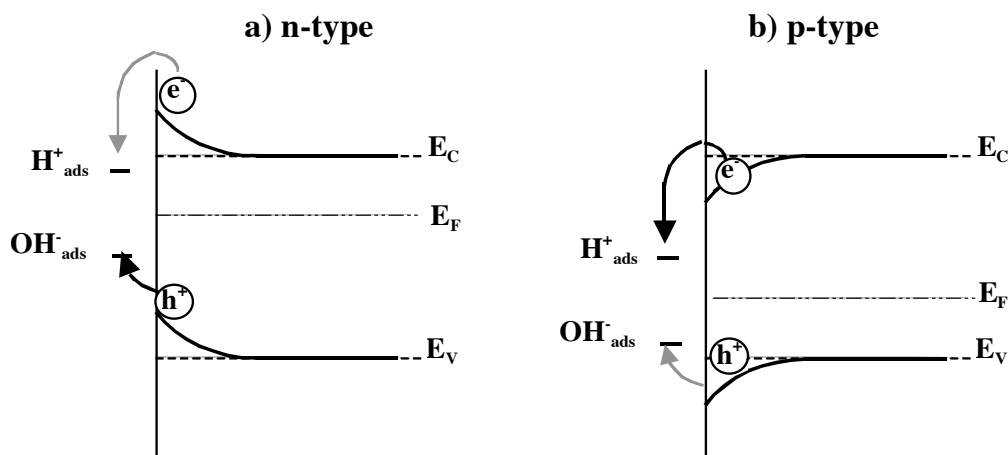


Figure 2.2: Schematic drawing of the effects of energy band bending in semiconductors. Note that the heavy arrows denote the “easy” reactions. (a) n-type. The upward band bending provides a barrier for an adsorbate to remove an electron but increases the ease of a hole being removed. (b) p-type. The bending of the bands downward allows for electrons, not holes, to be easily removed.

downward like the p-type semiconductor case because the dipolar field drives electrons to the surface where they are trapped and can react with adsorbates. Likewise, holes are trapped at the negatively charged end (bands are bent like n-type). Therefore, for this crystal, photochemical reduction of adsorbed species is more likely to happen on the positively charged surface while oxidation is more likely to occur on the negatively charged end. The schematic pictures in Figures 2.1 – 2.3 all assume an isotropic electronic structure. In fact, the energy levels of the electrons and holes vary with the wave vector of the charge carrier. In other words, electrons traveling in different directions can have different energies. As we shall see later, this anisotropy may explain the anisotropy of the reactivity.

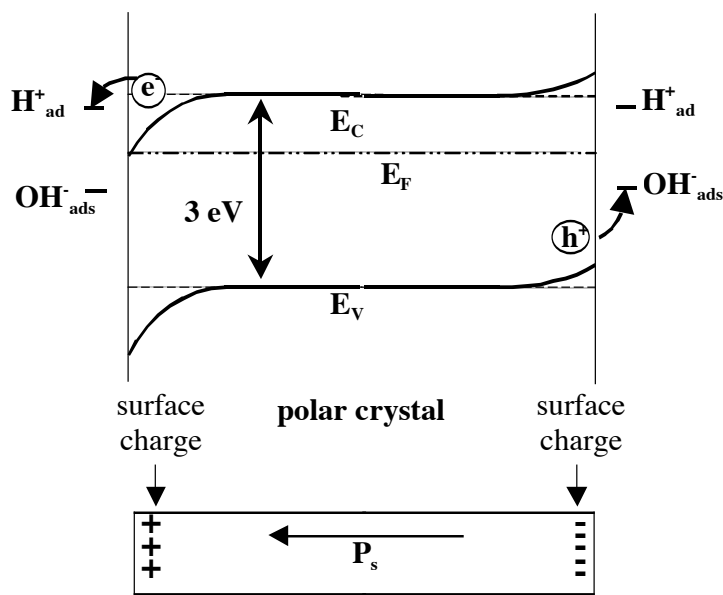


Figure 2.3: Energy band diagram for an illuminated polar crystal [2]. The positively charged surface behaves like a p-type semiconductor and photochemical reduction is easy on this surface. The negatively charged surface behaves like an n-type semiconductor and photochemical oxidation is easy on this surface.

2.4 Water Photolysis

In the water photolysis reaction, aqueous H^+ is reduced by photogenerated electrons to form H_2 and aqueous OH^- is oxidized by photogenerated holes to form O_2 and H_2O . Note that this simple description does not consider the various intermediates that are assumed to be short-

lived. Titania, TiO_2 , was the first oxide material used as a catalyst for water photolysis. The experiments by Fujishima and Honda [8] in the early seventies used n-type TiO_2 as the photoanode in a photoelectrochemical cell with Pt as the photocathode. Fujishima and Honda showed that water photolysis could take place with only UV light as the energy input – no external bias was applied. Unfortunately, this cell exhibits low efficiencies without an external bias. Also, the excitation of electrons through titania's bandgap ($E_g = 3.0 \text{ eV}$) is activated by light in the near UV range which is not abundant in the available solar spectrum.

TiO_2 is also the most researched particulate oxide for photolysis in colloidal suspensions. Generally, high surface area colloidal TiO_2 particles with Pt deposits are used. The Pt metal is thought to get the photogenerated electrons and, thereby, increase the amount of H_2 produced. These TiO_2/Pt particles in aqueous solutions also exhibit low efficiencies, on the order of $\sim 1\%$, under band gap radiation. Because of the close proximity of oxidation (TiO_2) and reduction (Pt) sites, there is a high incidence of charge carrier recombination and back reaction of intermediate products (for example, atomic H and hydroxyl radicals).

Recently, researchers have focused on developing catalysts with crystal structures that will internally separate oxidation and reduction sites. This research has primarily focused on oxides with tunnel [9,10] or layered [11-13] structures. These compounds have exhibited relatively high efficiencies for water splitting. The water photolysis efficiency of 23% for $\text{Sr}_2\text{Nb}_2\text{O}_7$ is the highest reported [14-16]. Interestingly, the majority of the compounds are also polar and/or related to the perovskite structure.

To determine if the polarity of these materials or their surface structures are important, the reactivities of the highly active materials BaTi_4O_9 and $\text{Sr}_2\text{M}_2\text{O}_7$ ($\text{M} = \text{Nb}, \text{Ta}$) were tested. BaTi_4O_9 has a pentagonal prism tunnel [17] and $\text{Sr}_2\text{Ta}_2\text{O}_7$ [18] and $\text{Sr}_2\text{Nb}_2\text{O}_7$ [19] have layered

perovskite structures. All of these structures are made up of either edge or corner sharing MO_6 octahedra and distortions of these octahedra in BaTi_4O_9 and $\text{Sr}_2\text{Nb}_2\text{O}_7$ cause the formation of dipolar fields within these crystals. The results from experiments conducted on BaTi_4O_9 and $\text{Sr}_2\text{M}_2\text{O}_7$ ($\text{M} = \text{Nb}, \text{Ta}$) are presented in Chapter 7, and their crystallography is described in Chapter 3.

2.5 Orientation Dependence of TiO_2

As stated in the previous section, TiO_2 is one of the most important and highly studied photocatalytic materials. Several studies have focused on determining the orientation dependence on the reactivity of the rutile phase of this material for photochemical reactions and these findings have partially motivated the experiments presented in this thesis. Rutile has a tetragonal crystal structure ($P4_2/mnm$ $a = 4.5937 \text{ \AA}$, $c = 2.9581 \text{ \AA}$, $E_g = 3.0 \text{ eV}$) and is made up of edge and corner-sharing TiO_6 octahedra. Based on surface energy considerations, the $\{110\}$, $\{101\}$, $\{100\}$, and $\{114\}$ surfaces typically appear on the equilibrium crystal shape and are the orientations that have been considered in most studies. The results on the orientation dependence of TiO_2 are presented here as a reference to the results to be discussed in the following chapters.

Some of the first comparisons of the reactivity of different orientations of rutile were done on homoepitaxial and heteroepitaxial (on alumina) thin films [20]. It was shown that the (001), (101), and (111) films, regardless of substrate, are more active for the photochemical silver reduction than (110) and (100) films. This trend was consistent even over various experimental conditions of film thickness, light intensity, and wavelength. Some of the surface and charge transport properties of rutile that may contribute to the anisotropy in the photochemical reactivity of these films were considered. All of the properties discussed pointed to the (001) surface

having a greater reactivity than the (100) surface. The (001) films had both a higher surface area and a higher Ti site density than the (100) films. Also, (001) has a higher surface energy and tends to break up into {101} and {114} facets. The {114} has a higher number of 4-coordinated Ti that has been shown to be a preferred site for reactions with organics, the dissociation of H₂O, and the adsorption of H₂ and CO. The high dielectric constant of rutile along [001] implies that the Debye length, the characteristic distance describing the depth of the space charge region adjacent to a surface, is longer for the (001) surface than the (100) surface. Because the photogenerated charge carriers that are created in the space charge region are separated by the electric potential, the number of recombination events will be lower for the (001) surface. Finally, charge carrier mobility and ion diffusivity is higher along [001] than [100], most likely because of the channels present in the crystal structure parallel to [001]. It was concluded that the efficiency of photogenerated charge carrier utilization was a more important factor for the anisotropic reactivity than the efficiency of photogenerated charge carrier generation.

In the same study as above, the activity of both as-polished and annealed rutile substrates for the photochemical reduction of silver was studied. For all substrates studied, there was no selective reactivity based on orientation. There was, however, selective reactivity along surface defects, such as scratches. Also, overall, the annealed substrates had lower reactivity than the as-polished substrates, presumably from a lower amount of surface defects and an increase in impurities at the surface caused by the heat treatment.

The above study motivated experiments to examine the reactivity of randomly oriented surfaces in a rutile ceramic compact [21]. This experiment was the basis of the polycrystal experiments described in the next chapter and was carried out in a similar manner. Briefly, a polycrystalline ceramic pellet was polished flat and annealed. The relative reactivity for many

grains for the photochemical reduction of silver was determined as was each grain's orientation and the orientations of any bounding facets. The activity-orientation relationship for rutile was obtained by combining the all the data. The observed stable orientations at the temperatures studied were $\{100\}$, $\{001\}$, $\{110\}$, $\{101\}$, and $\{112\}$. It was found that the presence of $\{101\}$ and/or the intersections between $\{101\}$ facets and neighboring facets were important for high photochemical reactivity. It was proposed that the longer distance between neighboring titanium atoms might be lead to a more efficient use of these sites and the high photochemical reactivity of the $\{101\}$ surface. Interestingly, the surface of the highly active $\{001\}$ film in the previous study [21] was exclusively bounded by $\{101\}$ facets.

Finally, two studies of the reactivity of small crystals for photochemical reduction and oxidation reactions were carried out. The first was an AFM study examining the formation of silver particles on small rutile particles during the photochemical reduction of silver [22]. Although the objective of this work was not to determine any reactivity-orientation relationships, it was observed that silver was deposited mostly on defects on the $\{110\}$ surfaces. In a separate study, faceted particles having $\{110\}$ and $\{101\}$ surfaces were examined [23]. The goal of this work was to determine the relative activities for the photochemical reduction of Pt and the oxidation of lead. They observed that the $\{110\}$ surface was preferred for Pt reduction and the $\{101\}$ surface was best for lead oxidation. Obviously these results contradict the bulk reactivity found with the thin films and ceramics. The authors explained this difference in reactivity as a result of the synergy between the energy levels and band bending of the adjacent crystal faces.

To make a comparison between the thin film, polycrystal, and particle experiments is difficult. The samples from different laboratories were created and treated under different conditions with varying impurity and defect concentrations. It is also difficult to find appropriate

surfaces to compare. None of the crystallites in the polycrystal experiment had a surface that was bounded by both $\{110\}$ and $\{101\}$ facets. The surface of the heteroepitaxial (100) film was bounded by $\{100\}$, $\{110\}$, and $\{101\}$ facets but the facets were much finer than the facets on the particles (~ 1 nm vs. ~ 750 nm) and it is probably not possible to make a meaningful comparison. The difference in reactivity observed may also be caused by specific conditions of the photochemical experiments such as deaerated (particles) vs. aerated (others) metal salt solutions or lamp output.

2.6 References

- (1) R.W. Whatmore, *Electronic Materials: from silicon to organics*; L.S. Miller and J.B. Mullin, Eds.; Plenum Press: New York, New York, 1991, p. 283.
- (2) M.E. Lines and A.M. Glass, *Principles and Applications of Ferroelectrics and Related Materials*; Oxford University Press, Oxford, England, 1977, p. 124.
- (3) H. Van Damme and W.K. Hall, *J. Catalysis*, **69** (1981) 371.
- (4) P.W. Tasker, *J.Phys. C: Solid State Phys.*, **12** (1979) 4977.
- (5) A. Wander, F. Schedin, P. Steadman, A. Norris, R. McGrath, T.S. Turner, G. Thornton, and N.M. Harrison, *Phys. Rev. Letters*, **86**[17] (2001) 3811.
- (6) A.N. Mariano and R.E. Hanneman, *J. Appl. Phys.*, **34** (1965) 384.
- (7) G. Heiland and P. Kunstmann, *Surface Science*, **13** (1969) 72.
- (8) A. Fujishima and K. Honda, *Nature*, **238** (1972) 37.
- (9) Y. Inoue, T. Kubokawa, and K. Sato, *J. Phys. Chem.*, **95** (1991) 4063.
- (10) Y. Yamashita, K. Yoshida, M. Kakihana, S. Uchida, and T. Sato, *Chem. Mater.*, **11** (1999) 61.

- (11) R. Abe, K. Shinohara, A. Tanaka, M. Hara, J.N. Kondo, and K. Domen, *Chem. Mater.*, **9** (1997) 2184.
- (12) S. Ikeda, M. Hara, A. Tanaka, J.N. Kondo, K. Domen, H. Takahashi, T. Okubo, and M. Kakihana, *Chem. Mater.*, **10** (1998) 72.
- (13) M. Machida, J. Yabunaka, and T. Kijima, *Chem. Mater.*, **12** (2000) 812.
- (14) H.G. Kim, D.W. Hwang, J. Kim, Y.G. Kim, and L.S. Lee, *Chem. Comm.*, (1999) 1072.
- (15) D.W. Hwang, H.G. Kim, J. Kim, K.Y. Cha, Y.G. Kim, and J.S. Lee, *J. Catalysis*, **193** (2000) 40.
- (16) A. Kudo, H. Kato, and S. Nakagawa, *J. Phys. Chem. B*, **104** (2000) 571.
- (17) E. Tillmanns and W.H. Baur, *Acta Crystallogr.*, **B26** (1970) 1645.
- (18) N. Ishizawa, F. Murumo, T. Kawamura, and M. Kimura, *Acta Crystallogr.*, **B32** (1976) 2464
- (19) N. Ishizawa, F. Murumo, T. Kawamura, and M. Kimura, *Acta Crystallogr.*, **B31** (1975) 1912.
- (20) P.A. Morris-Hotsenpiller, J.D. Bolt, W.E. Farneth, J.B. Lowekamp, and G.S. Rohrer, *J. Phys. Chem. B*, **102** (1998) 7323.
- (21) J.B. Lowekamp, G.S. Rohrer, P.A. Morris-Hotsenpiller, J.D. Bolt, and W.E. Farneth, *J. Phys. Chem. B*, **102** (1998) 3216.
- (22) W.E. Farneth, R.S. McLean, J.D. Bolt, E. Dokou, and M.A. Barteau, *Langmuir*, **15** (1999) 8569.
- (23) T. Ohno, K. Sarukawa, and M. Matsumura, *New J. Chem.*, **26** (2002) 37.

3 Crystallography

3.1 Introduction

The purpose of this chapter is to describe the crystal structures of the materials studied during this research. Important features of these structures will be described. Also, the similarities between the structures will be highlighted.

3.2 SrTiO₃ – Cubic Perovskite

Strontium titanate, SrTiO₃, was chosen to study the effect of polar terminations on photochemical activity. SrTiO₃ has a cubic perovskite structure ($a = 3.905 \text{ \AA}$, $E_g = 3.2 \text{ eV}$) as shown in Figure 3.1. This material was chosen because of the similarity of its structure to BaTiO₃ and similar Ti coordination to rutile. The $\{100\}$ surface of SrTiO₃ is nonpolar with either a TiO₂ or SrO termination and a projection of this surface is illustrated in Figure 3.2. This representation shows the TiO₂ plane above the SrO plane. The TiO₂ and SrO layers are separated

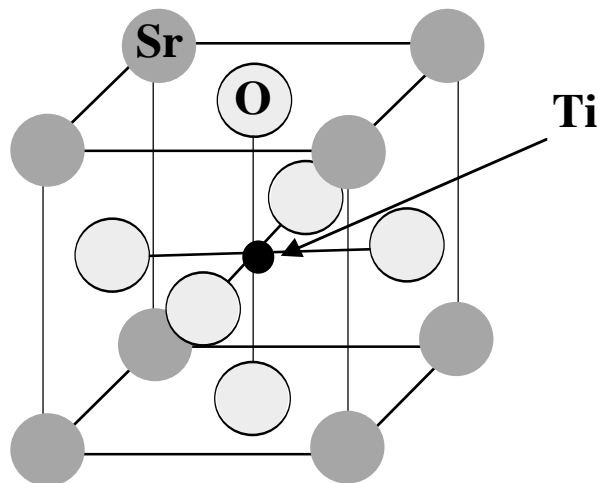


Figure 3.1: Cubic perovskite crystal structure of SrTiO₃.

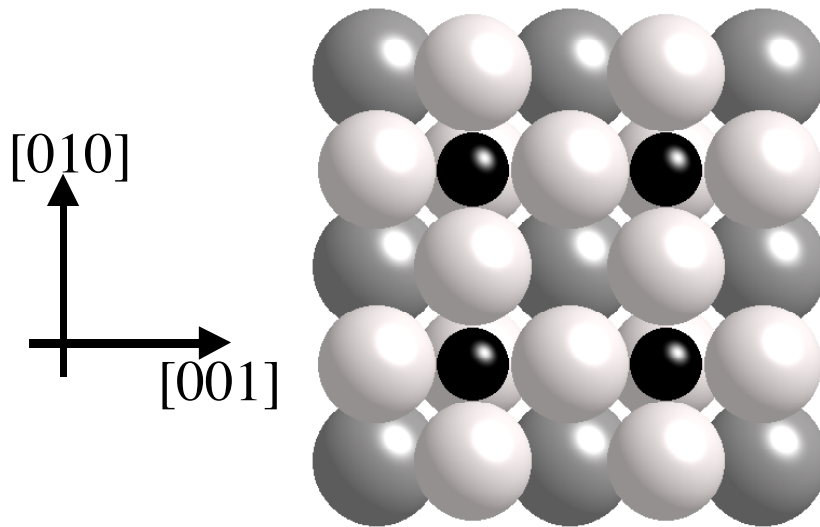


Figure 3.2: Projection of the $\text{SrTiO}_3(100)$ surface. The TiO_2 plane is above the SrO plane.

by $\frac{1}{2}d_{100} = \frac{1}{2}a = 1.95 \text{ \AA}$. The Ti in the TiO_2 terminated (100) surface has a 5-fold coordination with oxygen and is the SrTiO_3 surface most similar to the $\{110\}$ and $\{011\}$ rutile surfaces pictured in Figure 3.3. All of the Ti on the $\{011\}$ surface are 5-fold coordinated while only half of the Ti on the $\{110\}$ surface are 5-fold coordinated. The other half of the rutile $\{110\}$ Ti are 6-fold coordinated because of the rows of bridging oxygen.

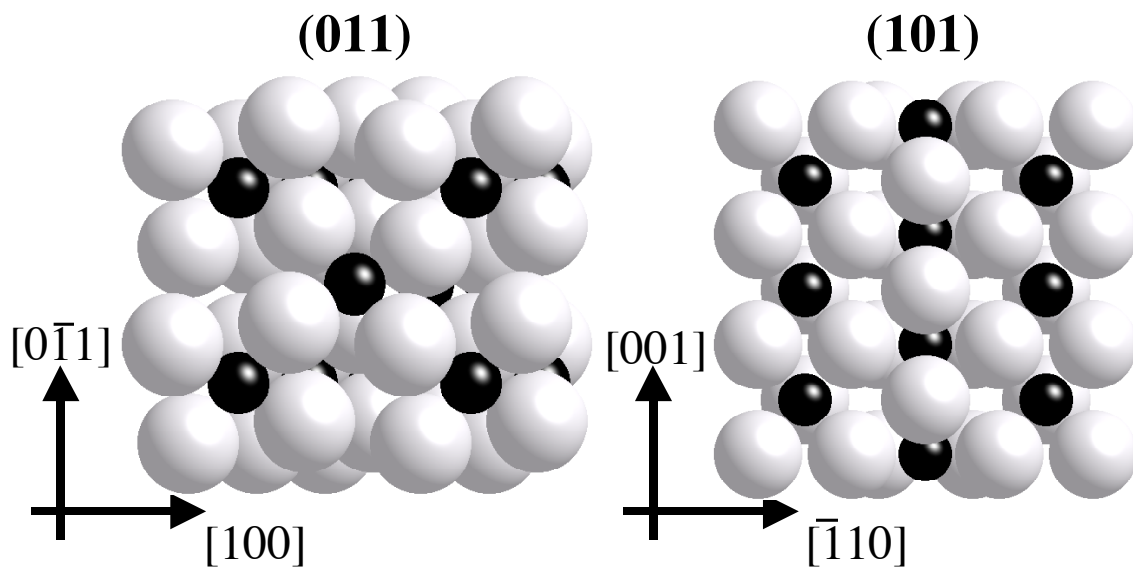


Figure 3.3: Projections of the rutile $\text{TiO}_2(011)$ and (110) surfaces.

Both of the $\{110\}$ and $\{111\}$ SrTiO_3 terminations are polar. The unreconstructed $\{110\}$ surface, shown in Figure 3.4, can have either a SrTiO^{4+} termination or an O_2^{4-} termination. As it is drawn in Figure 3.4, the SrTiO^{4+} plane is above the O_2^{4-} plane. The spacing between layers is $\frac{1}{2}d_{110} = \sqrt{2}a/4 = 1.38 \text{ \AA}$. The Ti atoms on the SrTiO^{4+} surface have four bonds with oxygen. The unreconstructed, polar $\{111\}$ surface (Figure 3.5) can have either a Ti^{4+} termination (three bonds each with oxygen) or a SrO_3^{4-} termination. The schematic in Figure 3.5 shows a projection of the $\{111\}$ surface with the Ti^{4+} above the SrO_3^{4-} plane. The spacing between the different layers is $\frac{1}{2}d_{111} = \sqrt{3}a/6 = 1.12 \text{ \AA}$.

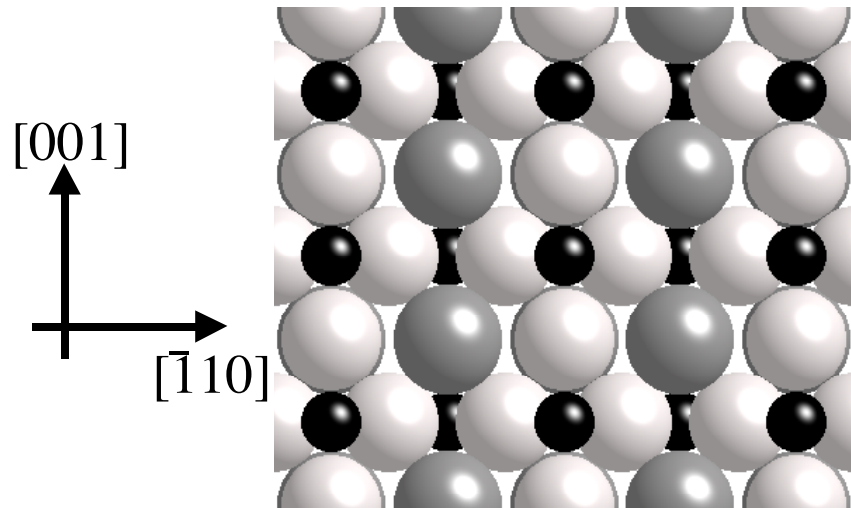


Figure 3.4: Projection of the SrTiO_3 (110) surface. The SrTiO^{4+} plane is above the O_2^{4-} plane.

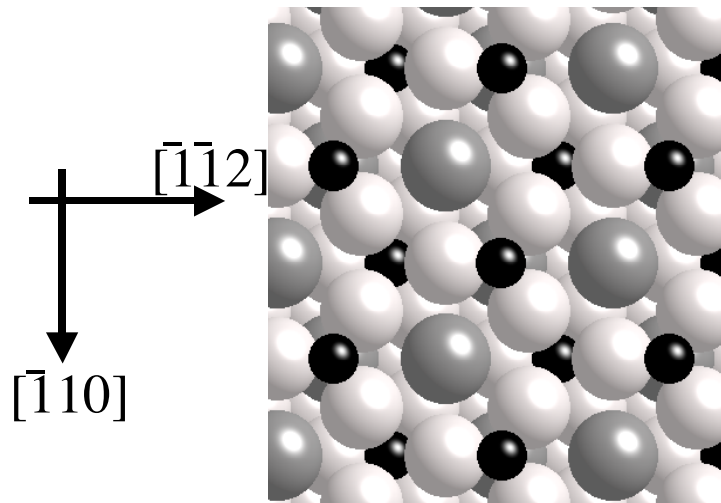


Figure 3.5: Projection of the SrTiO_3 (111) surface. The Ti^{4+} plane is above the SrO_3^{4-} plane.

1.3 BaTiO₃ – Tetragonal Perovskite

In this study, barium titanate, BaTiO₃, is used to examine the effects of spontaneous polarization on photochemical activity. BaTiO₃ undergoes a paraelectric-to-ferroelectric phase transition when cooled below $T_c = 120\text{ }^\circ\text{C}$ ($P_s = 26\text{ }\mu\text{C}/\text{cm}^2$ at $23\text{ }^\circ\text{C}$). Figure 3.6 depicts the crystal structure of the room temperature phase ($a = 3.98\text{ }\text{\AA}$, $c = 4.03\text{ }\text{\AA}$), which is a slight, tetragonal distortion of the higher temperature cubic perovskite phase. When looking at a cube face of a BaTiO₃ crystal, the new unique [001] axis is taken to point in the positive direction of the dipole in each domain and can point in the $\pm x$, y , or z directions. We refer to those domains where the polarization vector is in the $+z$ direction as being “up” domains, those domains where the polarization vector is in the $-z$ direction as “down” domains, and those domains where the polarization vector lies in the surface plane ($\pm y$ or $\pm x$) as lateral domains. The three types of domains can be differentiated by an acid etch; the up domains etch the fastest, the down the slowest, and the lateral domains etch at an intermediate rate [1].

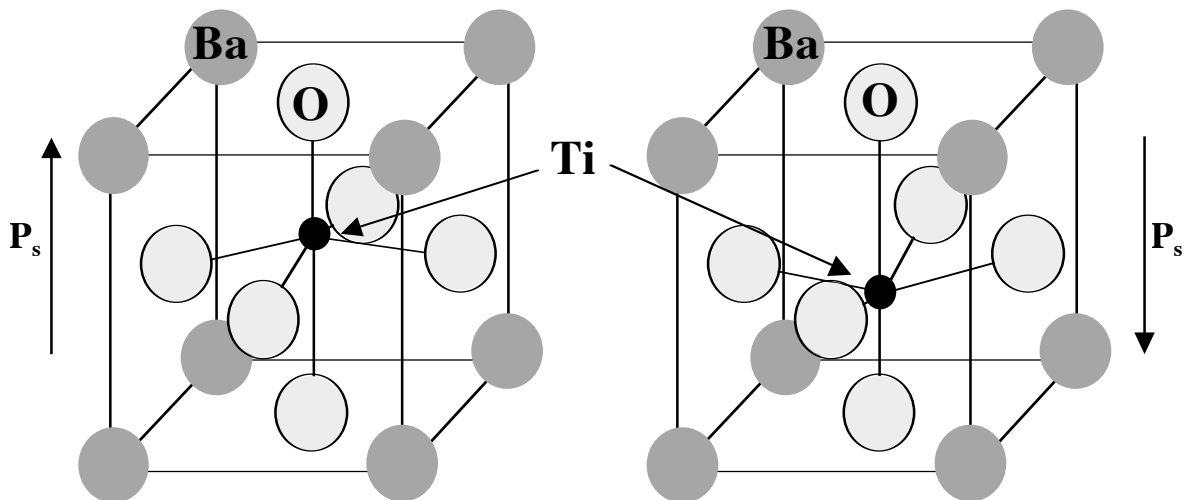


Figure 3.6: Ferroelectric perovskite phase of BaTiO₃ showing how the distortion of the Ti-O octahedra causes the tetragonal distortion of the unit cell and the occurrence of a spontaneous polarization in the direction of the Ti displacement.

Macroscopic bodies of BaTiO₃ are typically made up of many polarized domains and there are two types of boundaries that can separate the domains. The 90° boundaries (the name specifying the angle between the polarization vectors in adjacent domains) lie on {110} habit planes and, therefore, appear as straight lines on the BaTiO₃ {100} surface. There are also 180° boundaries that are not confined to a single habit plane and intersect the {001} surface along curved lines [1]. Figure 3.7 is a schematic drawing of a BaTiO₃ domain structure as well as the polarization vectors of each domain. The results of experiments on BaTiO₃ are presented in Chapter 5.

BaTiO₃ shows interesting ferroelectric and dielectric properties based on particle or grain size, most of which can be attributed to minimizing the stress or depolarization energy. For example, the dielectric constant decreases with grain size in BaTiO₃ ceramics most likely because of the increased volume of domain walls. Also, it has been observed that the width of 90° domain walls decreases with decreasing grains size in order to relieve the higher stress associated with the tetragonal phase. The depolarization effect has been attributed to causing

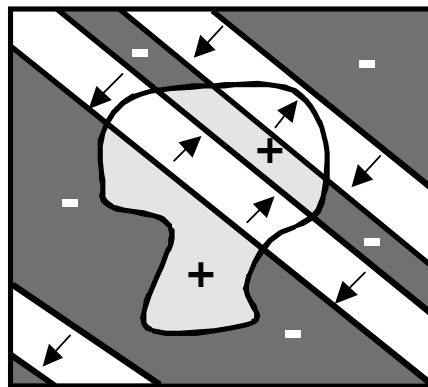


Figure 3.7: Schematic drawing of a typical BaTiO₃ domain structure. Domains with up polarization vectors (+) are shaded light gray, domains with down polarization vectors (-) are shaded dark gray, and domains with in-plane polarization vectors (arrows) have no shading. Notice that straight lines indicate 90° domain boundaries and curved lines indicate 180° domain boundaries.

the decrease in Curie temperature, or a stabilization of the cubic phase, with decreasing particle size [2]. In fact, it has been observed that there is a critical particle size below which the cubic phase is stable at room temperature. This observed critical size varies between approximately 14 nm and 150 nm and is dependent on preparation method (defect and space charge state) [2-4].

1.4 $\text{Sr}_2\text{Ta}_2\text{O}_7$ and $\text{Sr}_2\text{Nb}_2\text{O}_7$ – (110) Layered Perovskite Structure

$\text{Sr}_2\text{Ta}_2\text{O}_7$ (Cmcm: $a = 3.937 \text{ \AA}$, $b = 27.198 \text{ \AA}$, $c = 5.692 \text{ \AA}$; $E_g = 4.8 \text{ eV}$) [5] and $\text{Sr}_2\text{Nb}_2\text{O}_7$ (Cmc2₁: $a = 3.933 \text{ \AA}$, $b = 26.726 \text{ \AA}$, $c = 5.683 \text{ \AA}$; $P_s = 9 \text{ \mu C/cm}^2$, $E_g = 4 \text{ eV}$) [6] have high photolysis efficiencies and anisotropic crystal structures. They both have layered perovskite structures made up of corner sharing MO_6 octahedra, arranged in (110) perovskite-type slabs parallel to (010), that are separated by Sr_2O layers (Figure 3.8). Like {110} perovskite, the {010} $\text{Sr}_2\text{M}_2\text{O}_7$ planes should be polar and have two different chemical terminations. The $\text{Sr}_2\text{M}_2\text{O}_7$ orientations near the {710} and {015} planes have a similar structure to the nonpolar {100} perovskite planes. Since these $\text{Sr}_2\text{M}_2\text{O}_7$ structures have a strong similarity to the structure of SrTiO_3 , we might expect them to have similar trends in reactivity.

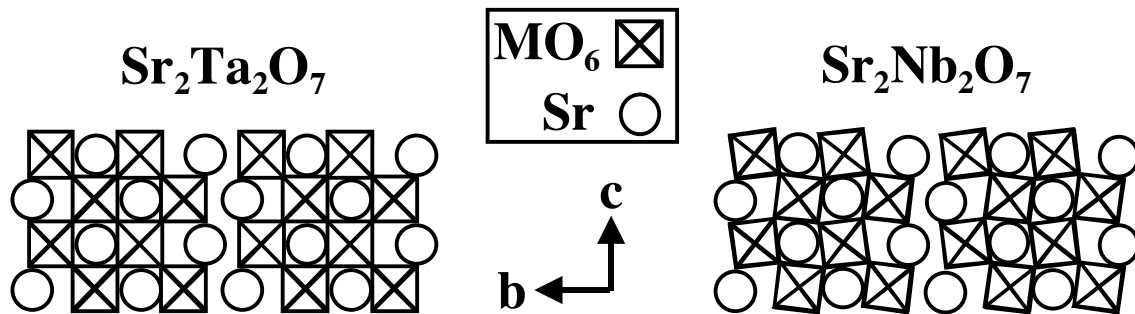


Figure 3.8: Schematic drawing of the layered perovskite structures of $\text{Sr}_2\text{Ta}_2\text{O}_7$ (Cmcm) and $\text{Sr}_2\text{Nb}_2\text{O}_7$ (Cmc2₁) parallel to [100].

As Fig. 3.8 shows, the main difference between these materials is the distortion of the NbO_6 octahedra in $\text{Sr}_2\text{Nb}_2\text{O}_7$ which makes it ferroelectric ($P_s \parallel c$ -axis). If the presence of dipolar fields is an important materials property for the photochemical reactivity of $\text{Sr}_2\text{Nb}_2\text{O}_7$, then we

would expect that it might have an anisotropic reactivity that depends on the inclination of the polar axis with the surface. The reactivities of these materials are discussed in Chapter 7.

1.5 BaTi₄O₉ – Pentagonal Prism Tunnel Structure

BaTi₄O₉ has a pentagonal prism tunnel structure (Pmmn, $a = 14.53 \text{ \AA}$, $b = 3.79 \text{ \AA}$, $c = 6.29 \text{ \AA}$) [7] and is another photolysis catalyst whose structure has been hypothesized to be responsible for its reactivity. A schematic of its structure is illustrated in Figure 3.9. This structure is composed of distorted edge and corner sharing TiO₆ octahedra arranged to form tunnels oriented along the [010] axis of the crystal. The Ba atoms have positions within these tunnel openings. The distortion of the octahedra create a dipole field that is directed towards the center of the tunnels (towards the Ba atom) [8]. However, this is a microscopic dipole and is not expected to have the same effect as the long range dipoles caused by polar surfaces or ferroelectric domains. Crystals exposing (010) planes reveal the maximum number of tunnel openings while those crystals with orientations along the line connecting (100) and (001) are parallel to the tunnel direction. We would therefore expect that there would be an anisotropy in the reactivity depending on the inclination of the tunnels with the surface. The reactivity of BaTi₄O₉ is also discussed in Chapter 7.

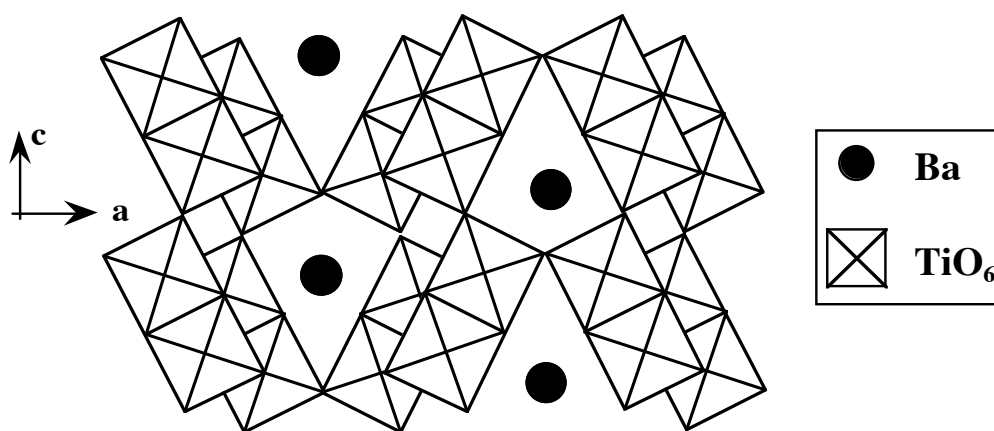


Figure 3.9: Schematic drawing of the pentagonal prism tunnel structure (Pmmn) parallel to [010]. The black circles represent Ba atoms that are surrounded by TiO₆ octahedra.

1.6 References

- (1) Y.H. Hu, H.M. Chan, Z.X. Wen, and M.P. Harmer, *J. Am. Ceram. Soc.*, **69** (1986) 594.
- (2) M.E. Lines and A.M. Glass, *Principles and Applications of Ferroelectrics and Related Materials*; Oxford University Press, Oxford, England, 1977.
- (3) J.F. Scott, *Aust. J. Phys.*, **52** (1999) 903.
- (4) E.K. Akdogan and A. Safari, *Jpn. J. Appl. Phys. Part 1*, **41**[11B] (2001) 7170.
- (5) N. Ishizawa, F. Murumo, T. Kawamura, and M. Kimura, *Acta Crystallogr.*, **B32** (1976) 2464.
- (6) N. Ishizawa, F. Murumo, T. Kawamura, and M. Kimura, *Acta Crystallogr.*, **B31** (1975) 1912.
- (7) E. Tillmanns and W.H. Baur, *Acta Crystallogr.*, **B26** (1970) 1645.
- (8) D.H. Templeton and C.H. Dauben, *J. Chem. Phys.*, **32**[5] (1960) 1515.

4 Experimental Approach

4.1 Introduction

The experimental approach is based on the use of photochemical "probe" reactions that leave insoluble products on the surface at the sites of oxidation and reduction on oxide surfaces. The reaction sites are determined by examining the surfaces before and after the probe photochemical reaction with atomic force microscopy (AFM). Ceramic polycrystals were used to examine the activity over the entire range of crystallographic orientations to determine if these reactions exhibit any crystallographic anisotropy, while single crystals were used to examine the activity of specific orientations. Particulate materials were used to see if the bulk reactivity applies to micron-sized particles. This method was recently used to study the anisotropy of the photochemical reduction of silver for rutile surfaces [1] and showed that {101} was the most active orientation for this reaction.

4.2 Sample Preparation

4.2.1 Polycrystalline ceramics

The compounds that were not commercially available (BaTi_4O_9 and $\text{Sr}_2\text{M}_2\text{O}_7$) were obtained by reacting the available powders in stoichiometric ratios in air for the times and temperatures listed in Table 4.1. Powder X-ray diffraction was used to confirm the phase purity of these powders. Ceramics were then produced in the following way. The powders were uniaxially compacted under 150 MPa to form disk-shaped pellets with a thickness of 3 to 12 mm and an approximate diameter of 25 mm (BaTiO_3) or 11 mm (all others). The pellets were then

placed in an alumina crucible with an excess of the parent powder to ensure that the pellet did not contact the crucible. The samples were then heated (all ramp rates were between 2 and 10 °C / min) in air to burn off any residual organics, sinter, and grow the grains. The particular temperatures and times for these steps are listed for each material in Table 4.1.

The sintered samples were then lapped flat using a 9 μm Al_2O_3 or 3 μm Al_2O_3 (Buehler) aqueous solution and polished with a basic 0.02 μm colloidal silica solution (Buehler). Polished samples were annealed in air to remove polishing damage, facet the surface, and thermally etch the grain boundaries. The times and temperatures for this annealing step are also included in Table 4.1 along with the average grain size for the ceramics with equiaxed grains.

Table 4.1: Preparation information for the polycrystalline ceramics.

	BaTiO₃	SrTiO₃	BaTi₄O₉	Sr₂Nb₂O₇	Sr₂Ta₂O₇
Powder source	AA*, 99.7%	AA*, 99.5%	BaCO ₃ : AA*, 99.95% TiO ₂ : from TiCl ₄	SrCO ₃ : AA*, 99% Nb ₂ O ₅ : AA*, 99.5%	SrCO ₃ : AA*, 99% Ta ₂ O ₅ : Cerac, 99.5%
Reaction step	—	—	1250°C 20 hr	1400°C 100 hr	1400°C 100 hr
Burn-off	900°C 12 hr	900°C 12 hr	875°C 6 hr	800°C 12 hr	800°C 12 hr
Sintering	1230°C 10 hr	1360°C 12 hr	1150°C 6 hr	1200°C 10 hr	1200°C 10 hr
Grain growth	1360°C 3 hr	1470°C 3 hr	1330°C 53 hr	1500°C 10 hr	1600°C 48 hr
Final anneal	1200°C 6 hr	1200°C 6 hr	900°C 6 hr	1200°C 6 hr	1200°C 10 hr
Grain size	40 μm	25 μm	20 μm	—	—

* AA = Alfa Aesar

1.1.2 Single Crystals

Mechano-chemically polished (100), (110) and (111)-oriented SrTiO₃ single crystals were obtained from Crystal GmbH (Berlin). The as-received crystals were annealed at 1200 °C in air for 6 h. Single domain, (100)-oriented BaTiO₃ single crystals were obtained from MTI

Corporation. The as-received crystals were heated to 150 °C, and then cooled to form a domain structure.

1.1.3 Faceted single crystals

Small, faceted crystals were produced using a molten salt flux method. Equal weights of commercially available powders or powders prepared as described in Section 4.2.1 and KCl (Fisher Scientific) were combined by wet grinding in ethanol for several minutes. The slurry was then transferred to a Pyrex beaker and was mixed by magnetic stirring for 2 h. Following mixing, the excess ethanol was decanted with a pipet and the powders were dried in air at 70 °C. The dried powder was transferred to an Al₂O₃ crucible and reacted according to the programs listed in Table 4.2. The KCl was removed by filtering with boiling deionized water and the remaining product was dried in air at 70 °C.

Table 4.2: Preparation information for the faceted single crystals.

	Powder source	Heating rate	Reaction step	Cooling rate
BaTiO₃	Alfa Aesar, 99.7%	5 °C/min	1100°C 6 hr	3 °C/min
SrTiO₃-1	Alfa Aesar, 99.5%	5 °C/min	1200°C 10 hr	3 °C/min
SrTiO₃-2	Cerac, 99%	5 °C/min	1200°C 10 hr	3 °C/min
Sr₂Nb₂O₇**	SrCO ₃ :AA*, 99% Nb ₂ O ₅ : AA*, 99.5%	5 °C/min	1100°C 6 hr	3 °C/min
Sr₂Ta₂O₇**	SrCO ₃ :AA*, 99% Ta ₂ O ₅ : Cerac, 99.5%	5 °C/min	1100°C 6 hr	5 °C/min

* AA = Alfa Aesar

** = Followed method in Reference [2] with wt. KCl : wt. (2SrCO₃ + M₂O₅) = 2 : 1.

1.3 Probe reactions

1.3.1 Photochemically Stimulated Inorganic Redox Reactions

The experiment described here relies on two established photochemical reactions: the reduction of Ag^+ by photogenerated electrons [3,4] and the oxidation of Pb^{2+} by photogenerated holes [5,6], as described by the reactions below:



Since both reactions leave an insoluble product on the surface (Ag and PbO_2 , respectively), microscopic analysis can be used to correlate the formation of each phase with the surface structure of the sample.

The photochemical reaction experiments are setup in the following way. A viton O-ring, 1.7 mm thick, was placed on the sample surface and the interior volume was filled with a solution containing a dissolved metal salt (0.115 M aqueous AgNO_3 (Fisher Scientific) or 0.0115 M aqueous $\text{Pb}(\text{C}_2\text{H}_3\text{O}_2)_2$ (Fisher Scientific)). A 0.2 mm thick quartz cover slip was then placed on top of the O-ring and held in place by the surface tension of the solution. The sample was illuminated using a variable power Hg lamp. The exposure times and lamp power for the silver reduction and the lead oxidation experiments are listed in Table 4.3. After exposure, the sample was rinsed with deionized H_2O , dried with forced air, and then imaged using atomic force microscopy (AFM). In control experiments conducted with light made up of energies less than the sample's band gap, no photochemical reactions were observed.

Experiments were carried out on the particulate materials by dusting carbon tape that was mounted on an SEM stub with the powder, removing the excess powder with forced air, and then carrying out the experiment as described above. Scanning electron microscopy was used to

analyze the surfaces of the particles. The times and lamp power for the particle experiments are in parenthesis in Table 4.3.

Throughout this thesis, it is assumed that the location of the reaction product marks the site of the reaction two other scenarios can also be suggested. The first is that the particles form homogeneously and then bind to certain sites on the surface. The second is that reduced and oxidized products diffuse away from active sites and nucleate preferentially on certain features. The following control experiments using ferroelectric BaTiO₃ suggest that these alternative scenarios are not likely. When BaTiO₃ is exposed to the aqueous silver nitrate solution and light made up of energies less than its band gap no reaction occurred but when the samples were exposed to UV light and the solution, silver deposits form striped patterns on the surface that can be related to the ferroelectric domains. Because colloidal silver particles are known to have a surface charge, the striped patterns of silver may be a result of colloidal silver particles adsorbed on oppositely charged domains. To confirm that the silver deposits were formed by a reaction at the surface, and not created in solution and then deposited, two experiments with silver colloids were carried out.

The goal of the first experiment was to show that silver was not created in solution during the UV exposure. In this experiment, a glass slide was used in place of BaTiO₃ during the silver reduction reaction. That is, the silver nitrate solution was placed on top of the glass slide and exposed at 300 W for 10 s. A glass slide was used because previous experiments showed that no silver was deposited on the slide following the photochemical reaction. Therefore, if a colloid was formed in solution it would stay in the solution. Following the exposure, the irradiated solution was transferred from the glass slide to a BaTiO₃ polycrystal. The solution was allowed to stand for one minute then the sample was rinsed and dried. AFM images of the surface

showed no stripes of silver. This result implies that colloidal silver is not generated in solution and then deposited onto specific charged domains.

In the second experiment, a silver colloid was prepared using a chemical route based on Reference [2]. Briefly, a silver nitrate solution was prepared using 2-propanol as the solvent. Under stirring, base (NaOH in 2-propanol) is added to initiate colloid formation. After several minutes acid (HNO₃) and additional 2-propanol is added to stop the reaction. After several minutes of additional stirring, the silver colloid was transferred to the surface of a BaTiO₃ polycrystal and allowed to stand for five minutes. The sample was rinsed, dried, and imaged with AFM. Again, no striped patterns of silver were observed. Therefore, it can be concluded that the stripes of silver observed on the surface of BaTiO₃ polycrystals is the result of the photochemical reduction of silver on the surfaces of some domains and not because colloidal silver particles are attracted to oppositely charged domains.

Table 4.3: Exposure conditions for photochemically stimulated inorganic redox reactions.

	Ag⁺ reduction		Pb²⁺ oxidation	
	Time (sec)	Lamp power (W)	Time (sec)	Lamp power (W)
BaTiO₃	3 (10)	300	150 (210)	300
SrTiO₃	3 (10)	300	150 (210)	300
BaTi₄O₉	3	400	150	400
Sr₂Nb₂O₇	15* (75)	300* (400)	300 (300)	400
Sr₂Ta₂O₇	45 (75)	300 (400)	—	—

* Sr₂Nb₂O₇ was promoted with NiO for this experiment.

1.3.2 NiO Promotion

Before the photochemical reaction, some surfaces were promoted with NiO in the following way. A bare polycrystal as placed on a hotplate at approximately 150°C. A 0.05 M Ni(NO₃)₂ (aq) solution was sprayed on the surface until the coverage appeared macroscopically even. The sample was heated to 400 °C in air to calcine the solid residue. It was then pretreated

by reduction at 500°C for 1 h in flowing forming gas (10% H₂/ 90% N₂) and reoxidation at 200°C for 1 h in flowing O₂.

1.3.3 Photochemical Oxidation of Organics

The photochemical oxidation of stearic acid, CH₃(CH₂)₁₆COOH (chain length = 2.5 nm), has been used in the past to evaluate the activity of photocatalysts used for environmental clean-up [7,8]. Typically, a stearic acid film is deposited onto the sample surface and the degradation of the film can be followed using AFM. Unlike the inorganic reactions described in the previous section, stearic acid is decomposed to CO₂ and H₂O by photogenerated hydroxyl radical attack [8]. Therefore, the degradation of the film indicates the sites of hydroxyl radical attack rather than the sites at which photogenerated charge carriers reach the surface.

Stearic acid films were deposited by melting stearic acid over low heat in an evaporation dish in a fume hood. There was enough stearic acid in the dish to just cover the bottom and the heat was kept low enough that the stearic acid did not oxidize. Individually, BaTiO₃ single crystals were attached to a glass slide using double stick tape and suspended, face down over the fuming stearic acid. Finally, a paper cylinder was placed around the dish. This cylinder provided a smoother air flow and more uniform film. The crystals were exposed for 2.5 minutes.

1.4 Sample Characterization

1.4.1 Surface Characterization

Atomic Force Microscopy (AFM) (Park Scientific Instruments Cp or Thermomicroscopes M5) was used to examine the surface topography of the all the polycrystalline and bulk single crystal samples both before and after the probe reactions. In this way, reaction sites (Ag or PbO₂ deposits or missing stearic acid) could be directly correlated to preexisting surface features. Gold-coated, sharpened pyramidal Si₃N₄ probes (Thermomicroscopes ML06A-F) were used for

images obtained in contact mode on the Cp while uncoated probes were used on the M5. The force used depended on whether the sample had been reacted (low force) or unreacted (high force) and varied between 0.25 nN and 10 nN. Generally, contact mode was sufficient to image most surfaces even after the probe reactions were performed but, in cases when the probe moved the deposits, non-contact AFM (NC-AFM) was used. Conical Si probes (Thermomicroscopes UL20A-D) with resonant frequencies of about 90kHz (UL20A/B) or 360kHz (UL20C/D) were used for NC-AFM image. All topographs presented in this document are displayed in grayscale; light contrast indicates relatively high regions of the surface while dark contrast indicates relatively low areas of the surface.

It was necessary in some cases to measure step heights between adjacent terraces on single crystal surfaces. For these measurements, multiple line traces were made across the step in the fast scan direction. The traces with the best step profile were chosen and the step heights were measured by subtracting the mean vertical position of the pixels on the lower terrace from the mean vertical position of the pixels on the upper terrace. The standard deviation of such measurements is 0.2 Å.

Scanning electron microscopy (SEM, Phillips XL30FEG) was used to examine the surfaces of as-processed and as-reacted particles. Typical imaging conditions were: working distance = 10 mm, spot size = 3 or 4, and accelerating voltage = 5-10 kV.

1.4.2 Orientation Information

After the AFM imaging was completed, the crystallographic orientations of individual grains in the polycrystalline samples were determined from electron backscattered diffraction patterns (EBSP). The samples were imaged in a Phillips XL40FEG SEM. An EBSP was collected for each grain and the patterns were indexed using Orientation Imaging Microscopy

Software, version 2.6 (BaTiO₃, SrTiO₃) or OIM for Windows Software version 3 (BaTi₄O₉, Sr₂M₂O₇) (TexSEM Laboratories, Inc.). The software returns a set of Euler angles (ϕ_1, ϕ_2, ϕ_3) for each grain which are used to specify a relationship between the sample reference frame and the crystallographic axes. From these data, the components of the surface normals can be computed. However, when interpreting the results, it must be remembered that the polycrystalline samples were thermally etched and some orientations are not stable with respect to faceting. Therefore, the surface normals computed from the EBSPs do not necessarily correlate to the crystallographic planes that bounded the surface.

Laue backscattered X-ray diffraction patterns were obtained for the SrTiO₃ single crystals. These experimental patterns were compared to simulated patterns from the commercial software Desktop Microscopist (Virtual Labs, Inc.). These diffraction patterns were used to confirm the surface orientation of the crystals and to determine the in-plane orientations of surface features observed by AFM.

1.1.3 Chemical Analysis

Energy dispersive X-ray (EDX) spectroscopy (Oxford Isis) conducted in a scanning electron microscope (Phillips XL30FEG) was used to analyze the elemental composition of the deposits. It was confirmed that the deposits from the silver reduction reaction contained Ag and that deposits from the lead oxidation reaction contained Pb. Determining the phase of the deposits using X-ray diffraction (XRD) proved unsuccessful. Even though we recognize that the oxidation state and phase of the products are uncertain, we will refer to them as Ag and PbO₂. In fact, the Ag may be partially oxidized and the Pb might not be fully oxidized.

1.1.4 Ferroelectric Domain Etching

It is well known that ferroelectric domains in BaTiO₃ etch differently depending on their polarization [9]. Domains that have their polarization vector parallel to the surface normal, or the “up” domains, etch the fastest while domains with the opposite polarization, the “down” domains etch the slowest. Domains with intermediate polarizations have intermediate etch rates.

At the end of each experiment, BaTiO₃ single crystals were etched to determine the orientations of the polarization vectors in the different domains. The crystals were dipped into 20 mL 4M HCl + 3 drops 50% HF for 10 sec. Etching of BaTiO₃ polycrystals proved inconclusive because the facet structure was also sensitive to the acid etch.

1.5 References

- (1) J.B. Lowekamp, G.S. Rohrer, P.A. Morris Hotsenpiller, J.D. Bolt, and W.D. Farneth, *J. Phys. Chem. B* **102** (38), 7323 (1998).
- (2) Brahmarroutu, B.; Messing, G.L.; Trolier-McKinstry, S. *J. Am. Ceram. Soc.* **1999**, *82*, 1565.
- (3) Clark, W.C.; Vondjidis, A.G. *J. Catalysis* **1965**, *4*, 691.
- (4) Herrmann, J.-M.; Disdier, J.; Pichat, P. *J. Catalysis* **1988**, *113*, 72.
- (5) Tanaka, K.; Harada, K.; Murata, S. *Solar Energy* **1986**, *36*, 159.
- (6) Torres, J.; Cervera-March, S. *Chem. Eng. Sci.* **1992**, *47*, 3857.
- (7) Sawunyama, P.; Fujishima, A.; Hashimoto, K. *Langmuir* **1999**, *15*, 3551.
- (8) Sitkiewitz, S.; Heller, A. *New J. Chem.* **1996**, *20*, 233.
- (9) Hu, Y.H.; Chan, H.M.; Wen, Z.X.; Harmer, M.P. *J. Am. Ceram. Soc.* **1986**, *69*, 594.

5 The Effect of Ferroelectric Domains – Barium Titanate, BaTiO₃

5.1 Introduction

The purpose of this chapter is to report the results of experiments to determine the photochemical reactivity of BaTiO₃. These results illustrate that the oxidation and reduction halves of photochemical reactions occur on the surfaces of oppositely oriented ferroelectric domains. These results imply that the static electric fields in ferroelectric crystals can be used to separate photogenerated carriers by microscopic distances and that the electron and hole half reactions can occur on spatially distinct areas of the catalyst surface.

5.2 Polycrystal Results

The topographic AFM images in Figure 5.1 show the surfaces of two grains in a BaTiO₃ polycrystal before (a & c) and after (b & d) the photochemical silver reduction reaction [1]. Before the reaction, the contrast is dominated by the facets that form during the high temperature anneal. In Figure 5.1a, faint parallel lines of light and dark contrast can also be distinguished and are indicated by the arrows in the figure. This contrast results from surface relief associated with ferroelectric domains. When the surface is illuminated in the presence of aqueous AgNO₃, some of the domains become covered by silver (see Figure 5.1b). The image in Figure 5.1d illustrates that the silver does not preferentially deposit on certain facets and can be tightly confined to specific regions of the surface with linear dimensions smaller than 200 nm. By inspecting the surfaces of many grains, we determined that the silver deposits selectively on some, but not all of

the ferroelectric domains. Because of this domain specific reactivity, it was impossible to determine if BaTiO₃ has any orientation based reactivity anisotropy.

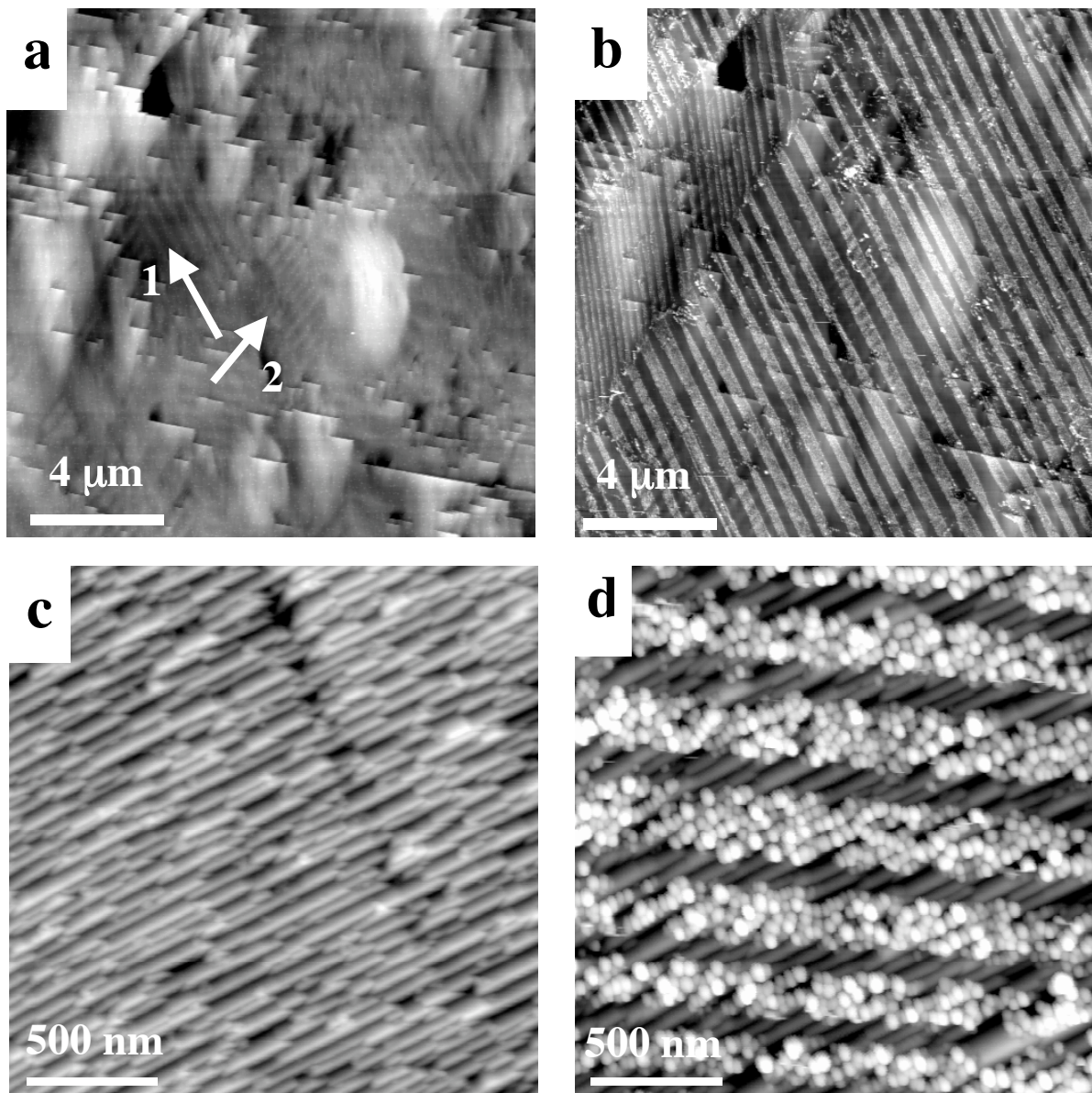


Figure 5.1: Topographic AFM images of the surfaces of crystallites in a BaTiO₃ polycrystal before (a&c) and after (b&d) the reaction. (a) Before the reaction. The white arrows draw attention to two sets of domains. (b) After illumination in AgNO₃ solution, deposited silver appears as white contrast. Silver is deposited on the set of domains labeled by arrow 1, but not by the one labeled 2. (c) A higher resolution image showing facets on a surface before the reaction. (d) After the reaction, the silver is selectively deposited. The vertical black-to-white contrast in (a) to (d) are 50 nm, 50 nm, 10 nm, and 30 nm respectively.

5.3 Single Crystal Results

5.3.1 Inorganic Redox Reactions

The topograph in Figure 5.2a shows a crystal before the silver reduction reaction. The vertical parallel lines of contrast show surface relief that is caused by the presence of 90° domain boundaries. The circular black features correspond to topographic depressions of unknown origin that are present on all of the as-delivered crystals. As successive steps of the experiment do not seem to alter these features, they serve as convenient fiduciary marks to compare images recorded at different stages of the experiment. After illumination in the presence of aqueous AgNO_3 , we find that silver has deposited only on some regions of the surface. The silver can be removed by carefully wiping the surface with a tissue and then sonicating the crystal in water and acetone. AFM was then used to confirm that all of the silver was removed and that the surface looked the same as it did before the reaction.

The surface was then etched to determine the polarity of the domains that accumulate Ag. The image in Figure 5.2c shows the same area of the surface after the acid etch. There is an obvious one-to-one correspondence between the domains that accumulated the most silver and the regions that etched the fastest. Therefore, it is the positive ends of the dipoles that accumulate the most silver. Note that on planes other than (001), some of the lateral domains will have at least a component of the polarization vector normal to the surface. Therefore, a high index surface may contain the positive end of a lateral domain's dipole and this explains the striped patterns of silver observed on the surfaces of polycrystals.

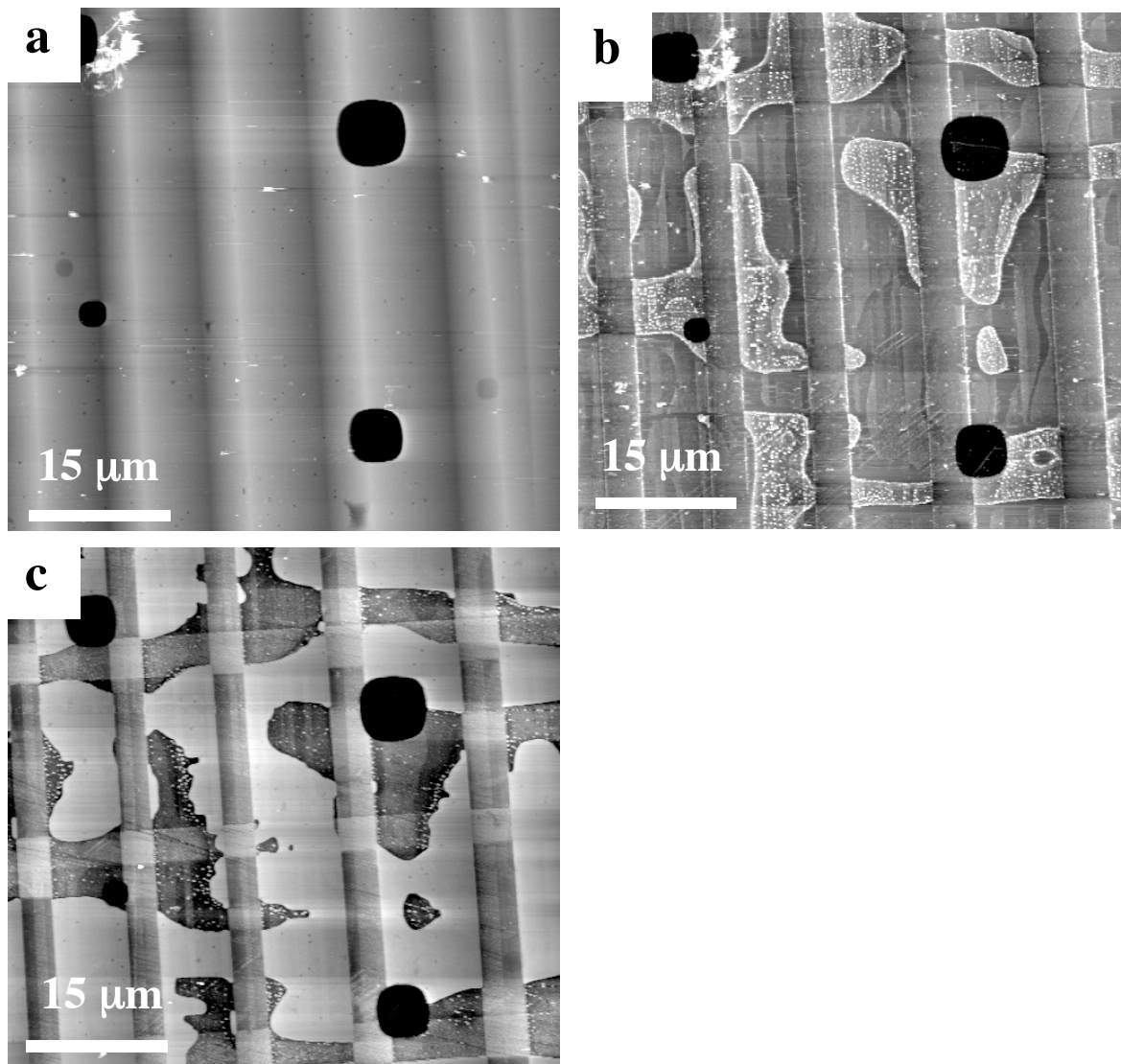


Figure 5.2: Topographic AFM images of the (001) surface of a BaTiO₃ single crystal. (a) before the reactions. (b) After the reaction, the white contrast corresponds to silver. (c) After etching treatment. The domains that etch fastest are topographically lower and have relatively darker contrast. The vertical black-to-white contrast in (a) to (c) are 80 nm, 100 nm, and 100 nm respectively.

The preferential deposition of silver is not likely to be connected to preferential adsorption of Ag⁺ cations before reduction; in up domains the surface is the positive end of the domain's dipole and it should, therefore, not attract the cations from solution. A better explanation for these observations is that the transport of photogenerated carriers in the bulk of the crystal is influenced by the static dipolar fields in the domains. In up domains, where the polarization

vector is pointed away from the crystal, the field will cause electrons to flow toward the surface where they can reduce Ag^+ to form Ag^0 on the surface. In down domains, the field urges the electrons away from the surface. The photogenerated holes should, obviously, behave in an opposite fashion. Under these conditions, it is anticipated that the holes oxidize adsorbed water and we expect that this reaction occurs on the surfaces of the down domains.

To confirm that the oxidation and reduction reactions do take place on oppositely polarized domains, both the silver reduction and the lead oxidation probe reactions were performed on the same crystal [3]. Figure 5.3a is a topograph of this crystal before either probe reaction. Figure 5.3b is an image after the silver reduction reaction. The crystal was then cleaned as described earlier and the lead oxidation reaction was performed (see Figure 5.3c). It is obvious from these images that the lead oxide deposits accumulate on areas of the surface that are different from those areas where silver deposits accumulate. Despite the fact that some of the domains migrate small distances during illumination, handling, and cleaning, it is clear that the areas on which oxidized lead is deposited are separated from those where silver deposits by 180° boundaries.

Since etching experiments showed that silver accumulates on the up domains, these images point to lead oxide accumulating on the down domains. This conclusion was confirmed by performing the lead oxidation experiment followed by the acid etch on a third crystal. Figure 5.4 shows the results of this experiment. The areas that accumulated the lead oxide deposits also etched the slowest (the down domains). Therefore, it is clear that reduction and oxidation photochemical reactions can be spatially separated on the surface of ferroelectric BaTiO_3 . The polarization field in up domains (+z, positive surface) drive photogenerated electrons to the surface while the polarization fields in the down domains (-z, negative surface) drive photogenerated holes to the surface.

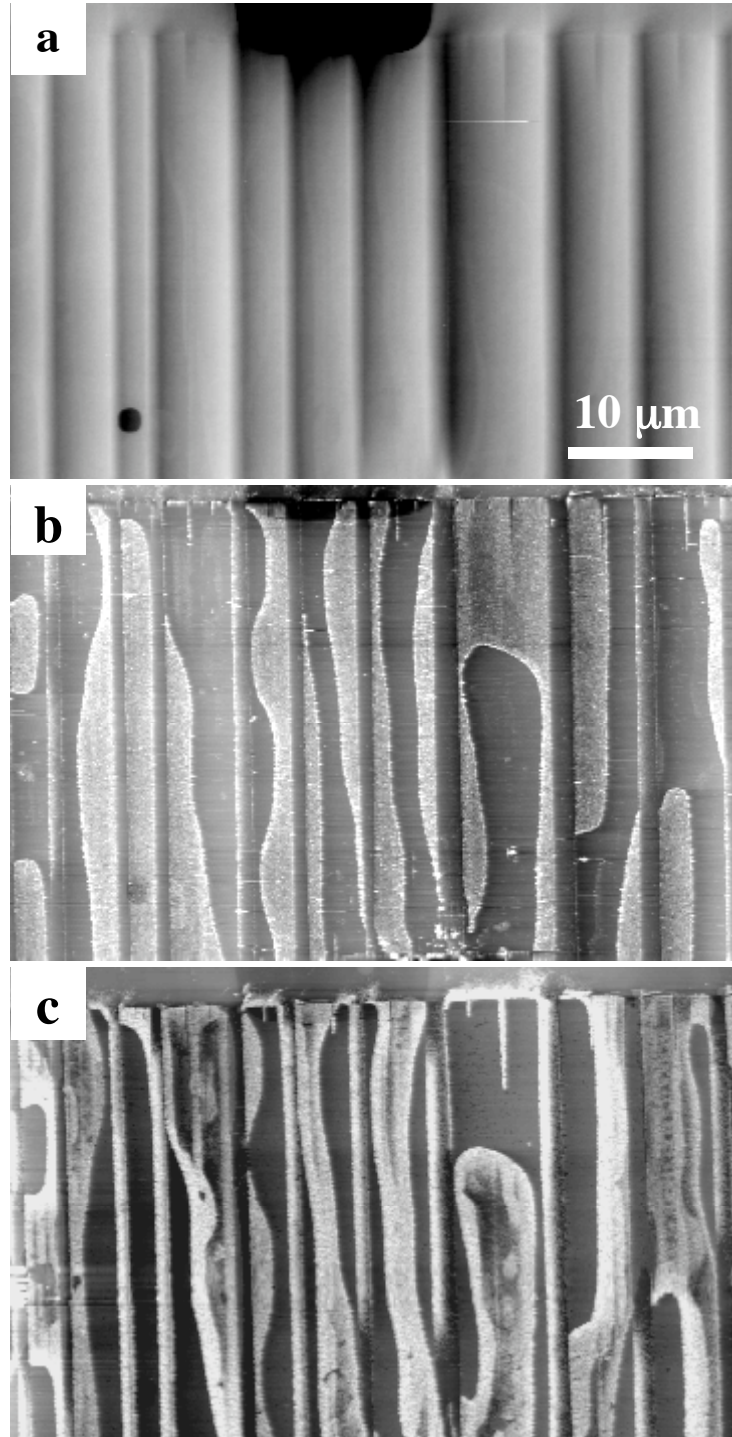


Figure 5.3: Topographic AFM images of the {001} surface of a BaTiO₃ single crystal. (a) Before the reactions. (b) The same area of the surface after illumination in an aqueous AgNO₃ solution. The white contrast corresponds to silver. (c) The same area of the surface after it was cleaned and illuminated in an aqueous lead acetate solution. The white contrast corresponds to lead containing deposits. The ranges of the vertical black-to-white contrast in (a) to (c) are 80 nm, 100 nm, and 110 nm, respectively.

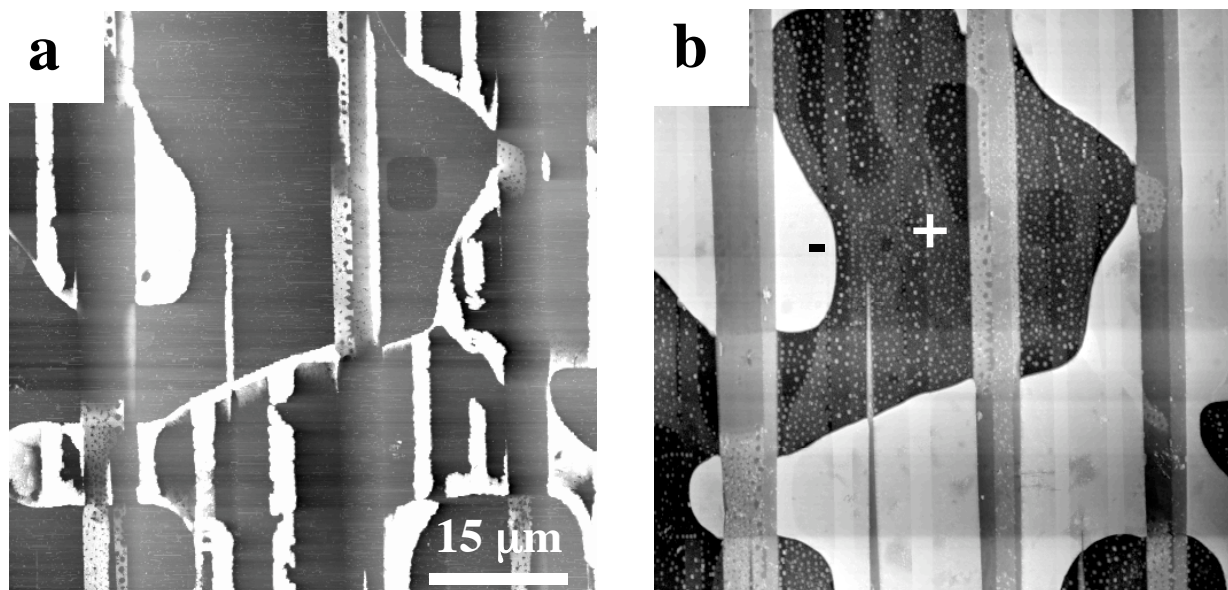


Figure 5.4: Topographic AFM images of the {001} surface of a BaTiO₃ single crystal. (a) After Pb oxidation reaction. (b) After etching treatment. The domains that etch slowest are topographically higher and have relatively lighter contrast. The vertical black-to-white contrast in (a) and (b) are 150 nm and 120 nm, respectively.

5.3.2 Organic Oxidation Reactions

A final experiment was performed to determine if the polarization fields in BaTiO₃ had any effect on the oxidation of stearic acid films. Figure 5.5a is a NC-AFM image of the clean surface [4]. The silver reduction reaction was performed in order to determine the areas of the surface where reduction by photogenerated electrons takes place and this image is shown in Figure 5.5b. The silver was removed from the surface in the normal way and the stearic acid film was deposited. The as-deposited film is shown in Figure 5.5c. The stearic acid does not form a continuous film on the surface but instead forms localized islands that are 10 – 20 μm in diameter and are separated by approximately 4 μm. After the film was irradiated, some of the film had been oxidized. Comparing the image of the oxidized film in Figure 5.5d to the image taken after the silver reduction reaction, it is obvious that there is no correlation between the areas where the film was oxidized and the areas where we would expect oxidation by

photogenerated holes. Therefore, once hydroxyl radicals are created through hydroxide oxidation by photogenerated holes, the radicals are no longer associated with these sites and are free to migrate on the surface to oxidize other species.

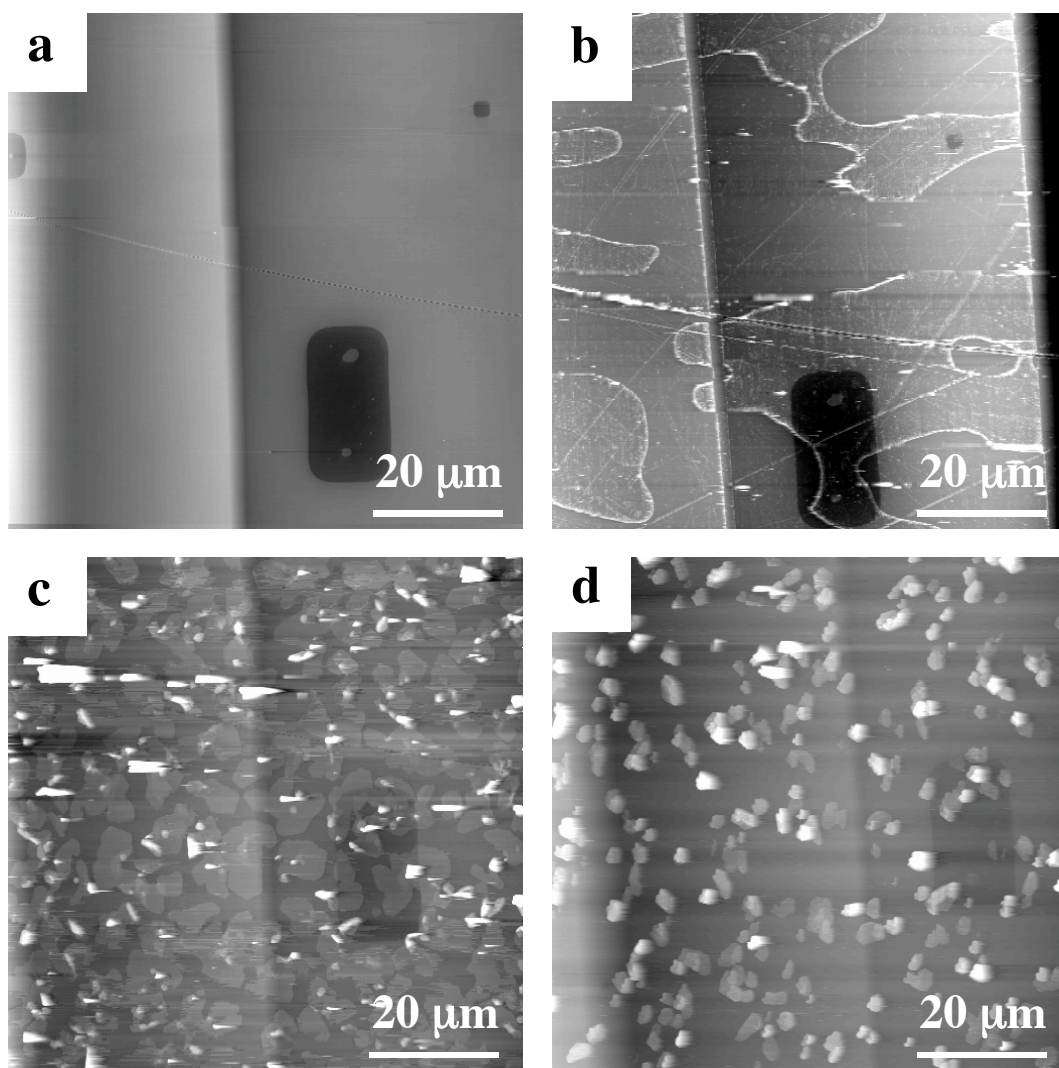


Figure 5.5: Topographic NC-AFM images of the (001) surface of a BaTiO₃ single crystal. (a) Before the reactions. (b) The same area of the surface after illumination in an aqueous AgNO₃ solution. The white contrast corresponds to silver. (c) The same area of the surface after it was cleaned and stearic acid was deposited. The white contrast corresponds to stearic acid islands. (d) The same area of the surface after it was illuminated and stearic acid was oxidized. Notice how the oxidation of stearic acid has no dependence on the domain structure. The ranges of the vertical black-to-white contrast in (a) to (d) are 80 nm, 100 nm, 150 nm and 150 nm, respectively.

1.4 Particle Results

The SEM image in Figure 5.6 below is of the as-prepared crystals. The contrast is dominated by the facets that form during the reaction in the salt flux. Most crystals are bounded by $\{100\}$, $\{110\}$, and $\{111\}$ type planes, as indicated in the figure, and have diameters in the range of 1 to 5 microns. Because these crystal shapes were formed above the Curie temperature, their habits are determined by the relative energies the low index surfaces in the KCl flux. Therefore, the assigned facet orientations (see labels in Figure 5.6) were simply determined using the symmetry of the respective planes (in the cubic phase (100): 4-fold, (110): 2-fold, (100): 3-fold). Obviously, indexing the facets by this method makes it impossible to determine the unique $[001]$ axis of these tetragonal crystals. Also, unlike the polycrystal and single crystal experiments described earlier, domain boundaries are not apparent on the as-prepared crystals.

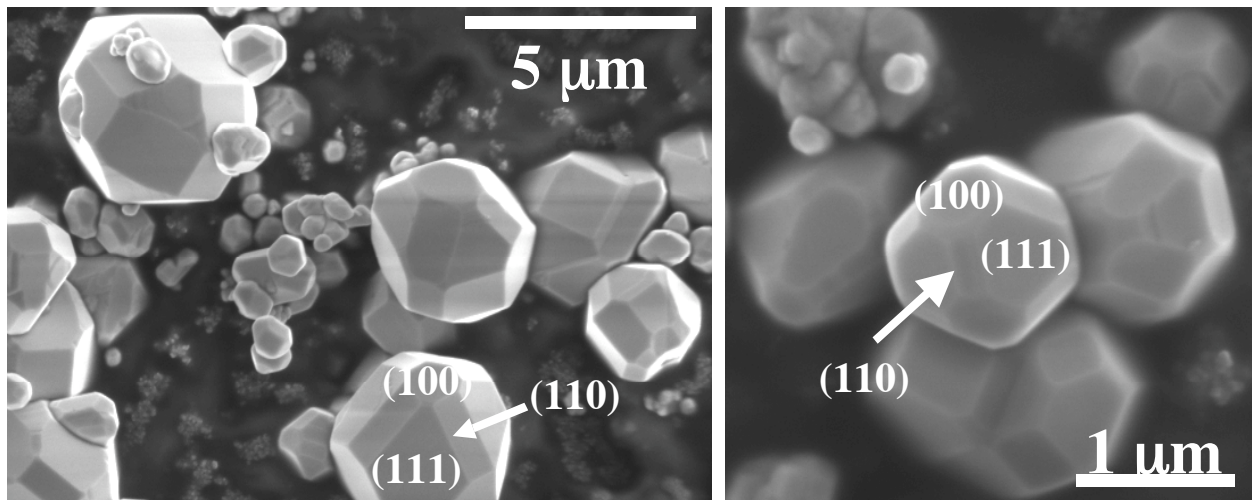


Figure 5.6 SEM images of the as prepared faceted BaTiO_3 crystals produced in a KCl flux. The crystallographic orientations of the faces are labeled.

When the crystals are illuminated in the presence of aqueous AgNO_3 , some of the domains become covered by silver (see Figures 5.7 and 5.8). The SEM images in Figure 5.7 clearly show

striped patterns of silver on the surface that are similar to the striped patterns of silver observed on the bulk BaTiO₃ samples and these patterns are indicative of domain patterns. These patterns demonstrate that the ferroelectric domains are the most important factor in determining the distribution of the product phase. However, since all of the facets show some reactivity, we can also see a secondary orientation effect; the relative reactivity of the faces can be ranked as {100}>{111}>{110}.

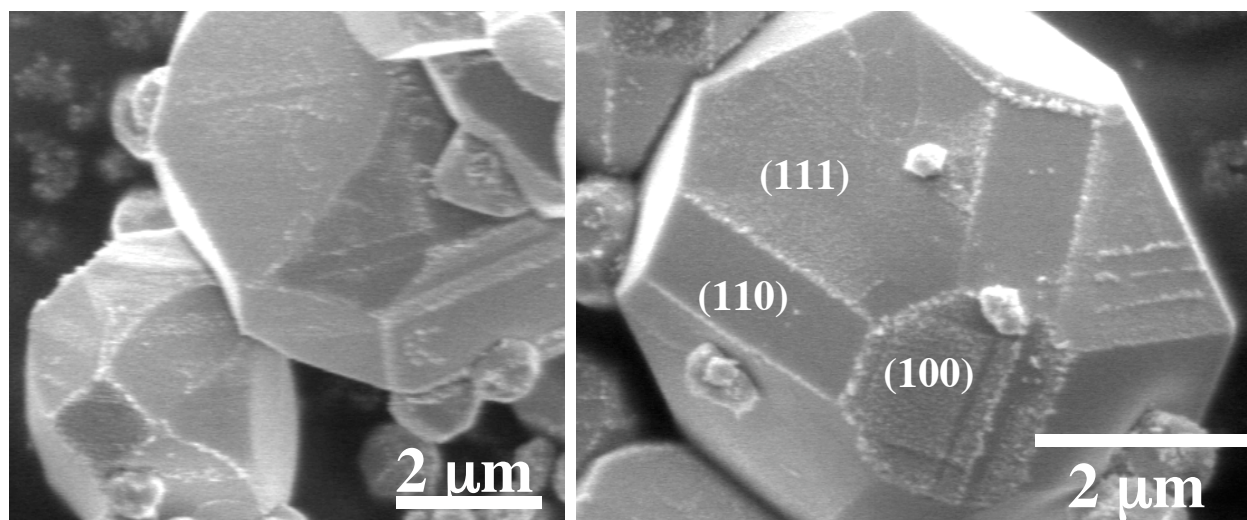


Figure 5.7: SEM images of the faceted BaTiO₃ crystals after reaction with AgNO₃. The circular white contrast indicates silver metal deposits. The striped pattern of these deposits is indicative of polarization specific reactivity.

In the previous section, acid etch experiments were used to determine the direction of the polarization vectors that reduced silver and those that oxidized lead on bulk BaTiO₃ samples. Those results showed that silver is photochemically reduced on domains that had positively charged surfaces and lead was oxidized on the oppositely polarized surfaces. For the particle experiments presented here, it is clear that the reactivity is controlled by the dipolar fields in certain ferroelectric domains but it is not possible to use acid etching to directly determine the polarization of the domains. However, we assume that the reactivity is the same for this case.

That is, that silver is also photochemically reduced on the surfaces of domains with their polarization vector pointed out the surface.

In other crystals, the characteristic stripes are not observed. The SEM images in Figure 5.8 show two crystals where the reactivity is predominately located on only one of the exposed {100}-type faces. The reactivity on this face is much higher than on any of the other faces (also see Figure 5.8 for comparison). Interestingly, the highly reactive face also has an abrupt border of unreactive region near the edge of the face. One possible explanation is that the area in the center of the reactive face is a more favorable nucleation site and the denuded zone near the edge of the particle is similar to the precipitate free zones seen in metal alloys. In these systems, the vacancy or solute concentration is decreased near grain boundaries because of higher diffusivity or precipitate formation in the grain boundary. It is possible that the edges of the crystal are a sink for vacancies or solutes, however, this explanation is unlikely since the reactivity of the edges of the crystal are not consistently reactive.

The most likely explanation for this “window effect” is the minimizing the depolarization field in these crystals. Calculations of electrostatic energy associated with a uniformly polarized polyhedral body have shown that the energy is maximized at the edges of flat faces perpendicular to the polarization [5]. Thus, the energy can be reduced if the crystal in this area is depolarized or the polarization is reversed. As long as the energy to form a domain boundary is comparable to the energy saved, this is a likely explanation for the unreactive region. The abruptness of the boundaries between the reactive and unreactive areas on the particles supports the idea that domains of opposite polarization were formed near the edges of the reactive face to minimize the depolarization energy.

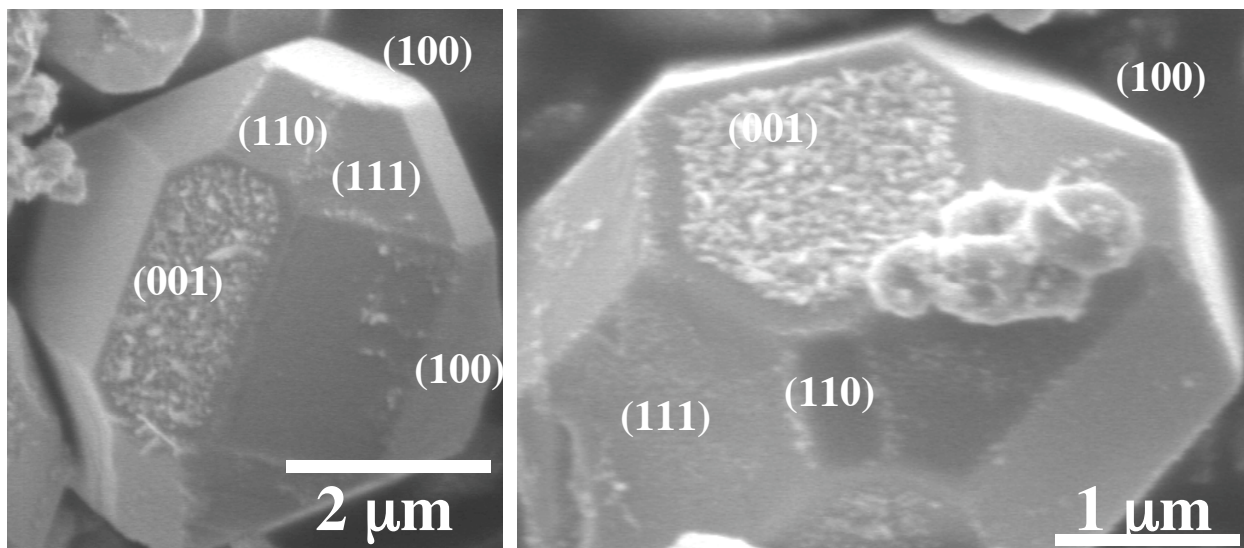


Figure 5.8: SEM images of the faceted BaTiO_3 crystals after reaction with AgNO_3 . The circular white contrast indicates silver metal deposits.

1.5 Discussion

The static electric fields associated with the ferroelectric domains in BaTiO_3 have been demonstrated to attract colloidal particles from solution [6] and influence both precipitation and vapor deposition processes [7]. In fact, these effects were used as the basis for domain decoration techniques developed several decades ago. Therefore, one might suggest that the patterns observed here are formed when insoluble Ag and Pb containing phases are formed in solution and then deposited in patterns on the surface. However, the colloidal silver experiments presented in section 5.2 show that this reaction mechanism is not the case. Also, no deposition is observed when photochemically inert materials such as alumina and silica are used in place of BaTiO_3 and unpatterned deposition is observed when photochemically active, but paraelectric materials such as titania [8] and SrTiO_3 (next chapter) are used. Therefore, we can be relatively certain that the reactions occur not in the solution phase, but on the surface. This is also confirmed by the stearic acid oxidation experiment; when the observable photochemical reaction does not directly rely on photogenerated charge carriers, then the reaction is free to occur at sites

on the surface that are unrelated to the site of hole transfer. Therefore, the distinct aspect of the spatially selective deposition process reported here is that it occurs because of a reaction between photogenerated charge carriers and species adsorbed from the solution. This process should make it possible to deposit Ag, PbO₂, or a number of other materials on predefined (or written) polarization patterns in thin film ferroelectrics and recent experiments by other researchers have showed this to be the case [9].

Two previous studies indicate that charge separation in polar oxides may affect photochemical activity and are worth mentioning. The first study focused on the activity of BaTiO₃ and SrTiO₃ powders for CO oxidation [10]. The researchers found that the both materials had the same apparent activation energy in the dark although the reaction rate in the dark was two orders of magnitude higher for SrTiO₃. Under illumination, the reaction rate increased for both powders indicating that there is a photocatalytic effect on the reaction. Interestingly, both BaTiO₃ and SrTiO₃ powders had the same room temperature reaction rate meaning that the rate of reaction on the BaTiO₃ powders increased significantly when illuminated. They suggest that the spontaneous polarization in BaTiO₃ accounts for large increase in its activity under illumination.

The effect of poling on the photochemical activity of potassium-doped lead niobate (PKN), Pb_{1-x}K_{2x}Nb₂O₆, was studied by comparing the activity of hydrogen production from water for poled and unpoled polycrystalline ceramics [11]. Ceramic discs (r = 10mm, t = 0.5mm) of PKN (x = 0.006) were prepared and Pt dots were deposited at regularly spaced intervals to act as a cocatalyst. PKN (x = 0.006) has a rhombohedral crystal structure and is paraelectric at room temperature but, when poled even at low temperature, a metastable orthorhombic phase is formed. This new phase is ferroelectric with a low spontaneous polarization ($P_s = 3 \text{ } \mu\text{C}/\text{cm}^2$).

Activities for hydrogen evolution of both poled and unpoled discs were tested. The researchers found that the positively charged polar surface had a higher activity than the negatively charged polar surface although both had a lower activity than the unpoled samples. They proposed that the positively charged surface had a higher rate of hydrogen evolution because the dipolar electric field transferred photogenerated electrons to this surface which agrees with the band model in Figure 2.3. The lower overall activity of the poled samples probably occurs because the population of the minority domain, and the opposite photochemical reaction, on each surface, becomes the rate-limiting step, as discussed below.

To understand why unpoled surfaces are more reactive than poled surfaces, we must consider that the oxidation and reduction half reactions must take place at the same rate in order to maintain charge neutrality in the system. Therefore, the reaction rates are lower for the polar surfaces of poled polycrystals because the more difficult reaction (oxidation on the (+) surface and reduction on the (-) surface) is hindered even more do to the charge separation caused by the electric field. It also is more difficult to separate the photogenerated charge carriers over the long distances required in this configuration. For the case of a BaTiO₃ (001) single domain crystal (thickness = 1 mm), we found that neither polar surface exhibited any activity for either the photochemical reduction of silver or photochemical oxidation of lead.

1.6 Summary and Conclusions

When BaTiO₃ is illuminated by ultraviolet light in the presence of aqueous Ag⁺ and Pb²⁺ ions, Ag⁺ is preferentially reduced on the surface of domains whose polarization vectors have their positive end directed toward the surface and, Pb²⁺ is preferentially oxidized on the surface of domains whose polarization vectors have their negative end directed toward the surface. As a result, the reduced and oxidized products are deposited on the surface in patterns determined by

the domain structure. These observations imply that the static electric fields in each domain separate photogenerated carriers by microscopic distances and that the electron and hole half reactions can occur on spatially distinct areas of the catalyst surface.

1.7 References

- (1) J.L. Giocondi and G.S. Rohrer, *Chem. Mater.*, **13** (2001) 241.
- (2) Z.Y. Huang, G. Mills, and B. Hajek, *J.Phys.Chem.*, **97** (1993) 11542.
- (3) J.L. Giocondi and G.S. Rohrer, *J.Phys.Chem. B*, **105** (2001) 8275.
- (4) J.L. Giocondi and G.S. Rohrer, in Structure-Property Relationships of Oxide Surfaces and Interfaces, edited by C.B. Carter, X. Pan, K.E. Sikafus, H.L. Tuller, and T. Wood (Mater. Res. Soc. Proc. **654**, Pittsburgh, PA, 2001) p. AA7.4.1-10.
- (5) M. DeGraef, personal communication.
- (6) G.L. Pearson and W.L. Feldmann, *J. Phys. Chem. Solids*, **9** (1958) 28.
- (7) A. Sawada and R. Abe, *Jap. J. Appl. Phys.*, **5** (1966) 401.
- (8) J.B. Lowekamp, G.S. Rohrer, P.A. Morris-Hotsenpiller, J.D. Bolt, and W.E. Farneth, *J.Phys. Chem. B*, **102** (1998) 3216.
- (9) S.V. Kalinin, D.A. Bonnell, T. Alvarez, X. Lei, Z. Hu, J.H. Ferris, Z. Qi, and S. Dunn, *Nano Letters*, **2**[6] (2002) 589.
- (10) H. Van Damme and W.K. Hall, *J. Catalysis*, **69** (1981) 371.
- (11) Y. Inoue, O. Hayashi, and K. Sato, *J. Chem. Soc. Faraday Trans.*, **86** (1990) 2277.

6 The Effects of Surface Termination and Orientation – Strontium Titanate, SrTiO₃

6.1 Introduction

The purpose of this chapter is to report the results of experiments conducted to determine the orientation dependence of the reactivity of SrTiO₃. These results show that SrTiO₃ has an orientation-based anisotropy in reactivity and that oppositely charged surface terminations affect the photochemical behavior of SrTiO₃. These results imply that the static electric fields adjacent to charged surfaces can be used to separate photogenerated carriers by macroscopic distances and that the electron and hole half reactions can occur on spatially distinct areas of the catalyst surface.

6.2 Polycrystal Results

The topographic AFM images in Figure 6.1 show the surfaces of two typical grains in a SrTiO₃ polycrystal after the photochemical silver reduction reaction. Facets that formed during the high temperature anneal are obvious in both images. It is also clear from both images that, unlike the BaTiO₃ case, silver deposits have formed on some facets and not others. In Figure 6.1a, the surface shown is bounded by three types of facets but only one of the facets, as indicated by the arrows, accumulated silver. The surface shown in Figure 6.1b is bounded by two types of facets and, again, only the facet indicated by the arrows accumulated silver.

To establish an orientation-reactivity relationship for this system, we need know what crystallographic planes are bounding the facets. As described in section 4.2.2, the surface normals computed from the OIM data simply tells us the macroscopic or average orientation of

the surface and not, for the case of faceted surfaces, the orientations of the bounding planes. To identify the stable facets, we develop a map of the smooth and faceted orientations, plotted on the standard stereographic triangle. We refer to this as an orientation stability diagram (OSD). The OSD or "n-diagram" has been compared to a ternary phase diagram, because it clearly shows separate fields comparable to single phase (flat surfaces), two phase (surfaces bounded by two facets) and three phase (surfaces bounded by three facets) regions [1].

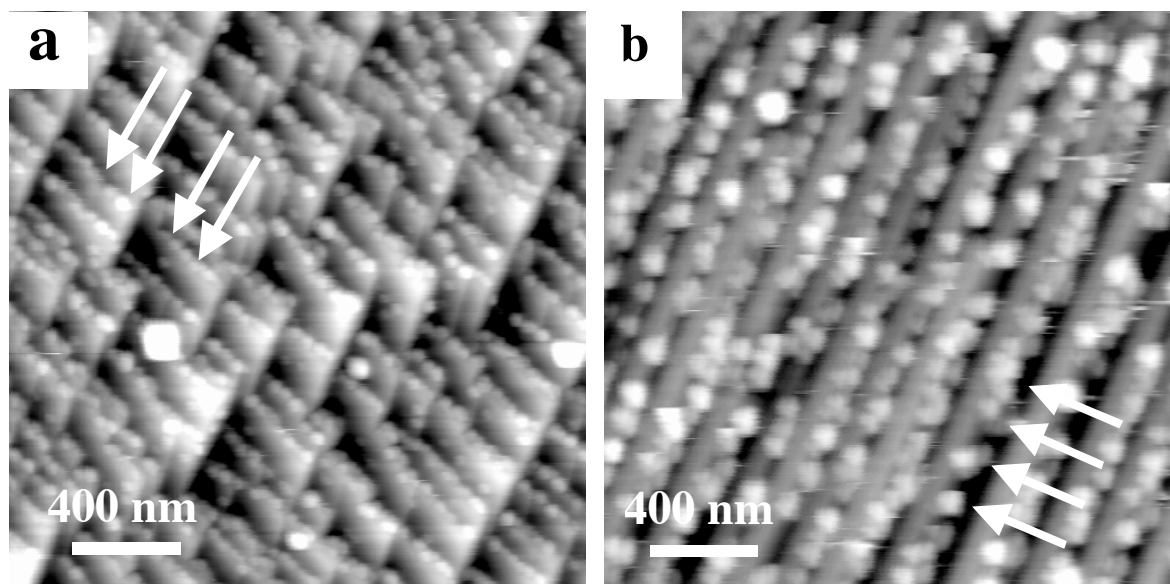


Figure 6.1: Topographic AFM images of the surfaces of crystallites in a SrTiO_3 polycrystal before after illumination in AgNO_3 solution. Notice how silver deposits (white contrast) selectively form on only some facets as indicated by the arrows. (a) Surface that is composed of three types of facets with only one facet type active for silver reduction. (b) Surface that is composed of two types of facets with only one facet type active for silver reduction. The vertical black-to-white contrast in (a) and (b) is 25 nm.

Figure 6.2 shows the OSD that was constructed using observations from approximately 75 grains in a single SrTiO_3 polycrystal [2]. Surfaces observed to be flat are indicated by the white circles. It is immediately clear that all of the flat surfaces are concentrated within 24° of the

{100} orientation. In the region between 19° and 25° from {100}, both faceted and smooth surfaces are observed. This overlap in the observations is probably the result of uncertainty in

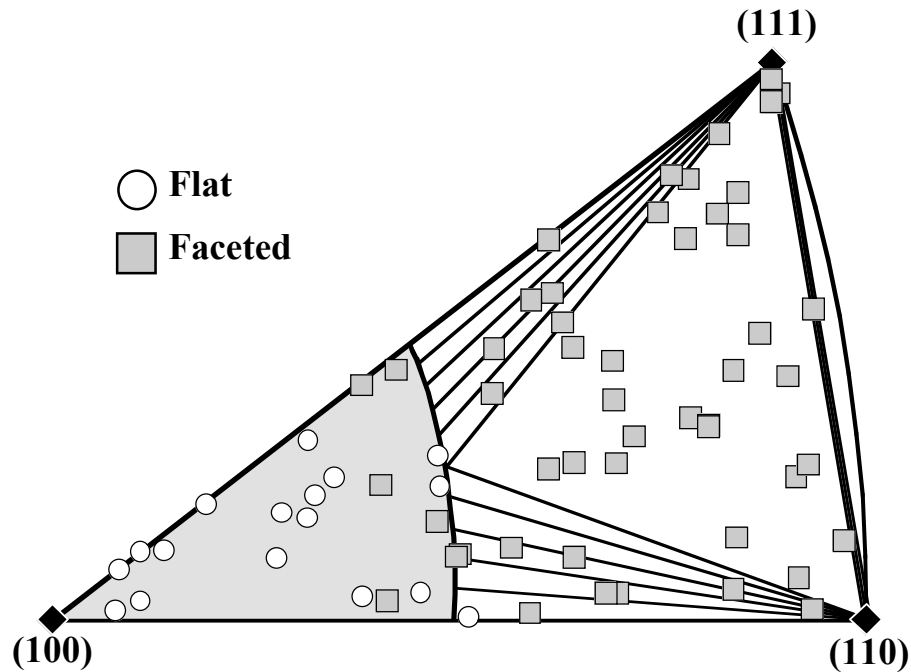


Figure 6.2: SrTiO₃ orientation stability diagram (OSD) for 6 h in air at 1200° C. Grains contained in the gray area within 24° of {100} have flat surfaces, grains on the tie lines are faceted to the two types of surfaces that lie at the ends of the lines, and the remainder of the grains (in the white area) are bounded by three types of surfaces: complex facet approximately 24° from {100}, a {110} facet, and a {111} facet.

the orientation measurements. Recognizing that the uncertainty in the orientation measurements is about 5°, we chose the set of complex facets inclined by 24° from {100} as the boundary between smooth and faceted orientations. In Figure 6.2, the range of orientations that are stable with respect to faceting is indicated with the light gray background. The observations also indicate that while {110} and {111} orientations are stable, surfaces inclined by more than a few degrees from these planes facet. The grains that lie on the tie lines in Figure 6.2 are bounded by two facets whose orientations can be found the ends of the tie lines. All of the other grains are

bounded by three types of facets. Therefore, every grain is bounded by three possible types of facets: a complex facet inclined $\sim 24^\circ$ from $\{100\}$, a $\{110\}$ facet, and a $\{111\}$ facet.

To estimate the relative reactivity of the different surfaces, the number of silver islands was counted on a typical area of each grain. Each grain was then classified as either a low reactivity grain (< 75 deposits/ μm^2), a medium reactivity grain (< 250 deposits/ μm^2), or a high reactivity grain (>250 deposits/ μm^2). One example for each of the three categories are shown by the topographic AFM images in Fig. 6.3. Grains with less than 75 deposits/ μm^2 , such as in Figure 6.3a, exhibited small silver islands that were scattered across the surface and were considered to have low activity. Grains with intermediate activity (Figure 6.3b) typically had more densely packed silver deposits but the surface structure remains clear. Grains with greater than 250 deposits/ μm^2 were considered to have high activity. The surface structure of these grains was usually obscured by the large number of silver deposits, as shown in Figure 6.3c.

The photochemical activity of each grain was plotted on the OSD (see Figure 6.4) to determine if there is a correlation between activity and the surface orientations. We found that all grains with high activity (>250 Ag islands/ μm^2) also had a complex $\{100\}$ facet. Since it is clear that silver deposits on only a subset of the facets, we suppose that it is the complex facet

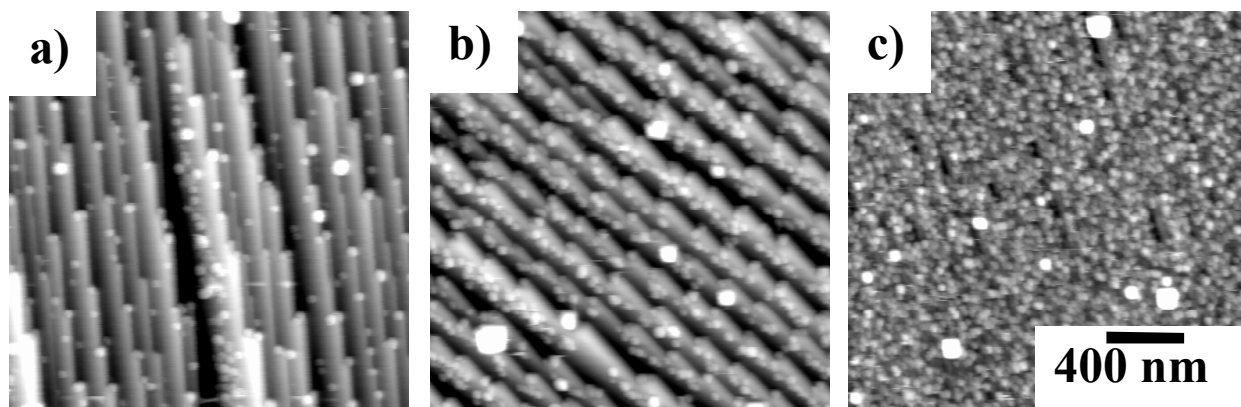


Figure 6.3: AFM topographs of grains with representative silver reduction activities. (a) low reactivity. (b) medium reactivity. (c) high activity. The vertical black-to-white contrast in a) to c) are 250 nm, 300 nm, and 200 nm, respectively.

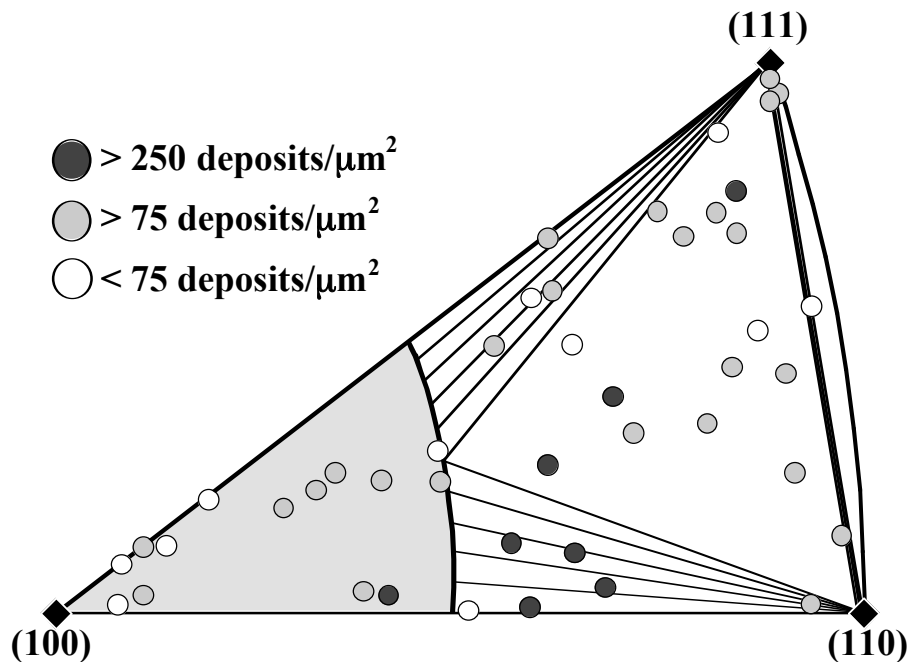


Figure 6.4. SrTiO₃ silver reduction activity plotted on the OSD. Dark circles indicate high activity, gray circles indicate medium activity, and white circles indicate low activity.

that selectively reduces silver. In principle, it should be possible to determine the index of the active facet by measuring its inclination with respect to the macroscopic surface normal in the topographic AFM images. However, because of tip convolution effects, accurate measurements of the inclination are only feasible when the area of the facet is relatively large (greater than a few hundred square nanometers). This situation makes it difficult to identify the indices of these facets with any degree of certainty. Therefore, the photochemical activity of single crystals of the low index orientations were used as a model for the polycrystal surface.

1.3 Single Crystal Results

1.3.1 (100) Single Crystal Results

The topograph in Figure 6.5a shows an annealed (100)-oriented SrTiO₃ single crystal. The surface consists of (100) terraces with step edges whose orientations are determined by the local

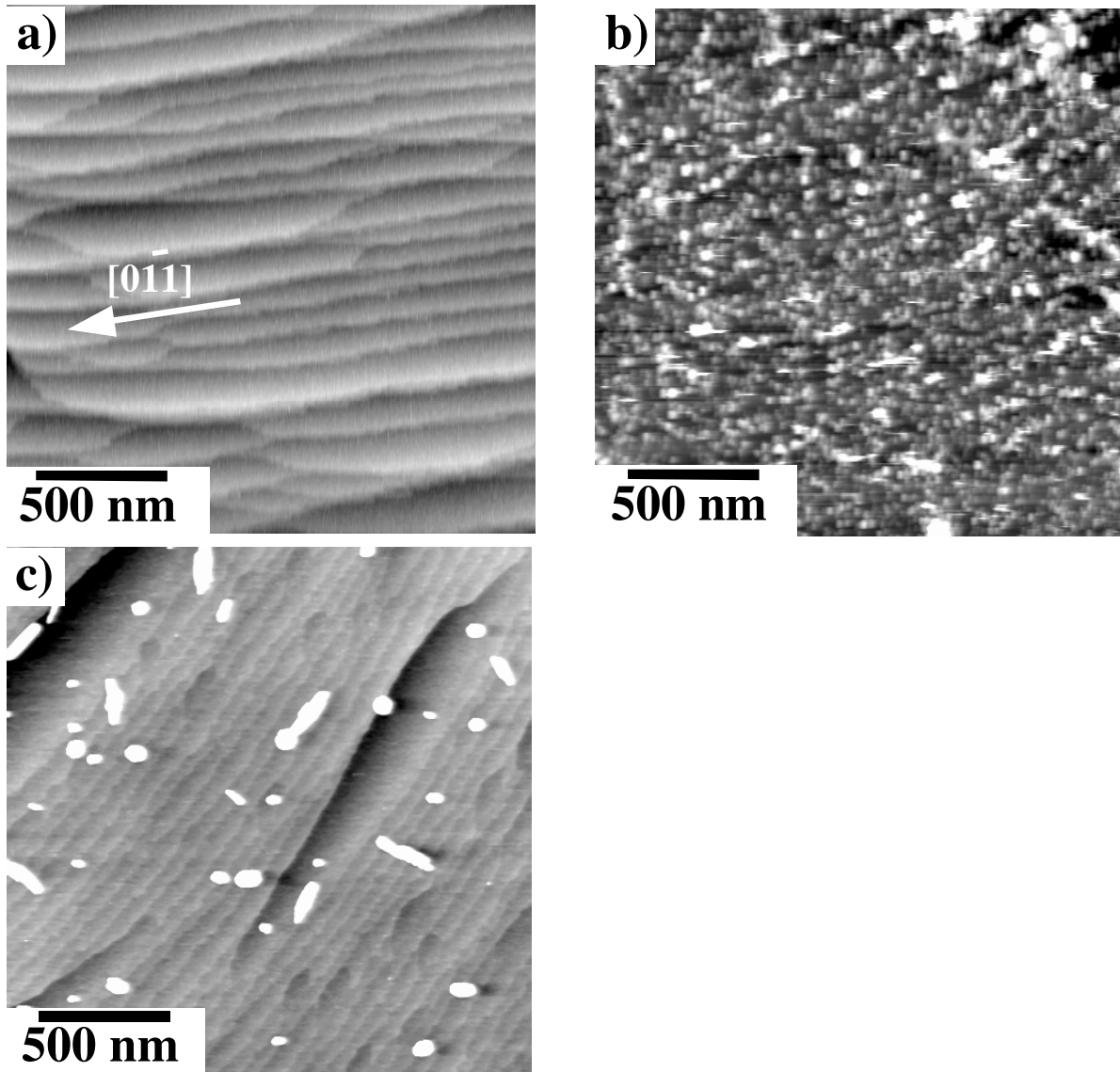


Figure 6.5: Topographic AFM images of the surfaces of (100)-oriented SrTiO_3 single crystals. (a) Before the reactions. (b) The same surface after illumination in an aqueous AgNO_3 solution. The white contrast corresponds to silver. (c) A different surface after illumination in an aqueous lead acetate solution. The white contrast corresponds to lead oxide deposits. The ranges of the vertical black-to-white contrast in (a) to (c) are 25 nm, 100 nm, and 25 nm, respectively.

miscut. Based on the stacking of atomic planes parallel to (100), the heights of all possible steps are equal to $(N/2)d_{100}$, where N is an integer, d_{100} is the spacing between (100) planes, and the smallest possible step has $N=1$. Because the crystal can be terminated by a TiO_2 or SrO plane, we can distinguish odd- N steps, that change the termination, from even- N steps, that preserve the

termination (see Figure 6.6). While the current data does not allow us to determine which terrace has which termination, the mixture of even- and odd-N steps allows us to be certain that both terminations are simultaneously present on this surface. The observation of mixed terminations is consistent with earlier studies of this surface [3].

The topograph in Figure 6.5b shows the surface after illumination in the presence of aqueous AgNO_3 . After this treatment, it is no longer possible to identify individual steps and the entire surface is uniformly covered with Ag deposits. The lead oxidation reaction was performed on another crystal prepared in the same way and the result is illustrated in Figure 6.5c. In this case, the lead oxide deposits (isolated white contrast) are found only on widely spaced, localized regions of the surface. For both the reduction and oxidation reactions on the $\{100\}$ surface, there is no obvious correlation between the reactivity and terrace composition.

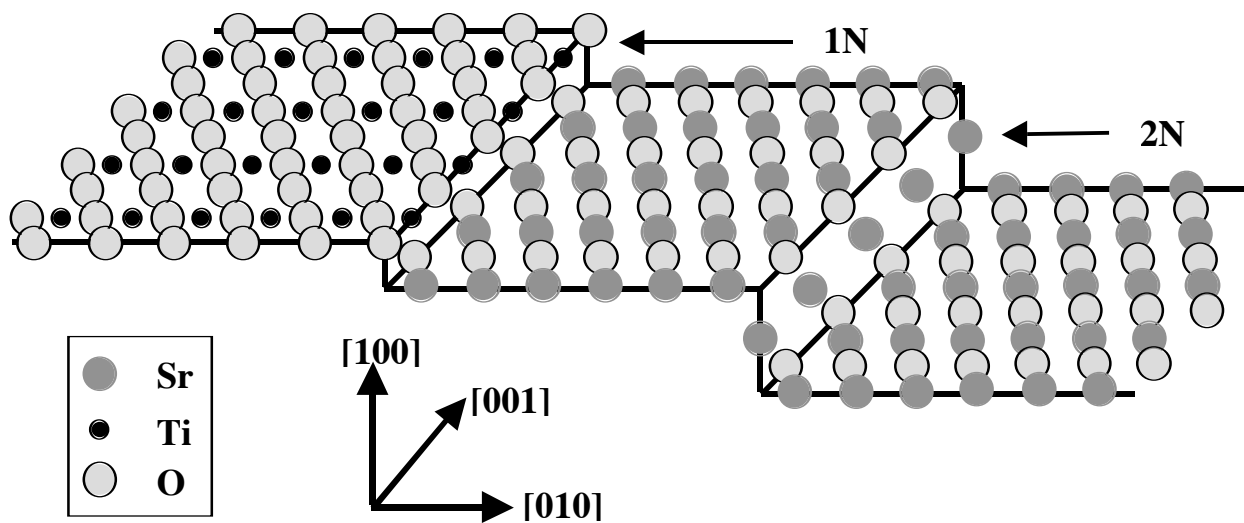


Figure 6.6: Schematic drawing of the possible $\text{SrTiO}_3(100)$ surface terminations. The left hand terrace has a TiO_2 termination. Traversing an odd-N step changes the termination to SrO (middle terrace) while traversing an even-N step does not change the chemical termination (right terrace). Layer spacing (N) = $1/2a = 1.95 \text{ \AA}$.

1.3.2 (111) Single Crystals

The topograph in Figure 6.7a shows the surface of an annealed SrTiO₃(111) surface. Adjacent (111) terraces are separated by a combination of straight and curved steps. The straight steps are orientated in <110> directions. The curved step edges are typically much smaller than the other features and therefore have only very weak contrast in the topographic image. Illumination in the presence of aqueous AgNO₃ causes silver to deposit on only some of the terraces (see Figure 6.7b). Note that the unreactive terraces comprise a minority fraction of the total surface area. The lead oxidation reaction was performed on another crystal prepared in the same way and the results are shown in Figure 6.7c. This image, which is characteristic of many areas that were examined, shows that lead oxide deposits accumulate on only a minority fraction of the terraces. The differential reactivity of the terraces suggests the possibility that they are structurally and chemically distinct. As was the case for the (100) surface, there are two possible terminations for the (111) surface (see Figure 6.8). All step heights are constrained to be $(N/2)d_{111}$, and the smallest possible spacing is $d_{111}/2 = 1.12 \text{ \AA}$. Again, steps with odd-N heights separate terraces with different terminations and steps with even-N heights separate terraces with the same termination. When the step heights are measured, we find steps of both odd- and even-N and this indicates that both the positively charged Ti terminated surface and the negatively charged SrO₃ surface are simultaneously present on the SrTiO₃(111) surface.

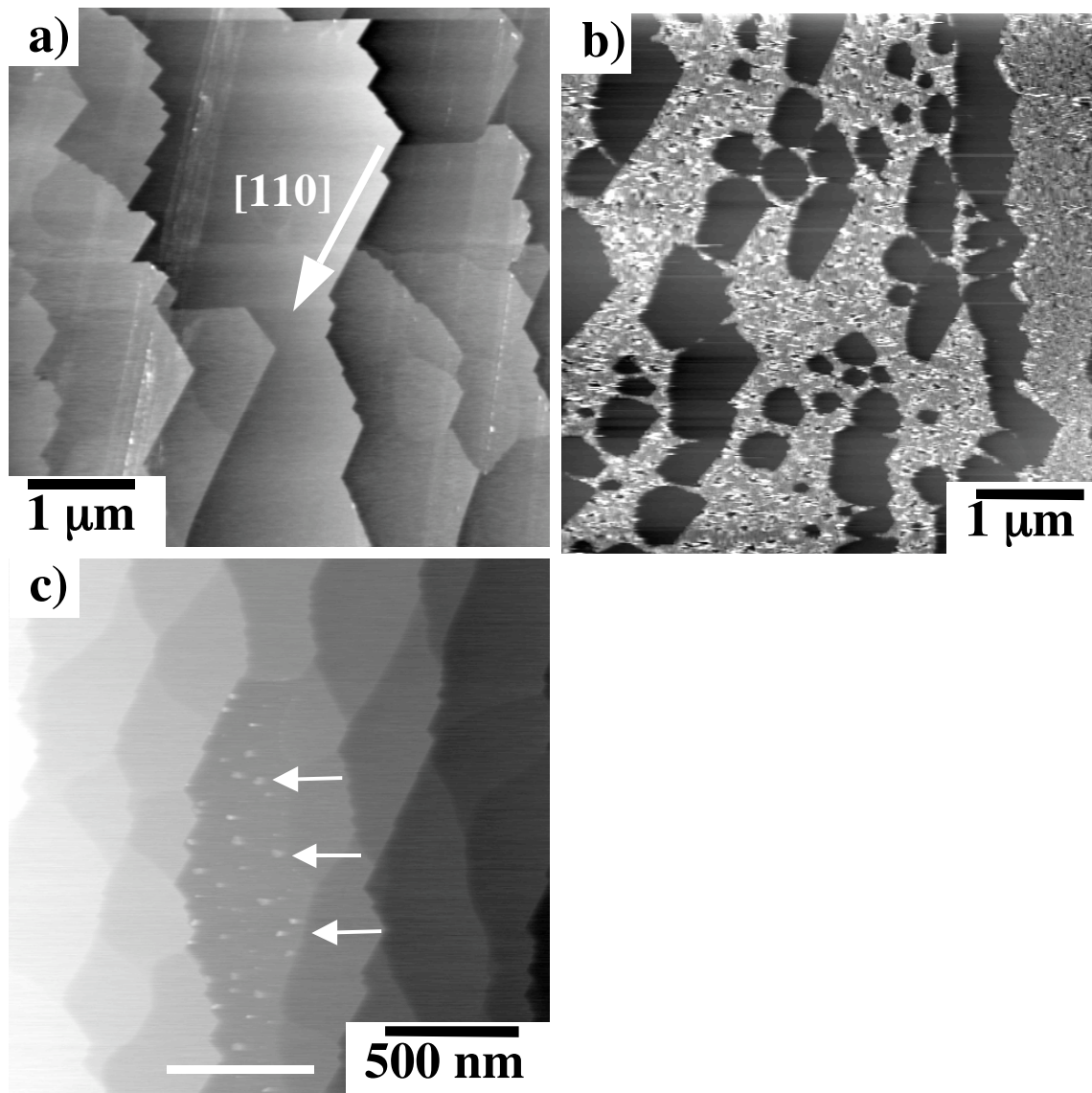


Figure 6.7: Topographic AFM images of the surfaces of (111)-oriented SrTiO₃ single crystals. (a) Before the reactions. (b) The same surface after illumination in an aqueous AgNO₃ solution. The white contrast corresponds to silver. (c) A different surface after illumination in an aqueous lead acetate solution. The white contrast corresponds to lead oxide deposits. The white line indicates where the data in Figure 6.9 is located. The ranges of the vertical black-to-white contrast in (a) to (c) are 60 nm, 200 nm, and 60 nm, respectively.

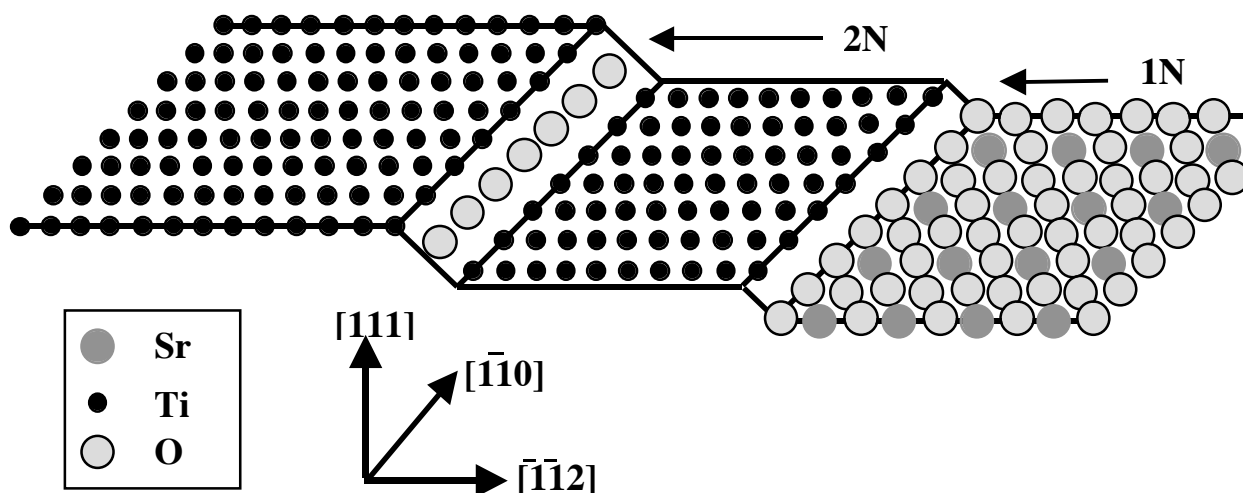


Figure 6.8: Schematic drawing of the possible SrTiO₃(111) surface terminations. The left hand terrace has a Ti⁴⁺ termination. Traversing an even-N step does not change the chemical termination while traversing an odd-N step changes the chemical termination to SrO₃⁺ (right terrace). Note that the step edges are {100} type. Layer spacing (N) = $\sqrt{3}a/6 = 1.12 \text{ \AA}$.

To test the idea that each type of reaction was limited to terraces with the same termination, we correlated the reactivity of the terrace with the heights of its bounding steps. For example, Figure 6.9 shows a sample line scan from Figure 6.7c, along the line indicated in the topograph. The height measurements can be used to differentiate steps separating terraces of constant termination from terraces with different terminations. We find that the steps that change the terrace termination separate the active and inactive terraces. Conversely, steps that preserve the termination separate terraces that have the same reactivity. The same phenomenon was observed for the Ag reduction reaction.

Because the silver reduction and lead oxidation reactions were not performed on the same crystal (removing the deposits after the first reaction irreversibly changed the surface), it is impossible to be sure that the reactions are taking place on different terraces. However, because there is a consistent difference in surface area between terraces that accumulate silver and those

that accumulate lead oxide, it is likely that these photochemical reactions take place on complementary terraces.

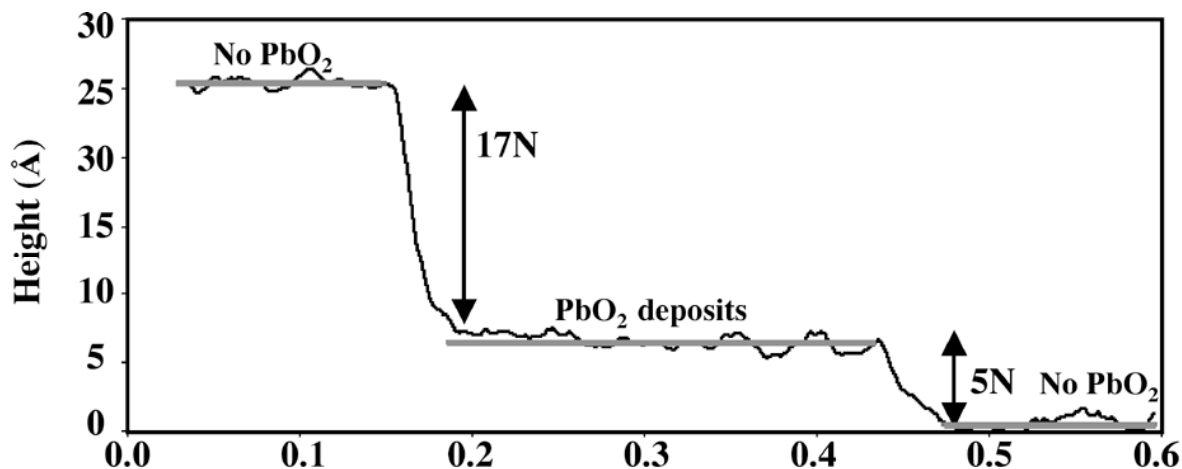


Figure 6.9: Height profile on the SrTiO₃(111) surface (see white line in Figure 6.7) showing how the change in reactivity is related to a change in chemical termination. The terrace in the middle contains PbO₂ deposits while the adjacent terraces do not. The left and middle terraces are separated by a step of ~17N (19.4 Å) and the middle and right terraces are separated by a step of ~3N (5.42 Å).

1.1.3 (110) Single Crystals

The AFM topograph in Figure 6.10a shows an annealed SrTiO₃(110) surface. The surface consists of (110) terraces with straight step edges; the long steps are along $\langle 100 \rangle$. A previous UHV STM study concluded that after repeated annealing above 1000 °C, the (110) surface is a reconstructed SrTiO termination composed of {100}-type microfacets [4]. The current observations provide no evidence for the existence of microfacets on this surface and this can be attributed to the difference in the preparation conditions (temperature and partial pressure of oxygen). The image in Figure 6.10b is a NC-AFM topograph of this surface after illumination in the presence of aqueous AgNO₃. In this case, we see that the white contrast (Ag) has accumulated only along the step edges. The lead oxidation reaction was performed on another

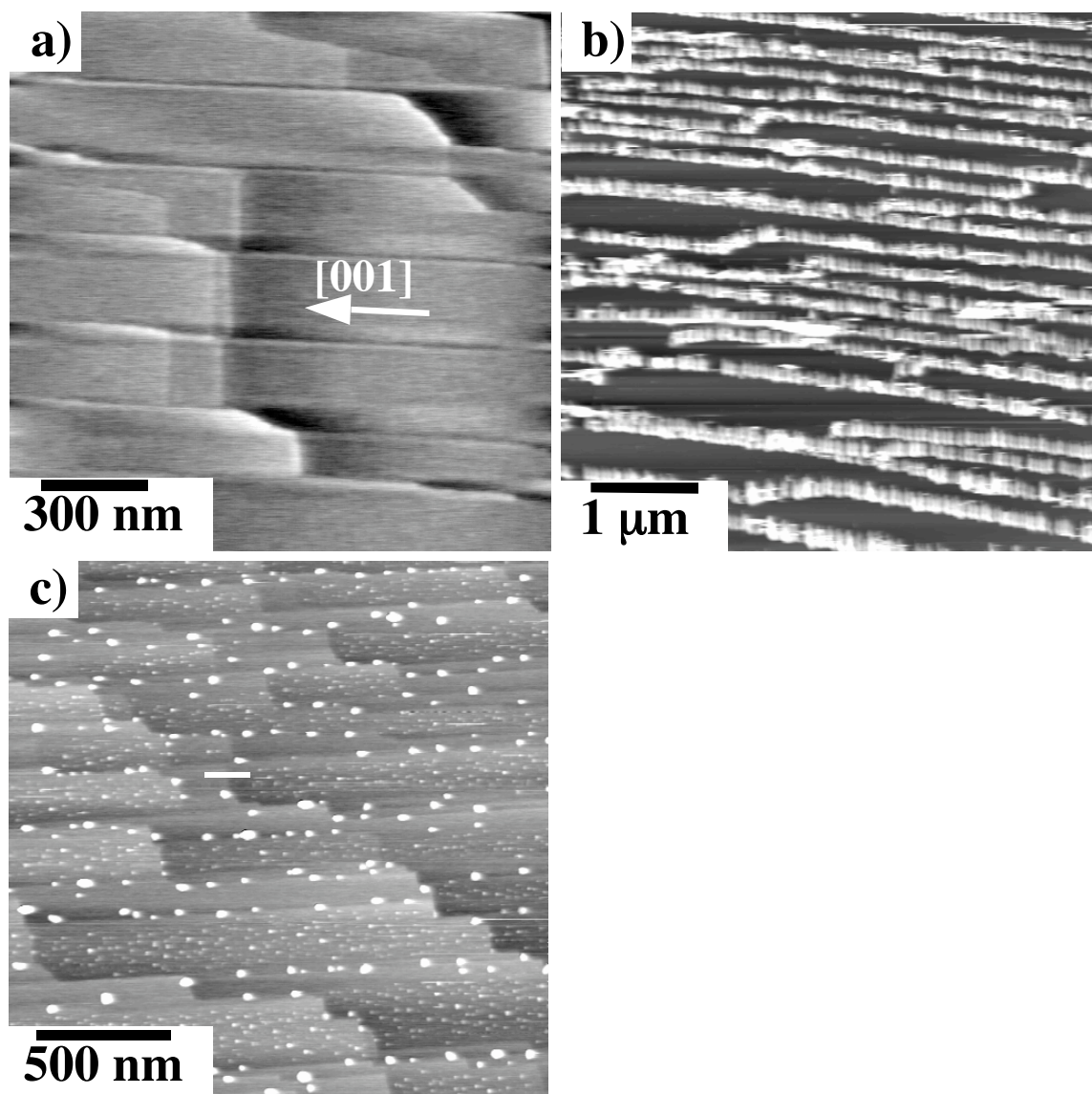


Figure 6.10: Topographic AFM images of the surfaces of (110)-oriented SrTiO₃ single crystals. (a) Before the reactions. (b) A NC-AFM topograph of same surface after illumination in an aqueous AgNO₃ solution. The white contrast corresponds to silver. (c) A different surface after illumination in an aqueous lead acetate solution. The white contrast corresponds to lead oxide deposits. The white line indicates where the data in Figure 6.12 is located. The ranges of the vertical black-to-white contrast in (a) to (c) are 30 nm, 300 nm, and 35 nm, respectively.

crystal prepared in the same way and the results are shown in Figure 6.10c. This image shows that large lead oxide deposits occur, widely spaced, along the step edges and smaller lead oxide deposits accumulate on certain terraces; other terraces are nearly free of the oxidized products.

The (110) surface can also be terminated by two different and oppositely charged polar layers, as

illustrated in Figure 6.11. As with the (111) surface, step height measurements indicate that termination preserving steps separate terraces with the same reactivity while termination changing steps separate terraces with different reactivities (see Figure 6.12).

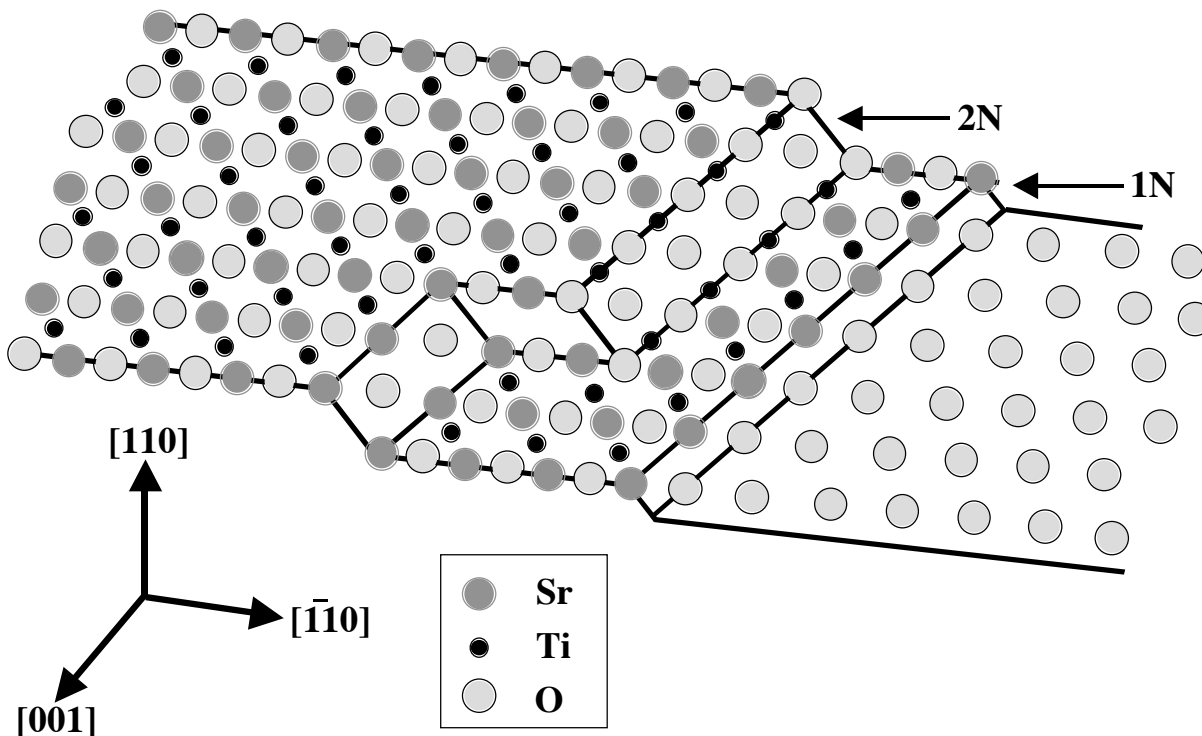


Figure 6.11: Schematic drawing of the SrTiO₃(110) surface terminations. The left hand terrace has a SrTiO⁴⁺ termination. Traversing an even-N step does not change the chemical termination while traversing an odd-N step changes the chemical termination to O₂⁺ (right-hand terrace). Note that the step edges are {100} type. Layer spacing = $\sqrt{2}a/4 = 1.38 \text{ \AA}$.

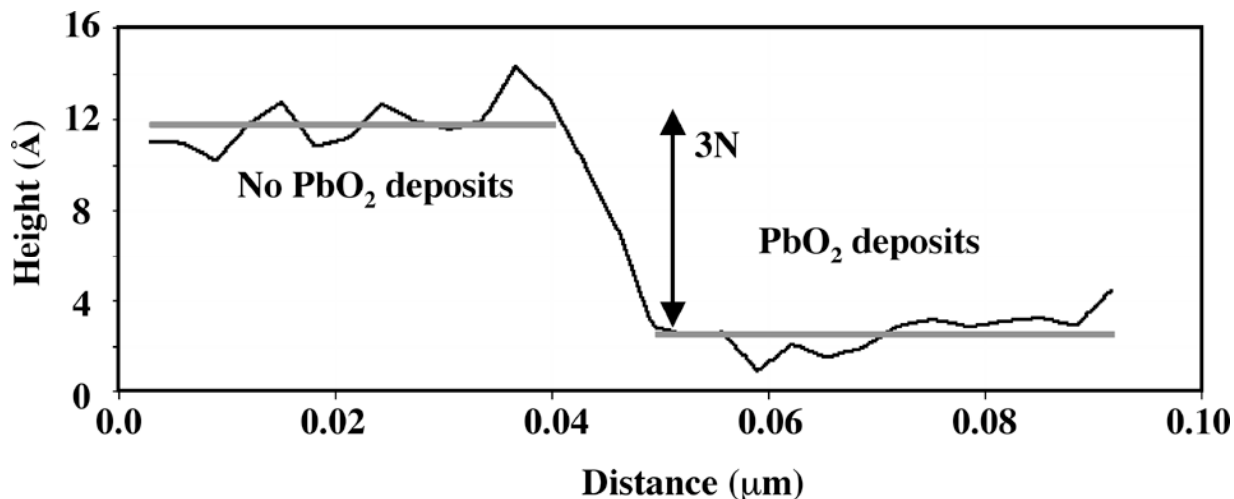


Figure 6.12: Height profile on the SrTiO₃(110) surface (see white line in Figure 6.10) showing how the change in reactivity is related to a change in chemical termination. The terrace on the left contains PbO₂ deposits and is separated by a step of $\sim 3N$ (4.3 Å) from a terrace without PbO₂ deposits.

1.4 Particle Results

Figure 6.13 shows a series of SEM images of SrTiO₃ crystals produced in a KCl flux following the photochemical probe reactions. The images in Figure 6.13a and b show particles produced using the powder from Alfa Aesar (labeled SrTiO₃-1 in Table 4.2) following the silver reduction and lead oxidation reactions, respectively. The overall shape of these particles is similar to the BaTiO₃ particles in Figures 5.6 - 5.8 which is not surprising since they were both cubic perovskites when the particle shape was determined at high temperature in molten KCl. These SrTiO₃ particles are predominately bounded by {100}, {110}, and {111} type planes and the orientations labeled in Figure 6.13a were determined by the symmetry of the particles. It is clear from Figure 6.13a that the {100} faces are active for silver reduction which is consistent with the previous results where the {100} oriented single crystals and the polycrystal grains with orientations near {100} had the highest activity for this reaction. Although not shown, some {111} facets showed some reactivity for Ag reduction but it was not as strong of that of the

{100} facets. In general, the reactivity of the silver particles for silver reduction ranked as {100}>{111}>{110}.

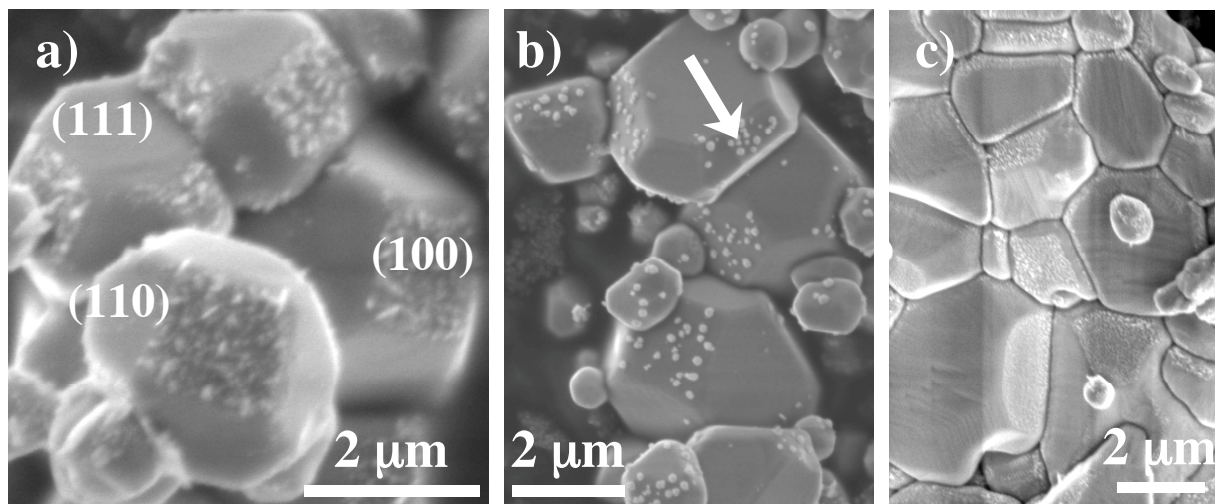


Figure 6.13: SEM images of the faceted SrTiO_3 crystals produced in a KCl flux. (a) Particles produced from the Alfa Aesar powder after silver reduction reaction. White deposits correspond to metallic silver. (b) Particles produced from the Alfa Aesar powder after the lead oxidation reaction. The circular white contrast corresponds to PbO_2 deposits. (c) Agglomerated particles produced from the Cerac powder following the silver reduction reaction.

The reactivity for the lead reaction is not as clear. The lead oxidation reaction yielded inconsistent results in both reactivity (amount of lead oxide deposited) and its apparent orientation dependence. Overall, {110} most consistently had the highest reactivity for this reaction. For example, the lead oxide particles, indicated by the arrow in Figure 6.13b, are deposited on the {110} faces but the orientation assignment on the other SrTiO_3 particles in this image is not as easy. Using particles where the facet orientations are clear, the reactivity of these particles for the oxidation of lead can be ranked as {110}>{111}>{100}.

Figure 6.13c shows an SEM image of an agglomerate of particles that were synthesized using the Cerac powder (see Table 4.2) following the silver reduction reaction. This agglomerate is similar to the others that were found in this batch of crystals but is different from Figures 6.13a

and b. The starting powder was probably agglomerated and faceted in the flux. Therefore, the agglomerates provide an intermediate link between the particle and polycrystal experiments. As shown in Figure 6.13c, silver deposits are located on only some of the facets in a similar way to both of the other particles and polycrystal grains. Although we cannot determine the orientations of the facets that are reactive for silver reduction, there is no reason to believe that the reactivity is any different from the previous experiments where surfaces exposing $\{100\}$ or orientations near $\{100\}$ had the highest reactivity for silver reduction.

1.5 Discussion

For the case of paraelectric SrTiO_3 , it is clear that surface orientation and termination has a significant effect on the photochemical activity. Unlike BaTiO_3 , whose orientation dependent anisotropy in activity was secondary in comparison to the effect of the domain structure, SrTiO_3 shows an obvious anisotropy in reactivity based on orientation. Observations from the SrTiO_3 polycrystals showed that only some facets were active for silver reduction and grains with complex $\{100\}$ facets had the highest activity. The faceted particles were also bounded by some combination of $\{100\}$, $\{110\}$, and $\{111\}$ faces. The reactivity of these particles were ranked as $\{100\} > \{111\} > \{110\}$ for silver reduction and inversely for lead reduction. These results are interesting considering the varying orientation dependence of the rutile's photochemical reactivity depending on the sample form (see Section 2.5). Unlike TiO_2 , SrTiO_3 has practically the same orientation dependent reactivity regardless of sample form. This common reactivity is probably a result of the common reaction conditions and the similar sample preparation.

Results from the SrTiO_3 single crystals were consistent with the observations made in the polycrystal experiments. These observations indicate that the relative photochemical reactivities of SrTiO_3 surfaces depend on both the crystallographic orientation of the surface and, in the case

of the polar surfaces, the composition of the atomic termination layer. Of the three low index SrTiO₃ surfaces, two distinct surface chemistries can be identified for each orientation if we assume bulk terminations and, therefore, there are six distinct possible surfaces. The observed step heights on the single crystals indicate that after the 1200 °C anneal in air, both possible terminations coexist on all three orientations. Our observations show that the nonpolar (100) surface is the most reactive and there is no evidence that the reactivity depends on the composition of the termination layer. On the other hand, for the polar (110) and (111) surfaces, terraces with distinct terminations do have different reactivities. These observations are discussed in more detail below in terms of what is already known, or can be reliably inferred about the SrTiO₃ surfaces.

As mentioned earlier and illustrated in Figures 3.2 and 6.6, the (100) surface of SrTiO₃ can be terminated by either a TiO₂ layer or by a SrO layer. Because calculated energies for these two terminations differed by only 0.2 J/m², Mackrodt [5] predicted that both terminations would coexist and this has proved to be the case [3]. Recent studies of the SrTiO₃ (100) surface composition conclude that the Ti-rich surface is more stable [3, 6-10]. In two of these cases, it was concluded that the surface is composed of TiO₂ with disordered Sr adatoms [7,8]. In these cases, however, the preparation of these surfaces (vacuum annealing) was so completely different from the experiments presented here, that the relevance to the present situation is questionable.

Even though step height measurements demonstrate the coexistence of SrO and TiO₂ terminated terraces, there was no sign of spatially selective reactions; this distinguishes the (100) surface from the (110) and (111) oriented surfaces. In this context, it is worth noting that this is the only one of the three orientations that is terminated by charge neutral layers. Furthermore,

the uniform coverage of reduced Ag on SrTiO₃(100) is similar to observations on the TiO₂(101), the most reactive surface of rutile [11]. While both the TiO₂ terminated SrTiO₃(100) surface and the TiO₂(101) surface reveal five-coordinate Ti atoms with similar Ti-Ti bond distances (3.57Å for TiO₂ vs. 3.905Å for SrTiO₃), the apparent equivalent reactivity of the SrO terminated terraces suggests that the details of the atomic structure on the surface might not be the deciding factor. The terrace termination also has no apparent influence the oxidation reaction, which leaves products dispersed at widely separated positions on this surface. The sparse distribution of products might arise if the reaction (or even the precipitation of the PbO₂) is initiated by defect sites not resolved in the images.

The idealized model of charge neutral SrO and TiO₂ terraces does not seem consistent with the relatively uniform photochemical properties of the SrTiO₃(100) surface. One possibility is that the surface is actually chemically more uniform than expected from the ideal bulk termination model. For example, one study of UHV annealed surfaces indicated more uniform Ti-rich terminations [6]. The assumption that these nonpolar layers are charge neutral might also be overly simplistic. Calculations have shown that these “non-polar” surfaces can actually possess a nonzero dipole moment perpendicular to the surface that results from incomplete charge transfer from the metals to the oxygen, or different vertical relaxations of the surface ions [12,13]. Goniakowski and Noguera refer to such surfaces as “weakly-polar” [12]. While a uniform dipolar field would be consistent with the present observations, the calculations do not agree on the sign or magnitude of the polarization.

In contrast to the (100) surface, the reaction products observed on the (111) surface are selectively deposited on specific terraces. As illustrated in Figures 3.5 and 6.8, the (111) surface can be terminated by a positively charged Ti layer or a negatively charged SrO₃ layer; the step

height measurements indicate the simultaneous presence of these terminations and the accumulation of products on terraces of the same character. The observation that the terraces that are inert for reduction comprise a minority fraction of the total area, and are comparable in area to the terraces that are active for oxidation, suggests that the reduction and oxidation products accumulate on terraces with complementary charges. Previous studies of the $\text{SrTiO}_3(111)$ surface indicate that the surface has a higher concentration of Ti than Sr [14-16]. These reports are consistent with the simultaneous presence of the Ti and SrO_3 terraces, with the Ti termination being predominant. Assuming this to be the case on the surfaces that we have examined, then the terraces that promote reduction are the predominant, positively charged, Ti terminated terraces and the terraces that promote oxidation are the negatively charged SrO_3 surfaces. This assignment, which is difficult to experimentally confirm, would be entirely consistent with the previous observations of BaTiO_3 (see Chapter 5) where the likely mechanism for this selective reactivity is that dipolar fields drive photogenerated charge carriers to oppositely charged surfaces. This same explanation can be applied to the $\text{SrTiO}_3(111)$ surface, except that in this case, the dipolar fields are created by charged surface termination layers.

The reactivity of the $\text{SrTiO}_3(110)$ surface also shows a strong surface structure sensitivity and that polar surface terminations are responsible for the accumulation of oxidation products on some, but not all terraces. As illustrated in Figures 3.4 and 6.11, the surface can be terminated by an O layer with a negative charge or by a SrTiO layer with a positive charge. Again, from the current data, it is not possible to determine which of these is responsible for the oxidation reaction. However, by analogy with the BaTiO_3 observations, the negatively charged oxygen terrace is the likely candidate. It should also be noted that all of the (110) terraces are apparently inert for reduction. The reduction products instead accumulate only on the step edges.

Oxidation products are also found both on step edges and (110) terraces, but with a different morphologies; they are larger and more widely dispersed on the step edges.

The reactivity of the inclined portion of the steps is easily explained if they have the (100) orientation. Based on the directions of the steps, we know that the orientation of the inclined portion of the surface is in the $\langle 100 \rangle$ zone. Since these steps are only a few Å high, the most likely orientation is (100), as illustrated in Figure 6.11. Therefore, the extensive Ag reduction that occurs on these steps is entirely consistent with observations of Ag reduction on the (100) surface. Moreover, oxidation products dispersed along the steps at irregular intervals are also consistent with observations on the (100) surface. Considering the fact that the majority of the reaction products accumulate at step sites, the ideal (110) surface is the least reactive of the orientations that have been examined.

It is interesting to consider the anisotropy in the reactivity in terms of strontium titanate's band structures. Electrons with wave vectors in the [100] direction are at the lowest point in the conduction band and should be easiest to remove from planes perpendicular to [100]. Conversely, holes with wave vectors in the [110] direction are at the highest point in the valance band and holes should be easiest to remove at the planes perpendicular to this direction. Therefore, it is not surprising that {100} oriented surfaces are the most reactive for reduction and the {110} surfaces are most active for oxidation. More research would be necessary to determine if the anisotropic reactivity based on the band structure is important for other photocatalysts.

1.6 Summary and Conclusions

The photochemical properties of SrTiO₃ depend on both the crystallographic orientation of the surface and the composition of the atomic termination layer. The charge neutral (100)

surface is the most reactive, the (110) surface is the least reactive, and the (111) surface has an intermediate reactivity. Two different surface terminations coexist on each of the low index single crystal surfaces. No difference in the reactivity of the two (100) terminations was observed. However, on the polar (111) and (110) surfaces, the reduction and oxidation reactions occur on terraces with different terminations and opposite charges; this leads to a non-uniform distribution of reaction products. These observations lead to the conclusion that dipolar fields arising from surface domains with uniform polar terminations influence the transport of photogenerated electrons and holes and promote spatially selective oxidation and reduction reactions.

1.7 References

- (1) J. Cahn and C. Handwerker, *Mat. Sci. Eng. A*, **162** (1993) 83.
- (2) J.L. Giocondi and G.S. Rohrer, *Mater. Res. Soc. Proc.*, in press.
- (3) G. Koster, B.L. Kropman, J.H.M. Rijnders, and D.H.A. Blank, *Appl. Phys. Letters*, **73**[20] (1998) 2920-22.
- (4) H. Bando, Y. Aiura, Y. Haruyama, T. Shimizu, and Y. Nishihara, *J. Vac. Sci. Technol. B*, **13**[3] (1995) 1150-54.
- (5) W.C. Mackrodt, *Phys. Chem. Minerals*, **15**[3] (1988) 228-37.
- (6) Q.D. Jiang and J. Zegenhagen, *Surface Science*, **425**[2-3] (1999) 343-54.
- (7) T. Kubo and H. Nozoye, *Phys. Rev. Letters*, **86** [9] (2001) 1801-04.
- (8) P.A.W. Van der Heide, Q.D. Jiang, Y.S. Kim, and J.W. Rabalais, *Surface Science*, **473**[1-2] (2001) 59-70.
- (9) G. Koster, G.J.H.M. Rijnders, D.H.A. Blank, and H. Rogalla, *Physica C*, **339**[4] (2000) 215-30.

- (10) G. Charlton, S. Brennan, C.A. Muryn, R. McGrath, D. Norman, T.S. Turner, and G. Thornton, *Surface Science*, **457**[1-2] (2000) L376-80.
- (11) J.B. Lowekamp, G.S. Rohrer, P.A. Morris Hotsenpiller, J.D. Bolt, and W.D. Farneth, *J. Phys. Chem. B*, **102**[38] (1998) 7323-27
- (12) J. Goniakowski and C. Noguera, *Surface Science*, **465**[2] (1996) L657-62.
- (13) E. Heiffets, E.A. Kotomin, and J. Maier, *Surface Science*, **462**[1-3] (2000) 19-35.
- (14) S. Sekiguchi, M. Fujimoto, N.-G. Kang, S. Koizumi, S.-B. Cho, and J. Tanaka, *Jpn. J. Appl. Phys.*, **37**[7] (1998) 4140-43.
- (15) S. Sekiguchi, M. Fujimoto, M. Nomura, S.-B. Cho, J. Tanaka, T. Nishihara, N.-G. Kang, and H.-H. Park, **108**[1- 4] (1998) 73-79.
- (16) W.M. Sigmund, M. Rotov, Q.D. Jiang, J. Brunen, J. Zegenhagen, and F. Aldinger, *Appl. Phys. A*, **65**[2] (1997) 219-20.

7 The Photochemical Reactivity of Materials with Anisotropic Tunnel and Layer Structures

7.1 Introduction

The experiments presented in Chapters 5 and 6 have shown how internal electric fields can separate the oxidation and reduction halves of photochemical reactions and that perovskites have orientation dependent photochemical reactivity. It has been hypothesized that materials with tunnels and layers have structural elements that promote the separation of photogenerated carriers and, therefore, also, lead to the spatial separation of oxidation and reduction half reactions. Most of these oxides are also polar. The purpose of this chapter is to report the results of experiments to test the relationship between the crystallography of BaTi_4O_9 and $\text{Sr}_2\text{M}_2\text{O}_7$ ($\text{M} = \text{Nb, Ta}$) surfaces and their photochemical reactivity over a wide range of orientations.

7.2 Pentagonal Prism Structure

7.2.1 BaTi_4O_9 Results

The topographic AFM image in Figure 7.1a shows the surface of the BaTi_4O_9 polycrystal before any reaction. In general, most surfaces are smooth so that the macroscopic surface orientation represents the actual surface orientation. In some cases (for example, the grain labeled 7), the surfaces are faceted and the actual facets bounding the surface are not the same as the macroscopic surface orientation. Of the more than 50 grains examined, approximately 25 % are faceted. The distribution of faceted orientations is illustrated in Fig. 7.2.

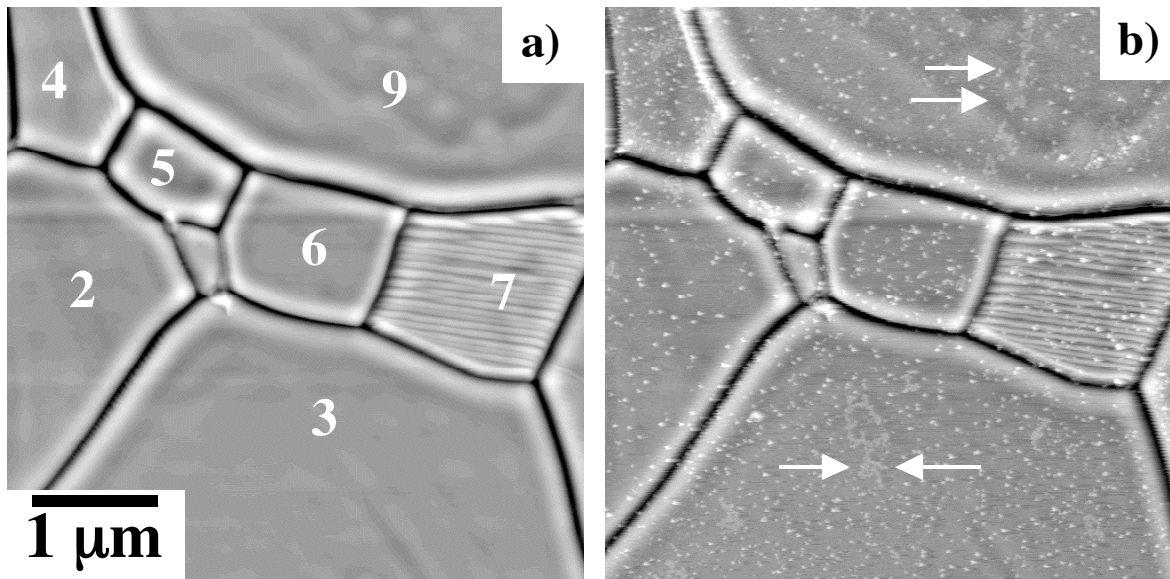


Figure 7.1: Topographic AFM images of the surfaces of crystallites in a BaTi_4O_9 polycrystal before and after illumination in a lead acetate solution. (a) Contact AFM image of eight grains (2 – 9) before the reaction. (b) NC-AFM image of the same area following the reaction. The areas of white contrast correspond to PbO_2 deposits. Continuous networks of reaction products are indicated by the arrows. The vertical black-to-white contrast in (a) and (b) are 15 nm and 20 nm, respectively.

When exposed to light in the presence of AgNO_3 , the surfaces of all of the grains were coated by silver, with no detectable orientation dependence. On the other hand, the reduced rate of the lead oxidation process allowed spatial variations to be detected. The topographic AFM image in Figure 7.1b shows the same area as Figure 7.1a after the photochemical oxidation of lead. The oxidized lead deposits appear as the white contrast in the AFM image. Some variation in the rate of lead oxidation is obvious. For example, grains labeled 4 and 6 have more deposits than the grains labeled 2 and 5. Similar observations were made on more than 50 grains, and the reactivities are classified as high (> 18 deposits / μm^2), medium (10 - 18 deposits / μm^2), or low (< 10 deposits / μm^2). These results are summarized in Figure 7.3 [1].

There are several noteworthy features of these results. First, the differences in the amount of reaction products found on different grains is not as large as observed in previous studies of

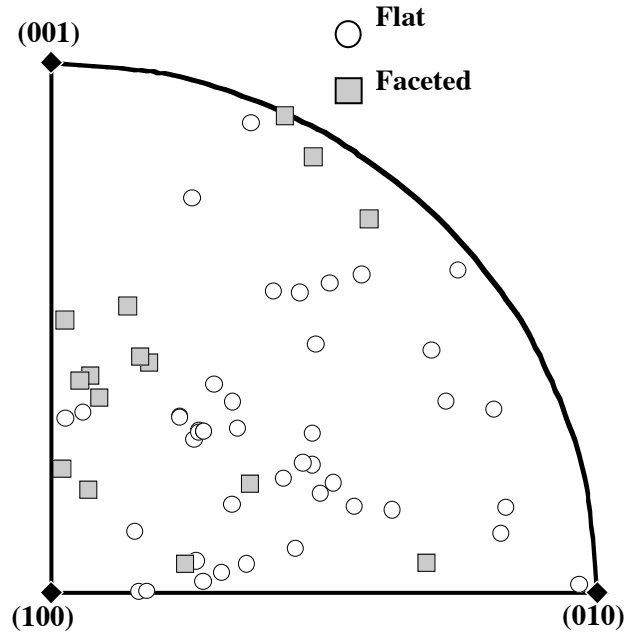


Figure 7.2: An inverse pole figure plotted on the standard stereographic triangle for orthorhombic crystals, showing the orientations of smooth and faceted grains for BaTi_4O_9 . The black diamonds indicate the locations of low index orientations.

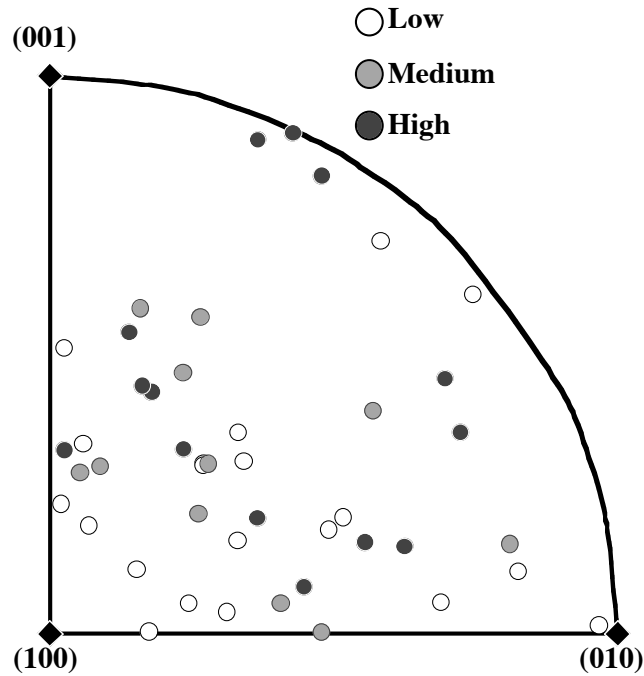


Figure 7.3: An inverse pole figure plotted on the standard stereographic triangle for orthorhombic crystals, showing relative reactivity of each BaTi_4O_9 grain for the oxidation of lead. The black diamonds indicate the locations of low index orientations.

TiO₂ [2] and the SrTiO₃ (see Chapter 6). In these cases, some grains were completely covered with reaction products while others were nearly free of products. By comparison, this reaction exhibits little anisotropy. Second, the differences in the reactivity within a single grain are almost as large as the differences between grains. For example, the arrows in Figure 7.1b point to continuous networks of lead oxide deposits while the remainder of deposits on the same grain are isolated. Finally, when the orientation dependence of the reactivity is examined, there are no distinct trends. Similar orientations can have very different reactivities and there are no clear trends in the plot of reactivity versus orientation. Finally, the data in Figures 7.2 and 7.3 also indicate that the rate of reaction is not correlated to either the presence of smooth surfaces or facets on the grains.

1.1.2 *BaTi₄O₉ Discussion*

The experiments described here were carried out to determine if the reactivity of BaTi₄O₉ was correlated to the orientations of the tunnels in the structure. The structure is illustrated in Figure 3.9, which shows that the tunnels are oriented along the [010] axis of the crystal. This means that crystals exposing (010) planes reveal the maximum number of tunnel openings while those crystals with orientations along the line connecting (100) and (001) are parallel to the tunnel direction (see Figure 7.2 or 7.3). The reactivity does not seem to be correlated with these special orientations. This can be seen most clearly in Figure 7.4. The surface of grain 5 is nearly perpendicular to the [010] direction so that this crystal exposes the highest density of tunnel sites. On the other hand, grains 7 and 2 expose surfaces that are nearly parallel to the tunnels. The AFM image in Figure 7.1b indicates that reactivities of grains 5, 7, and 2 are not significantly different.

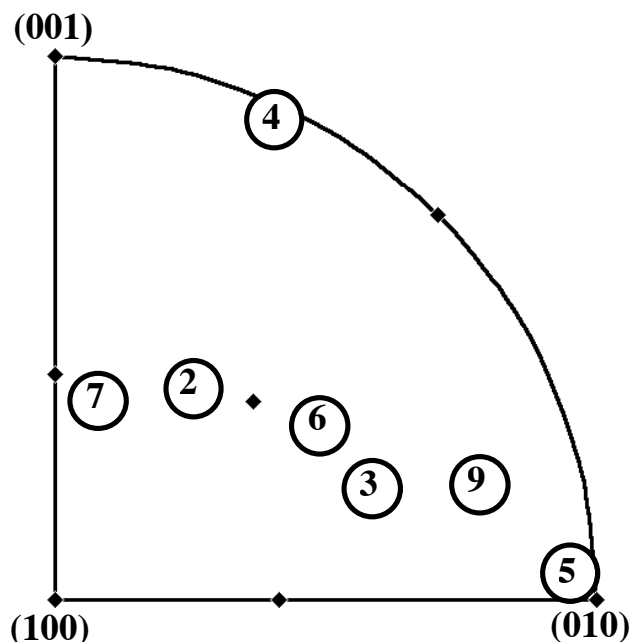


Figure 7.4: Inverse pole figure illustrating the orientations of the grains in Figure 7.2. Note that the surface of grain 5 is nearly perpendicular to the tunnels.

The results from both the reduction and oxidation experiments refute the hypothesis that sites associated with the tunnels in some way spatially isolate either the reduction or oxidation half reactions. The original proposal was that distortions in the octahedral units surrounding the pentagonal tunnels create large dipole moments that are directed towards the center of the tunnels and it is these internal electric fields that separate the photogenerated charges [3, 4]. The proposal for charge separation by dipolar fields is not unreasonable. As mentioned earlier, previous studies of the ferroelectric $(\text{Pb,K})_2\text{Nb}_2\text{O}_6$ indicated that poling influences its photochemical activity [5] and the BaTiO_3 experiments presented in Chapter 5 show that polarizations in ferroelectric domains influence the transport of photogenerated carriers and lead to the spatial separation of reaction products [6, 7]. It was also shown in Chapter 6 that the dipolar fields associated with polar surface terminations of the non-ferroelectric SrTiO_3 influence the transport of carriers to the surface and this also leads to a spatial separation of the

photochemical oxidation and reduction reactions [8]. Since localized variations in the reactivity on single grains observed in the current study are similar to variations observed on SrTiO_3 surfaces, it is possible that localized changes in the surface termination are responsible for the inhomogeneous distribution of oxidized products on BaTi_4O_9 surfaces.

1.3 Layered (110) Perovskite Structure

1.3.1 $\text{Sr}_2\text{Ta}_2\text{O}_7$ Results

A NC-AFM topograph of a typical area after the reaction is shown in Figure 7.5. The circular white contrast corresponds to silver deposits. The first feature to note is that the majority of the grains in this area are faceted. In fact, approximately 80% of the grains examined in this study have faceted surfaces (see Figure 7.6). Therefore, in most cases, the planes that bounded the surface are actually inclined with respect to the macroscopic surface normal.

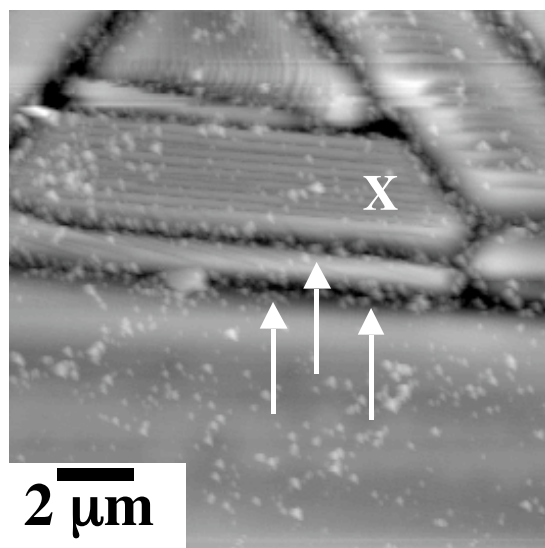


Figure 7.5: NC-AFM topograph of a typical area of a $\text{Sr}_2\text{Ta}_2\text{O}_7$ polycrystal after illumination in a silver nitrate solution. The areas of white contrast correspond to Ag^0 deposits. The white arrows indicate Ag^0 deposits accumulated in grain boundaries. “X” denotes a grain with inhomogeneous amount of Ag^0 . The vertical black-to-white contrast is 50 nm.

It is also obvious from Figure 7.5 that the silver islands are not deposited uniformly within the individual grains. The grain marked “X” in Figure 7.5 is probably the best example of this phenomenon. There are silver deposits concentrated on the left hand side of this grain while the remainder of the grain has relatively few silver deposits. Also notice how silver deposits have accumulated in the grain boundary grooves as indicated by the white arrows. Although this deposition does not occur at all grain boundaries, it is frequently observed. Overall, the observed differences in the amount of reaction products found on different grains is similar to that found on the BaTi_4O_9 grains but not as large as observed for TiO_2 or SrTiO_3 . In these studies, some grains were completely covered with reaction products while others were nearly free of products. By comparison, this reaction exhibits little anisotropy.

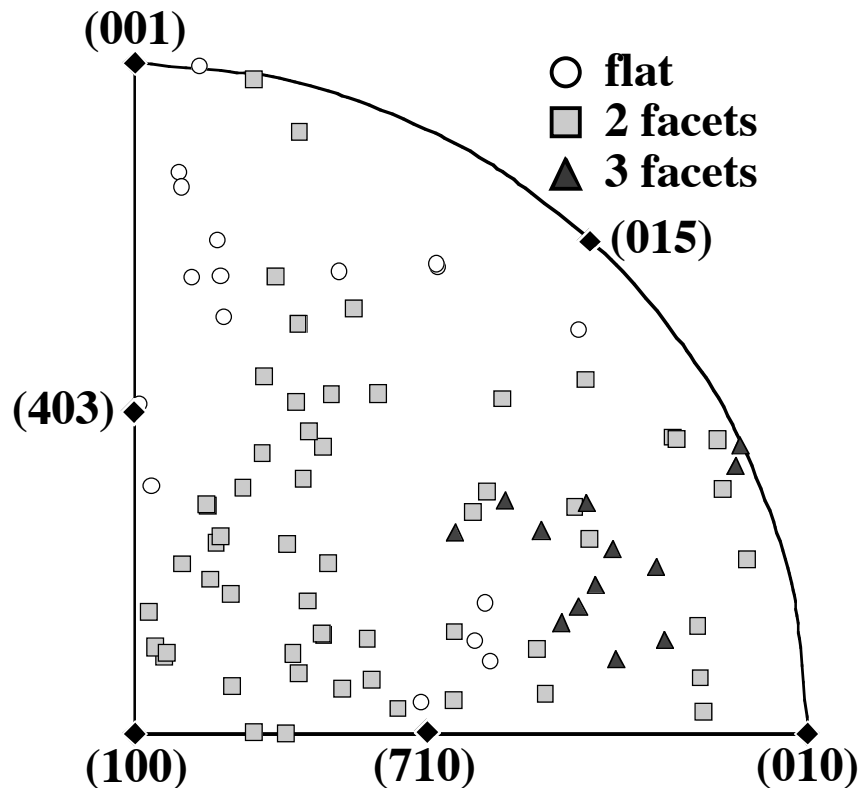


Figure 7.6: An inverse pole figure plotted on the standard stereographic triangle for orthorhombic crystals, showing the orientations of smooth and faceted grains for $\text{Sr}_2\text{Ta}_2\text{O}_7$. The black diamonds indicate the locations of low index orientations

The activity of individual crystallites was estimated by counting the number of silver deposits on a representative area of each grain. In cases where the silver coverage was inhomogeneous, two representative areas were counted and averaged. The silver islands that deposited in the grain boundary grooves were not counted. Figure 7.7 is a plot of the activity of each grain examined as a function of the surface orientation. All grains were placed into one of three categories: low (0 - 3 deposits/ μm^2), medium (3 - 6 deposits/ μm^2), or high (6 - 23 deposits/ μm^2). Grains with high activity typically had an even, dense, homogeneous coverage of silver. Low activity grains usually had a few deposits that were evenly spread across the surface. Most grains with an inhomogeneous silver coverage fell into the medium category. The grains that were most reactive are closer to (010) than the three other low index directions. In fact, most

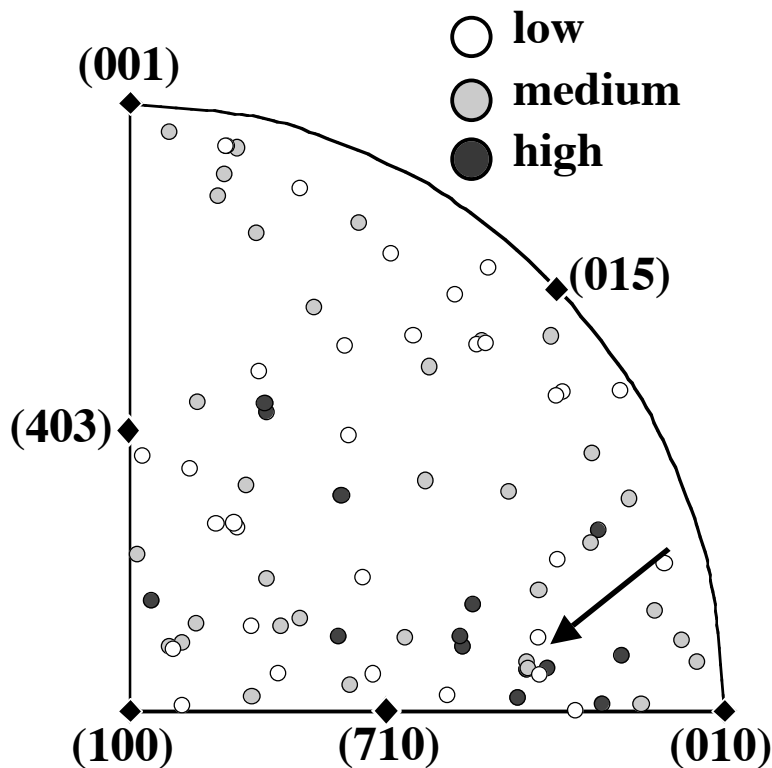


Figure 7.7: Orientation-activity relationship for $\text{Sr}_2\text{Ta}_2\text{O}_7$ surfaces plotted on the standard stereographic triangle for orthorhombic crystals. The arrow indicates a group of grains with nearly the same orientation but different activities.

of these grains lie between (010), which is structurally analogous to the cubic perovskite (110) plane, and (710) and (015) which have a similar structure to the cubic perovskite (100) plane. It should also be noted that there are several incidences of grains with nearly the same orientation that have very different activities (see arrow in Figure 7.7). The number of examples of these inconsistencies is larger than expected from experimental error and presumably arises from the inhomogeneous distribution of reaction products.

1.1.2 $Sr_2Nb_2O_7$ Polycrystal Results

Figure 7.8 is a plot of the distribution of faceted orientations for $Sr_2Nb_2O_7$ and shows that most of the grains are faceted. This can also be seen in Figure 7.9 which shows two NC-AFM images of the surface following the lead oxidation reaction. It is immediately clear that each of

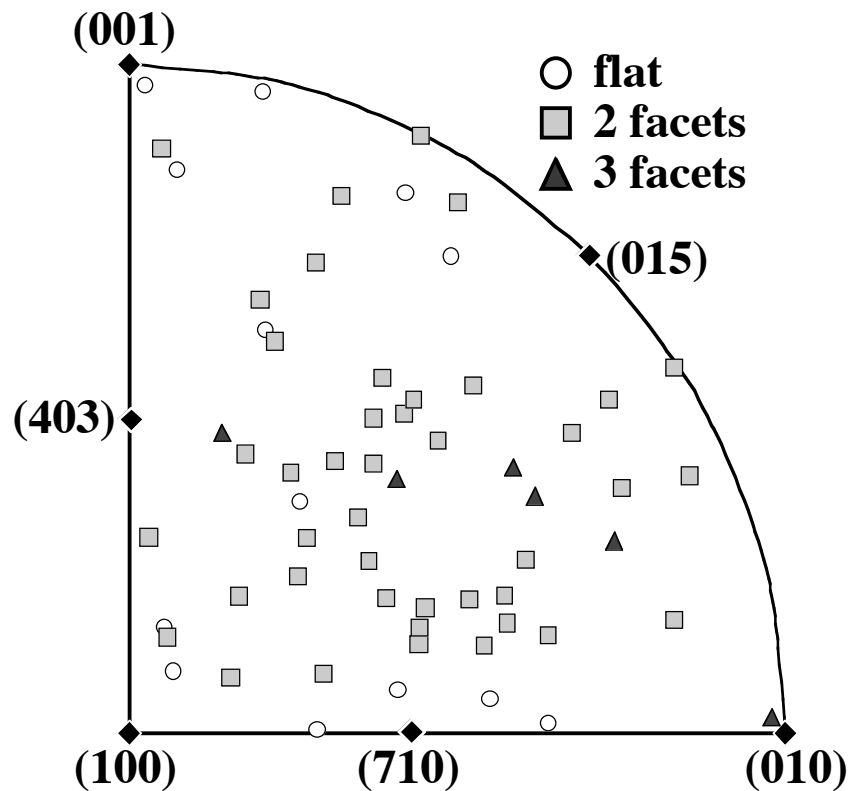


Figure 7.8: An inverse pole figure plotted on the standard stereographic triangle for orthorhombic crystals, showing the orientations of smooth and faceted grains for $Sr_2Nb_2O_7$. The black diamonds indicate the locations of low index orientations.

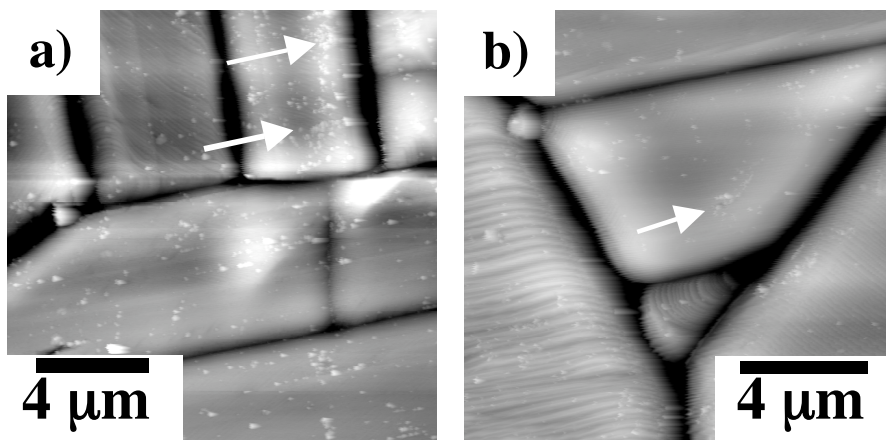


Figure 7.9: AFM image of the $\text{Sr}_2\text{Nb}_2\text{O}_7$ surface following the lead oxidation reaction. The arrows in this image indicate an example of the inhomogeneous distribution of lead oxide within individual grains.

the grains in this image has an inhomogeneous distribution of lead oxide and this was characteristic of most of the grains that were observed. The arrows in Figure 7.9 indicate an example of this inhomogeneous distribution. The number of lead deposits also did not vary much from grain to grain which can be seen when the amounts of oxidized lead are plotted as a function of orientation (Figure 7.10). This plot shows that there is not a strong orientation dependence on the reactivity. Further, since no orientations near (001) (\square to P_s) were observed, it is not possible to determine if the dipolar field effect influences the reactivity.

It has previously been reported that it is necessary to use a NiO promoter with $\text{Sr}_2\text{Nb}_2\text{O}_7$ to observe any activity for water photolysis [9,10] and, in our experiments, we find that the promoter is also required for the silver reduction reaction. Figure 7.11a is a topograph of the surface of a NiO-promoted polycrystal. The white contrast in this image corresponds to NiO (see arrows). The NC-AFM image in Figure 7.11b is of the surface in Figure 7.11a after the silver reduction reaction. New areas of light contrast correspond to Ag deposits. Notice that the grain marked “X” in Figures 7.11a and 7.11b had no noticeable NiO on the surface yet, it still

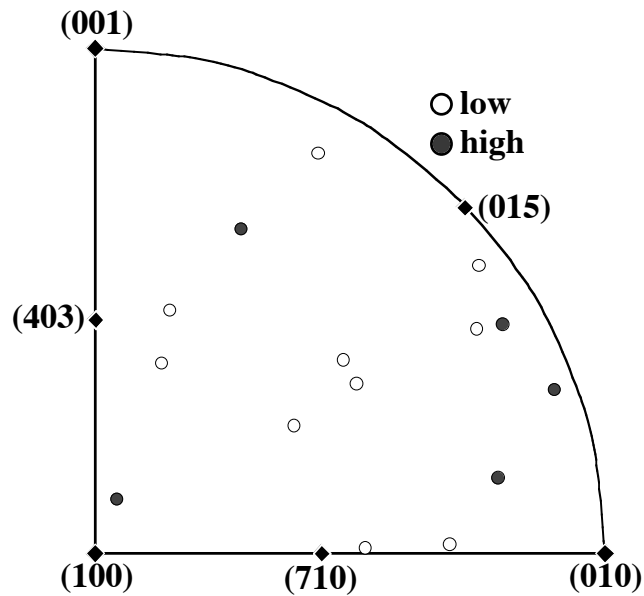


Figure 7.10: An inverse pole figure plotted on the standard stereographic triangle for orthorhombic crystals, showing the relative reactivity individual $\text{Sr}_2\text{Nb}_2\text{O}_7$ grains for the oxidation of lead. The black diamonds indicate the locations of low index orientations.

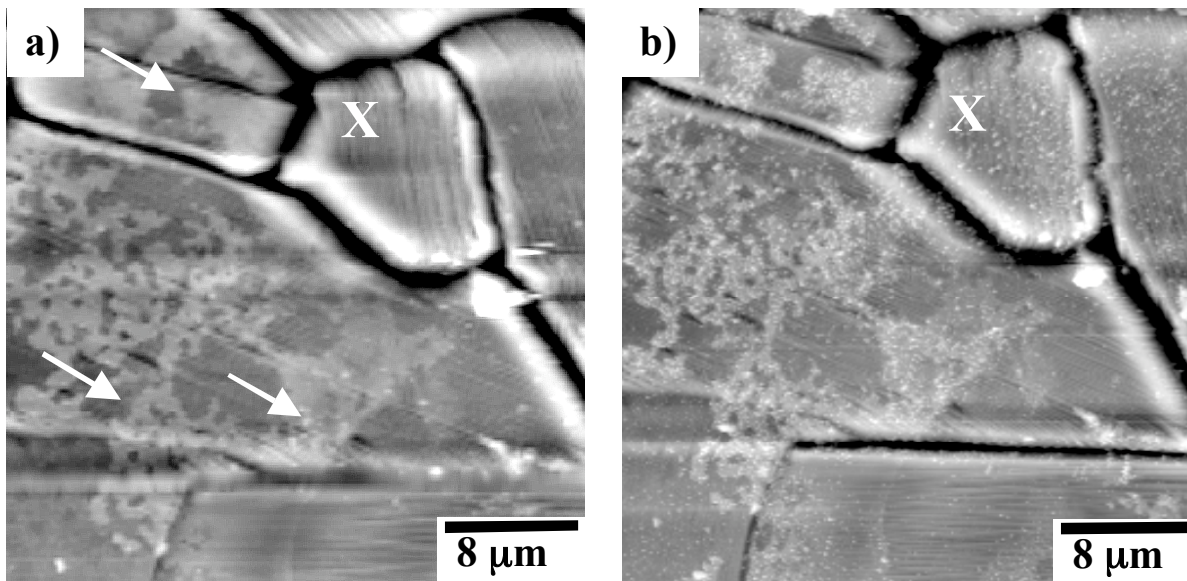


Figure 7.11 NC-AFM topographs the $\text{Sr}_2\text{Nb}_2\text{O}_7$ crystallites for reduction. (a) Area on a polycrystalline sample following the addition of a NiO promoter and the associated pretreatment. The areas of white contrast correspond to NiO deposits (see arrows). (b) The same area as in (a) following the reduction of silver. The new areas of white contrast correspond to Ag^0 deposits. Grain “X” appears to have no NiO in (a) but has silver deposits in (b). The vertical black-to-white contrast in (a) and (b) are 500 nm, and 500 nm, respectively.

had silver deposits after the reaction. We found that grains with high coverage of NiO did not necessarily have the highest amounts of silver. Experiments on the promoted surfaces were complicated by the fact that granular NiO and Ag are indistinguishable in AFM images. The amounts of silver were estimated from the most reliable images when the before and after images were easily compared and large differences could be measured. The results of this analysis are presented in Figure 7.12. This plot of reactivity with respect to orientation also shows that that the highest reactivity surfaces are near the line connecting (100) and (010).

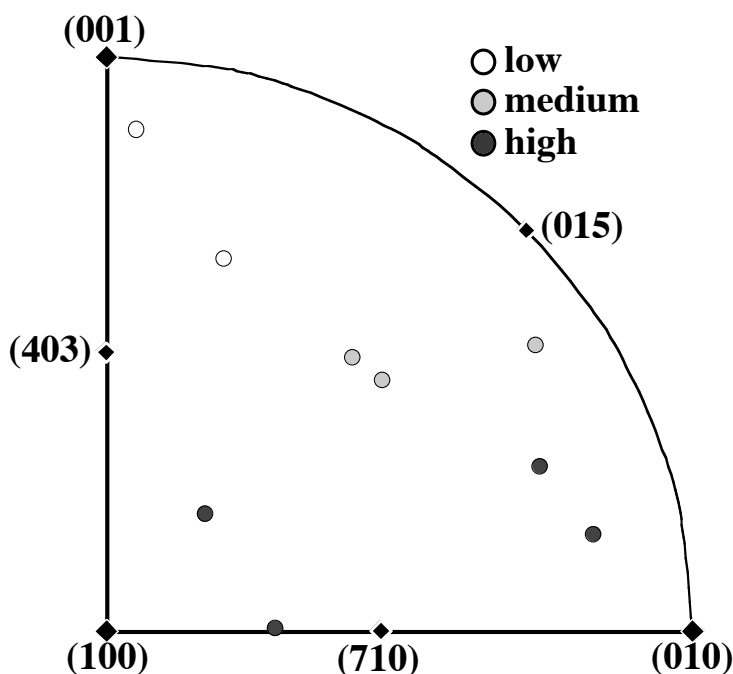


Figure 7.12: An inverse pole figure plotted on the standard stereographic triangle for orthorhombic crystals, showing the relative reactivity of NiO-promoted $\text{Sr}_2\text{Nb}_2\text{O}_7$ grains for the reduction of silver. The black diamonds indicate the locations of low index orientations.

1.1.3 $\text{Sr}_2\text{Nb}_2\text{O}_7$ Particle Results

Figure 7.13 shows images of the as-prepared $\text{Sr}_2\text{Nb}_2\text{O}_7$ particles. The majority of particles are found in agglomerates containing both large, thin platelet particles with high aspect ratios (large face parallel to (010)) and smaller, more equiaxed particles. The majority of crystals that showed reactivity for silver reduction (no particles were active for lead reduction) were the larger

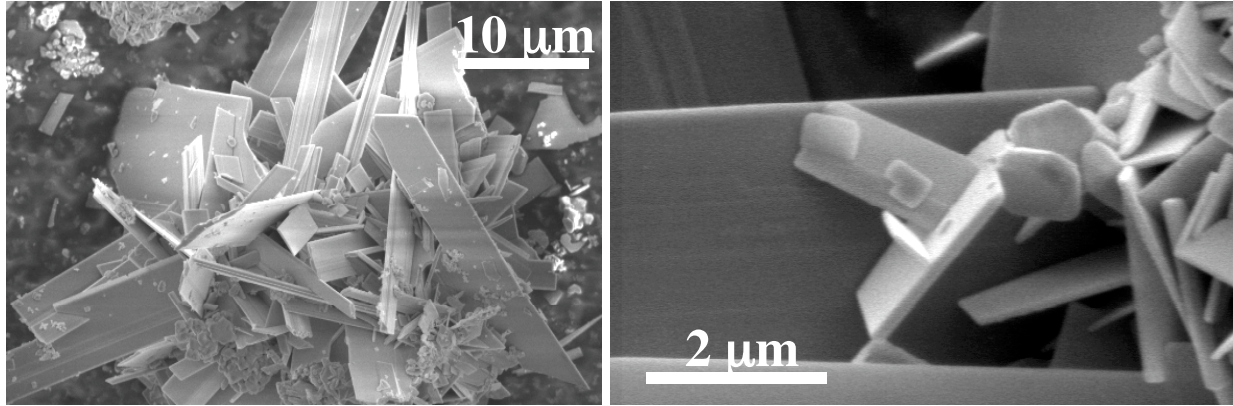


Figure 7.13: Faceted $S_2Nb_2O_7$ crystals prepared in a KCl flux.

particles. However, it should also be recognized that these crystals are also more easily observed.

The images in Figure 7.14 show the $Sr_2Nb_2O_7$ particles after the silver reduction reaction carried out on carbon tape for 45 s (see Section 4.3.1). The majority of silver deposits are located at the step edges that are along the long direction of the large crystals. OIM orientation measurements of these particles show that the steps are directed along the [100] direction. Therefore, the most likely orientation of the step edge is either (001) or (015), which is similar to cubic perovskite (100) and may be stable with respect to faceting (see Figure 7.10).

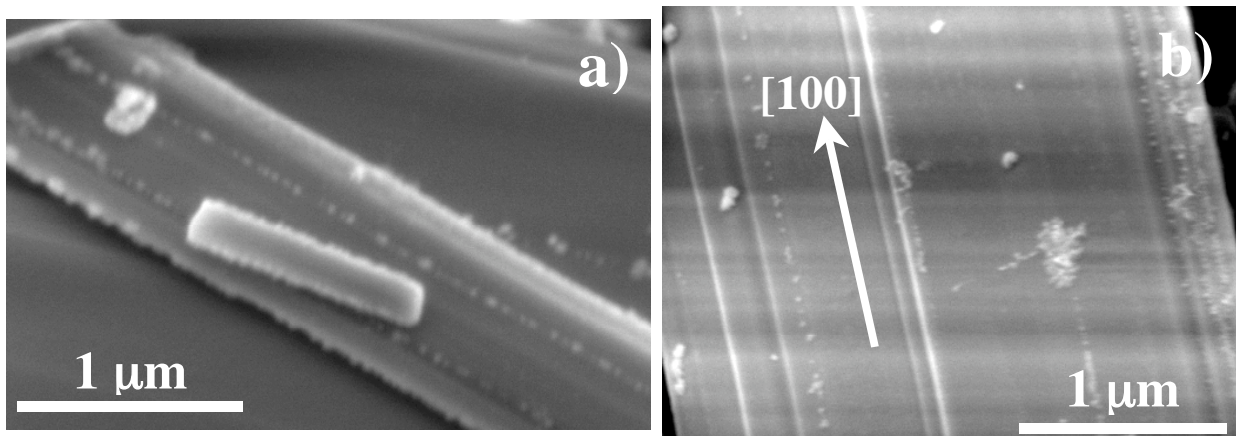


Figure 7.14: SEM images of faceted $S_2Nb_2O_7$ crystals following the silver reduction reaction (45 sec, 400 W). The (010) plane is the large face of these plates. These images all show silver deposited along [100] step edges.

Considering its high water photolysis efficiency, the relatively low reactivity of $\text{Sr}_2\text{Nb}_2\text{O}_7$ was surprising. This motivated a second attempt at the silver probe reaction using different experimental conditions. The experiment consisted of a suspension of particles in a continuously stirred, 0.0115 M aqueous AgNO_3 solution contained in a Pyrex reaction vessel. A water-cooled quartz inner irradiation cell (450 W high-pressure Hg lamp) was suspended into the bath. The reactor was evacuated and filled with Argon three times and then Ar was bubbled through the suspension for the remainder of the experiment. The particles were illuminated for 45 minutes, filtered, rinsed with deionized water, and dried.

Figure 7.15 shows two SEM images following the silver reaction. It is immediately obvious that the reactivity is much more extensive than was observed in the previous experiment (see Figure 7.14). This difference in reactivity could be a result of the slightly higher lamp power, the combination of a more dilute silver solution with a longer reaction time, or the decreased amount of dissolved oxygen in solution. The particles shown in Figure 7.15 also show a stronger orientation-based reactivity. The images show that not all of the apparently identical steps are reactive and that the reactivity is not even constant along the length of a single step. Figure 7.15a shows a particle with reactivity only along the long edges of the particle. The arrows in this image indicate how the silver deposits alternate between opposing edges. In other words, when the upper edge is reactive the lower edge is not and vice versa. As mentioned earlier, these edges are most likely to be bounded by either (001) or (015) planes. The reactivity shown in Figure 7.15a is best explained by these edges having the (001) orientation because the normal to this plane is parallel to the spontaneous polarization direction. One can imagine that the presence of the 180° domain boundaries could create this type of alternating reactivity, in a way analogous to the 180° domain boundaries in BaTiO_3 .

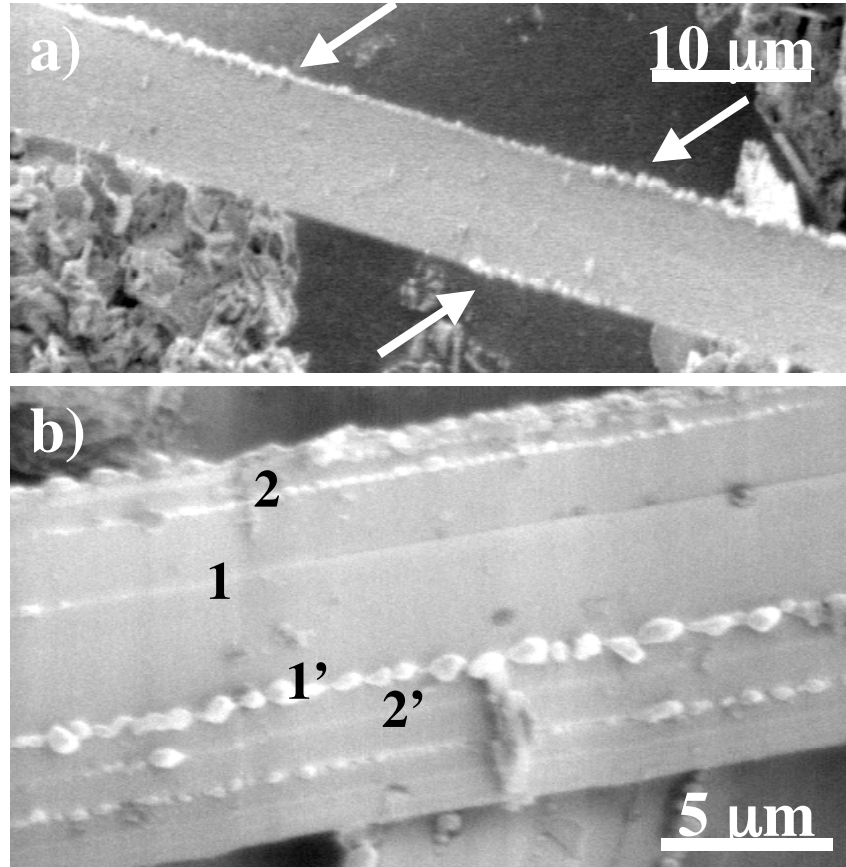


Figure 7.15: SEM images of faceted $S_2Nb_2O_7$ crystals following the silver reduction reaction (45 min, 450 W) using an accelerating voltage of 1 kV. (a) Arrows shows silver deposits alternating along the opposing long edges of the crystal. (b) Numbers indicate opposing terraces with different reactivity.

The reactivity shown in the image in Figure 7.15b can also be explained by the presence of dipolar fields from ferroelectric domains. The numbers in this image indicate opposite steps on the same terrace. For example, 1 and 1' indicate an unreactive and reactive step, respectively. The reactivity of this terrace can be explained if the direction of the spontaneous polarization points from 1 to 1'. Similarly, if the spontaneous polarization points from the unreactive 2' edge to the reactive 2 edge, the reactivity of this terrace can be explained. Therefore, a 180° domain wall lies within the (010) plane between terrace 1 and 2. Another potential explanation for this reactivity is that the opposing step edges are bounded by oppositely charged chemical

terminations and the associated dipolar field is the source of the reactivity difference. However, since this compound is a known ferroelectric with its polarization in the [001] directions, the domain structure is a more likely explanation for the inhomogeneous distribution of reaction products.

1.1.4 Discussion

The polycrystal results illustrate that both the oxidation and reduction reactions are slightly favored on surfaces with orientations between (010), (710), and (015). In other words, within the resolution of our experiment, the oxidation and reduction reactions occur predominantly on the same crystallographic planes. The differences in the reactivities of different orientations were on the order of differences in the reactivity within single grains and are similar to the reactivity of BaTi_4O_9 . The significant anisotropies previously observed in TiO_2 and SrTiO_3 are not detected here. The more isotropic reactivity of these layered compounds was unexpected. Reaction conditions and sample preparation most likely play an important role in this difference. Typical photolysis experiments are carried out in deaerated solutions on promoted and pretreated catalysts. In fact, the faceted particle experiment on $\text{Sr}_2\text{Nb}_2\text{O}_7$ in a deaerated silver solution showed that these conditions revealed an apparent orientation dependent reactivity.

In the case of ferroelectric $\text{Sr}_2\text{Nb}_2\text{O}_7$, it has also been proposed that internal fields help separate the photogenerated charges [10]. This hypothesis is reasonable given the observation that for BaTiO_3 the dipolar fields associated with the ferroelectric domains do, in fact, separate the charges and, therefore, the oxidation and reduction half reactions. If dipolar fields are the important charge separation mechanism for $\text{Sr}_2\text{Nb}_2\text{O}_7$, then we would expect to find grains with high reactivity oriented perpendicular to the direction of the spontaneous polarization, [001]. The one grain we observed with this orientation had relatively low reactivity and showed no

evidence for the domain patterns observed in studies of BaTiO_3 . However, the silver deposits on the particle were found on opposing (001) faces and this is a strong indication of a dipolar field effect due to either the spontaneous polarization or oppositely charged chemical terminations bounding the faces.

It is interesting to consider these results in comparison to the orientation dependence of the reactivity of SrTiO_3 where surfaces vicinal to (100) had the highest reactivity for silver reduction. In the current experiment, most grains with high reactivity also had orientations in the region between (010), (710) and (015). Since most of the grains were faceted, the macroscopic, average crystal orientations determined by EBSD were not identical to those of the planes terminating the surface. In fact, looking at the plots in Figures 7.6 and 7.8 it appears that the surfaces vicinal to {100}, {001}, {710}, {403}, and {015} are stable. Since the {100} orientation is known to be a stable plane in perovskites, it is likely that facets on the surfaces of $\text{Sr}_2\text{Nb}_2\text{O}_7$ and $\text{Sr}_2\text{Ta}_2\text{O}_7$ had the analogous (710) and (015) orientations. Therefore, the relatively higher reactive surfaces of $\text{Sr}_2\text{Nb}_2\text{O}_7$ and $\text{Sr}_2\text{Ta}_2\text{O}_7$ might be explained by the similarity of the local configuration of atoms to the perovskite (100) surface.

1.4 Summary and Conclusions

Observations of the spatial distribution of reduction and oxidation products on BaTi_4O_9 surfaces lend no support to the hypothesis that dipolar fields associated with the tunnels in this structure lead to a separation of charge carriers and the spatial isolation of one of the half reactions. Surfaces perpendicular and parallel to the tunnels have similar reactivities. However, the photochemical reduction of Ag and oxidation of Pb on $\text{Sr}_2\text{Nb}_2\text{O}_7$ and $\text{Sr}_2\text{Ta}_2\text{O}_7$ occurs more readily on surfaces oriented between (010), (710), and (015). The (710) and (015) surfaces are structurally similar to perovskite (100), which is the most reactive of SrTiO_3 surfaces. The low

activity of these materials for the photochemical probe reactions should be investigated further, especially in light of their high photolysis efficiencies. The $\text{Sr}_2\text{Nb}_2\text{O}_7$ particle experiment performed in the reactor did show evidence for a dipolar field effect and, therefore, more experiments with faceted $\text{Sr}_2\text{M}_2\text{O}_7$ and BaTi_4O_9 particles should be performed to more accurately describe the orientation dependence of their reactivity.

1.5 Acknowledgements

I would like to thank Ariana M. Zimbouski and Shahrzad Samadzadeh for their work on the $\text{Sr}_2\text{M}_2\text{O}_7$ and BaTi_4O_9 polycrystal experiments respectively.

1.6 References

- (1) J.L. Giocondi, S. Samadzadeh, and G.S. Rohrer, *Mater. Res. Soc. Proc.*, submitted.
- (2) J.B. Lowekamp, G.S. Rohrer, P.A. Morris Hotsenpiller, J.D. Bolt, and W.D. Farneth, *J. Phys. Chem. B*, **102**[38] (1998) 7323.
- (3) M. Kohno, S. Ogura, K. Sato, and Y. Inoue, in *Studies in Surface Science and Catalysis*, Vol. 101, edited by J.W. Hightower, W.N. Delgass, E. Iglesia, and A.T. Bell, (Elsevier Science, New York, 1996) p. 143.
- (4) M. Kohno, S. Ogura, K. Sato, and Y. Inoue, *J. Chem. Soc., Faraday Trans.*, **94**[1] (1998) 89.
- (5) Y. Inoue, O. Hayashi, and K. Sato, *J. Chem. Soc., Faraday Trans.*, **86**[12] (1990) 2277.
- (6) J.L. Giocondi and G.S. Rohrer, *J. Phys. Chem. B*, **105**[35] (2001) 8275.
- (7) J.L. Giocondi and G.S. Rohrer, *Chem. Mater.*, **13**[2] (2001) 241.
- (8) J.L. Giocondi and G.S. Rohrer, *J. Amer. Ceram. Soc.*, **86** [7] (2003) 1182.
- (9) T. Takata, Y. Furumi, K. Shinohara, A. Tanaka, M. Hara, J.N. Kondo, and K. Domen, *Chem. Mat.*, **9** (1997) 1063.
- (10) A. Kudo, H. Kato, and S. Nakagawa, *J. Phys. Chem. B*, **104** (2000) 571.

8 Summary, Conclusions, and Future Work

8.1 Summary

The research in this thesis has shown how internal electric fields, due to ferroelectric domains or polar surfaces, can separate the oxidation and reduction halves of photochemical reactions and that simple perovskites have orientation dependent photochemical reactivity. While experiments on BaTi_4O_9 , $\text{Sr}_2\text{Ta}_2\text{O}_7$, and $\text{Sr}_2\text{Nb}_2\text{O}_7$ polycrystals show no evidence that either dipolar fields or surface orientation are important materials properties, experiments on $\text{Sr}_2\text{Nb}_2\text{O}_7$ crystals do indicate that the dipolar field effect spatially separates charge carriers.

8.2 Conclusions

8.2.1 *Do permanent dipoles separate photogenerated charge carriers and the locations of photochemical oxidation/reduction half reactions on the surfaces of polar oxides?*

Yes, the dipolar fields due to ferroelectric domains and charged surface terminations have a significant effect on the photochemical reactivity of BaTiO_3 and SrTiO_3 , respectively. The ferroelectric domain structure also appears to influence the reactivity of $\text{Sr}_2\text{Nb}_2\text{O}_7$. The ability to separate photogenerated charge carriers and the locations of oxidation and reduction half reactions with these fields could have important implications for improving the efficiencies of water photolysis catalysts. For example, one could use ferroelectric materials as supports for high efficiency water photolysis catalysts to further improve their efficiencies.

8.2.2 *Do materials other than TiO₂ have orientation dependent photochemical reactivities?*

Yes, SrTiO₃ has a strong orientation dependent photochemical reactivity. For silver reduction, {100} was the most reactive followed by {111} and {110}. Looking at the reduction of silver on the BaTiO₃ particles, one can also infer the same orientation dependence. The reactivity of SrTiO₃ for lead oxidation had the inverse orientation dependence.

Interestingly, the orientation stability of the perovskite oxides studied are all similar and can be related to the number of broken transition metal bonds and the polarity of the surface. Polycrystal studies on SrTiO₃ showed that surfaces vicinal to {100} were the most stable with the {110} and {111} surfaces also having some stability. Both the SrTiO₃ and BaTiO₃ particles were bounded by some combination of {100}, {110}, and {111} facets with {100} being the largest followed by {110} and {111}. This order of stability is consistent with a broken bond model where the nonpolar {100} surface should be most stable with only one broken Ti-O bond and the polar {110} and {111} surfaces should have lower stability with two and three Ti-O broken bonds, respectively. Looking at the distributions of flat and faceted grains for Sr₂Nb₂O₇ and Sr₂Nb₂O₇, it appears that all the flat orientations are located near orientations that are structurally similar to cubic perovskite {110} and {100} orientations.

8.2.3 *Is the internal dipolar field or the crystal structure of the catalyst an important materials property for compounds with high photochemical activity such as Sr₂Nb₂O₇, Sr₂Ta₂O₇, and BaTi₄O₉?*

In this case, different experiments have led to contradictory answers. The polycrystals of the anisotropic compounds that were examined all had surprisingly isotropic reactivity, at least for the conditions of these experiments. Sr₂Nb₂O₇, a ferroelectric material, showed any anisotropy in reactivity with the direction of the field. Sr₂M₂O₇ showed only a slight orientation

dependent reactivity for orientations similar to perovskite {100}. They also have relatively low reactivity compared to the titanate compounds for these reactions, even though they are known to be good photolysis catalysts. The only trend between the three materials is that the reactivity within individual grains varied as much as between grains. This reactivity may indicate that there are microscopic differences in the chemistry of these surfaces that were not detected but are similar to the chemical termination effect seen on SrTiO₃. The results for Sr₂Nb₂O₇ particles contradicted the polycrystal study. These results suggest that the reduction of Ag is correlated to the direction of the internal polarization and that because of this the reactivity is anisotropic.

8.2.4 *Particle Reactivity versus Bulk Materials Reactivity*

Another encouraging result was that the micron-sized particles had the same reactivity as the bulk materials. Unlike the experiments that have been performed on rutile, the SrTiO₃ particles have the same orientation dependent reactivity that was observed in the bulk materials. For BaTiO₃, the bulk materials and particles both have reactivity that depends on the ferroelectric domain structure. Whether or not the reactivity relationships established in this research are significant for the water photolysis reaction is not yet clear. Experiments on crystals of Sr₂Ta₂O₇ and BaTi₄O₉ should be carried out under conditions that exactly mimic the reaction conditions used for the Sr₂Nb₂O₇ experiment.

8.3 **Future Work**

8.3.1 *Using the Dipolar Field Effect*

One way to determine the effect of the dipolar field on photolysis is to measure the rate of the evolution of H₂ and O₂ from illuminated Sr_xBa_{1-x}TiO₃ (0.20 ≤ x ≤ 0.40) and Sr₂(Nb_{1-x}Ta_x)₂O₇ (0.8 ≤ x ≤ 1) powders in aqueous solutions. Both the BaTiO₃/SrTiO₃ (BSTO) and the Sr₂Nb₂O₇/Sr₂Ta₂O₇ (SNTO) systems form complete solid solutions that have a linearly varying

Curie temperatures with $T_c = 20\text{ }^\circ\text{C}$ at $x = 0.3$ for BSTO and at $x = 0.93$ for SNTO. By evaluating the series of compositions in this way, these experiments can determine how the ferroelectric-to-paraelectric transition affects the efficiency of water photolysis at a constant temperature and as the Sr/Ba (or Nb/Ta) ratio is varied in a systematic way. We expect that the ferroelectric phases will show an increased efficiency because of the separation of charge carriers by the dipolar electric field.

Another experiment could be conducted to determine the dependence of photochemical activity on domain size. Over the course of the experiments already performed, several notable observations were made. First, 1 mm thick, single domain BaTiO_3 (001) crystals did not show any activity for the photochemical reduction of silver or oxidation of lead. We hypothesize that the large distance required for the separation of the carriers along the axis of the dipole limits the activity. Conversely, very thin domains (~ 10 nm wide) showed a low activity. In this case, the proximity of the domains to each other limits the effectiveness of the dipolar field for separating the charge carriers and/or preventing the back-reaction of products. Therefore, it is likely that there is an optimal domain size for which the highest activity could be achieved.

1.1.2 Textured Particles for Water Photolysis

Photolysis efficiency measurements on powders and particles with different habits should be used to determine the influence of these orientation-reactivity relationships on water photolysis efficiency. The goal of the experiment would be to compare the activity for water splitting of crystals with the same surface area but different habits. A change in activity between different particles can therefore be directly related to the surface orientations of these particles.